This pdf file consists of figures and their captions, extracted from:

Petrology, Petrogenesis, and Tectonic setting of Jurassic rocks of the Central Cascades, Washington, and Western Klamath Mountains, California-Oregon

by

James H. MacDonald, Jr.

A Dissertation

Submitted to the University at Albany, State University of New York

in Partial Fulfillment of

the Requirements for the Degree of

Doctor of Philosophy

College of Arts & Sciences

Department of Earth and Atmospheric Science

2006

Figure 1. Generalized geologic map of western Klamath terrane, including Galice Formation. Modified from Wyld and Wright (1988), Miller and Saleeby (1995), Harper (2003), and Giaramita and Harper (2006).

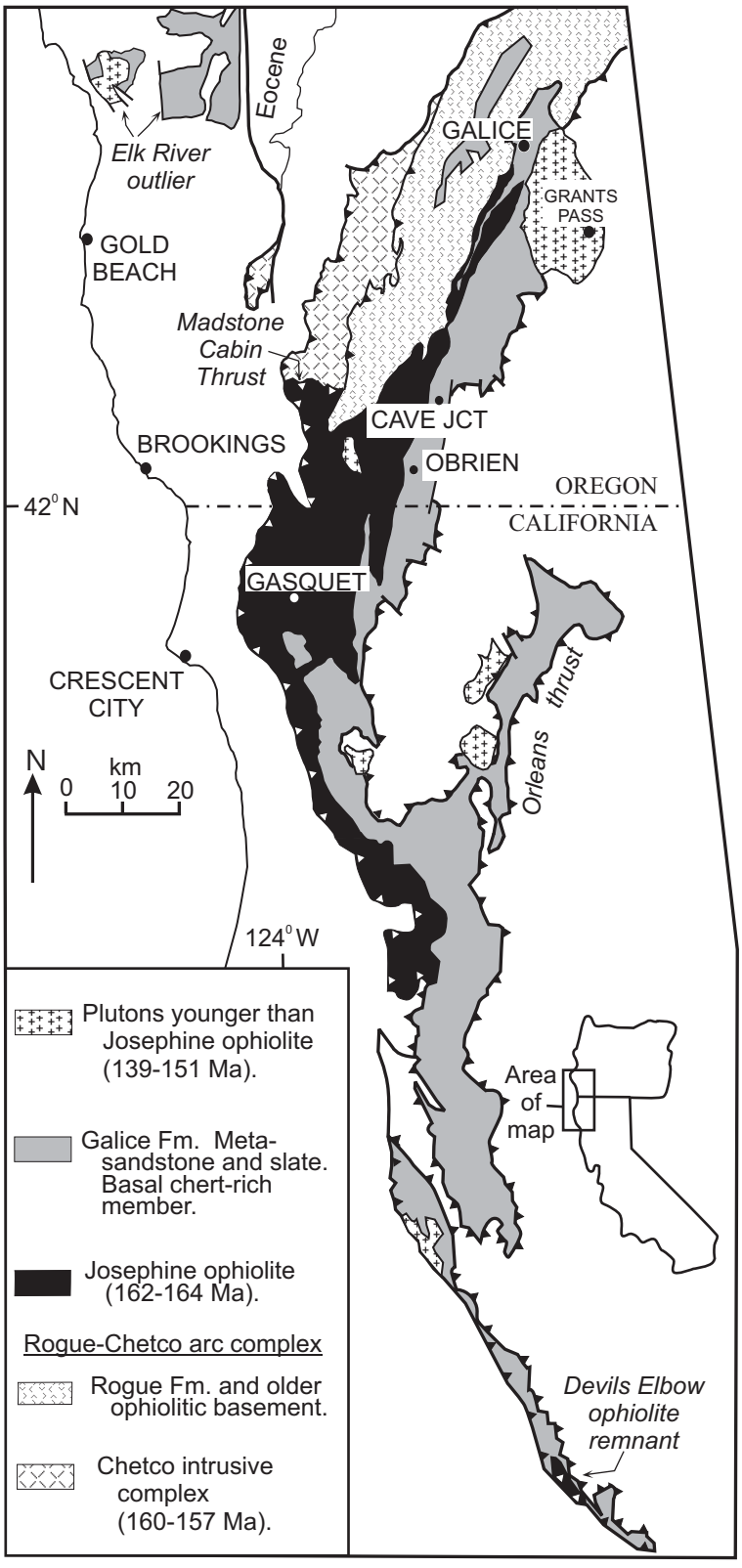
Eocene
Elk River outlier
GALICE
GRANTS PASS
GOLD BEACH
Madstone Cabin Thrust
CAVE JCT
BROOKINGS
OBRIEN
OREGON
CALIFORNIA
42° N
GASQUET
CRESCENT CITY
Orleans thrust
N
km
0 10 20
124° W
Area of map
Devils Elbow ophiolite remnant
Plutons younger than Josephine ophiolite (139-151 Ma).
Galice Fm. Meta-sandstone and slate. Basal chert-rich member.
Josephine ophiolite (162-164 Ma).
Rogue-Chetco arc complex
Rogue Fm. and older ophiolitic basement.
Chetco intrusive complex (160-157 Ma).

Figure 2. Sedimentary sequence overlying ~162 Ma Josephine ophiolite. Biostratigraphic ages are from Pessagno and Blome (1990) and Pessagno et al. (2000), and radiometric ages are from Harper et al. (1994). Location of metalliferous sediments is from Pinto-Auso and Harper (1985). Detrital-zircon sample (~153 Ma and ~227 Ma peaks; Miller et al., 2003) is from a locality of *Buchia concentrica* of middle Oxfordian to late Kimmeridgian age (Imlay et al., 1959). Modified from Harper (1994).

Josephine ophiolite
Galice Formation
sensu lato
pillow lava
hemipelagic sequence
hemipelagic-turbidite transition
turbidite
Orleans thrust
mudstone
sandstone
volcanic diamictite
hiatus?
level of detrital zircon sample
50 m
sill 146 ±1 Ma
soft sediment deformation
sill 150 ±1 Ma
metalliferous sediment
UPPER CALLOVIAN
OXFORDIAN
KIMMERIDGIAN

Figure 3. Drill core sample from the Turner-Albright mine showing siliceous argillite that is interbedded with lavas of the Josephine ophiolite. The black and green laminations are interpreted as terrigenous and tuffaceous in origin, respectively. The alternating black and green colors are also typical of the hemipelagic sequence overlying the Josephine ophiolite. Note coin for scale.

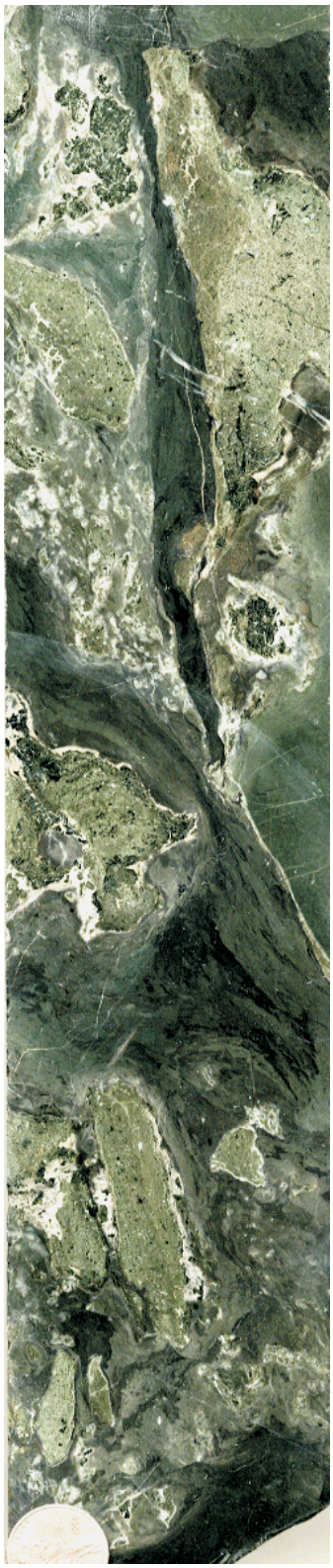

Figure 4. A. Photomicrograph of a tuffaceous chert showing bipyramidal (volcanic) quartz, and plagioclase. 0.25 mm scale is located on figure. Crossed polarizers. B. Photomicrograph of tuffaceous radiolarian argillite from the hemipelagic sequence showing well preserved cone-shaped Radiolaria (arrow), altered vesicular glass (left center), and angular quartz grains (clear). Plane light. Horizontal scale is 2 mm. C. Photomicrograph of metasandstone from the Galice Formation showing felsic volcanic clast with resorbed quartz phenocryst. Colorless high-relief grain below this clast is augite. Note foliation in the matrix. Horizontal scale is approximately 1.5 mm. D. Photomicrograph of metasandstone from the Galice Formation showing a clast of quartz-mica schist. At the lower left of this grain is a mafic volcanic clast. Dark seams are parallel to foliation. Horizontal scale is approximately 0.8 mm.

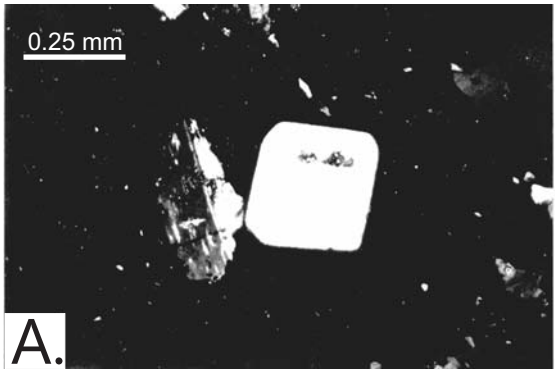
0.25 mm
A.

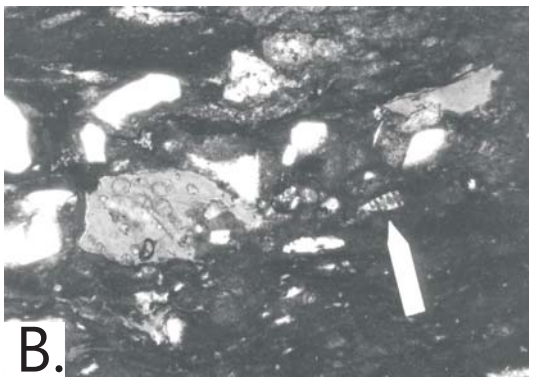
B.

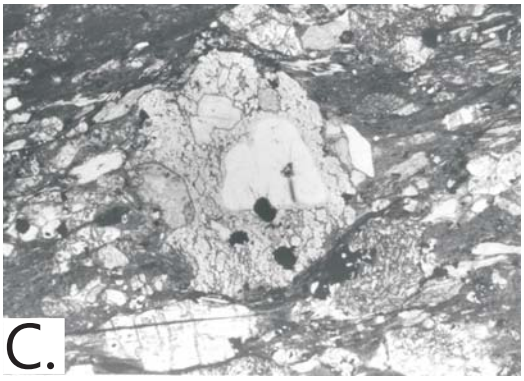
C.

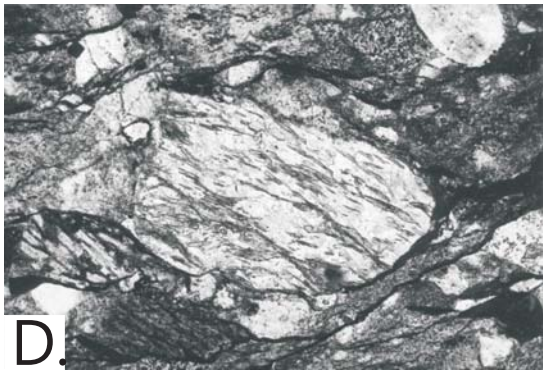
D.

Figure 5. Plot illustrating apparent mixing relationships for sediments within Josephine ophiolite, hemipelagic sequence, and Galice Formation. Mixing curves are for East Pacific Rise (EPR), hydrothermal sediment, and Pacific pelagic clay (PC), and EPR hydrothermal sediment and mid-ocean ridge basalt (MORB; values from Barrett, 1981). Also shown is field for Margi umbers, Cyprus, which are pure metalliferous sediment (Ravizza et al., 1999). Figure modified from Pinto-Auso and Harper (1985), and Harper et al. (1988).

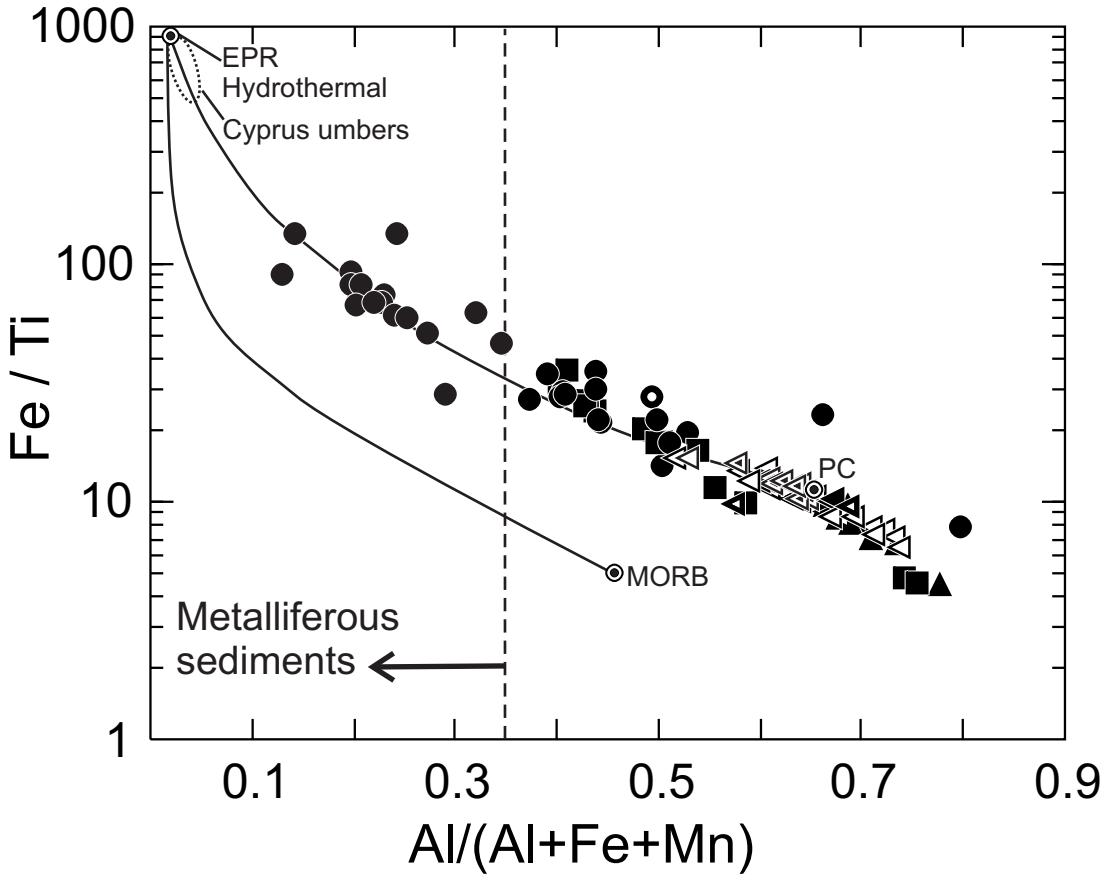

Galice Formation

Type Galice
- Slate
- Sandstone

Galice overlying Josephine ophiolite
- Sandstone
- Slate
- Elk River outlier

Hemipelagic sequence
- Siliceous argillite
- Chert

Intra-pillow sediment
- Siliceous argillite

Figure 6. Graded bed from hemipelagic sequence of the Galice Formation. Bed beneath pebbly sandstone is a radiolarian chert. On the back side of this sample there is a 3-cm subangular rip-up clast of underlying sediment located within pebbly sandstone.

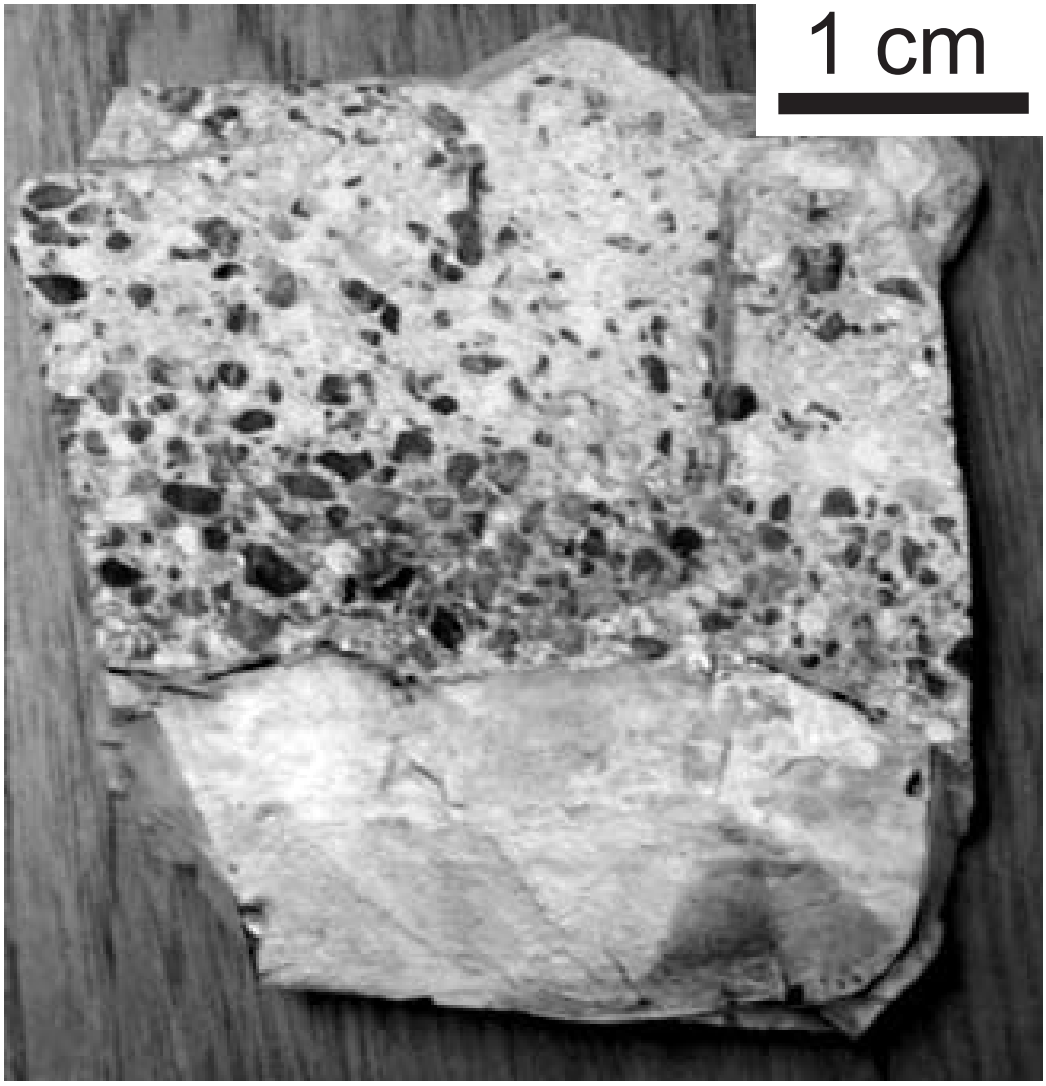
1 cm

Figure 7. Rose diagrams displaying paleoflow current directions. A. Type area of the Galice Formation, corrected for folding (from Park-Jones, 1988). B. Type area of Galice, also corrected for inferred ~65° oroclinal bending of the Klamath Mountains (Renne and Scott, 1988; Saleeby and Harper, 1993). C. Galice Formation that overlies Josephine ophiolite, corrected for folding. D. Galice Formation that overlies Josephine ophiolite, also corrected for inferred ~65° oroclinal bending of Klamath Mountains. Unidirectional data displayed in black, bimodal data are gray. Intervals of 15 degrees are used. Note the different scale in A and B, and C and D.

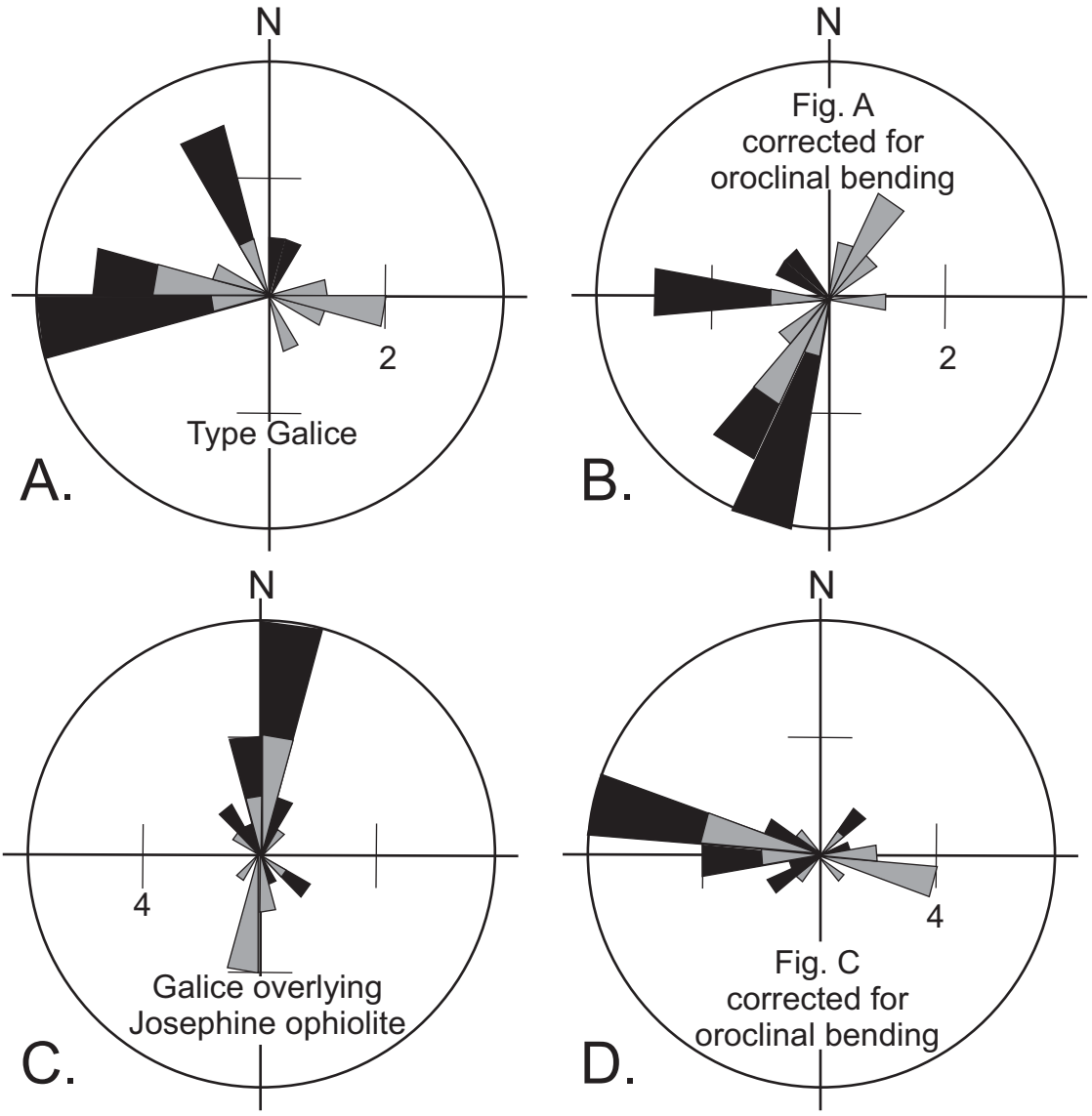
N
2
Type Galice
A.
N
Fig. A
corrected for
oroclinal bending
2
B.
N
4
Galice overlying
Josephine ophiolite
C.
N
4
Fig. C
corrected for
oroclinal bending
D.

Figure 8. Triangular plots of point-count data for sandstones from Galice Formation in its type area (Harper, 1980), where it overlies the Josephine ophiolite near the Oregon-California border (Harper, 1980; Norman, 1984), and overlying Devils Elbow remnant of the Josephine ophiolite in the southern Klamath Mountains (Wyld, 1985). Q = monocrystalline quartz + polycrystalline quartz + chert; F = feldspar (all plagioclase in these samples); L = unstable lithics; Q_m = monocrystalline quartz; L_t = total polycrystalline lithic fragments, including stable quartzose; Q_p = chert + polycrystalline quartz; L_v = lithic volcanics; L_{sm} = sedimentary + metasedimentary lithics. A. Q-F-L diagram after Dickinson et al. (1983). Shaded field is for correlative rocks in the Sierra Nevada foothills, including the Mariposa Formation (Behrman and Parkison; 1978). B. Q_m-F-L_t diagram after Dickinson et al. (1983). C. Q_p-L_v-L_{sm} diagram after Dickinson (1985). Inferred end-member sources for Galice sandstones are indicated. D. L_{sm}+Q_p-F-L_v diagram.

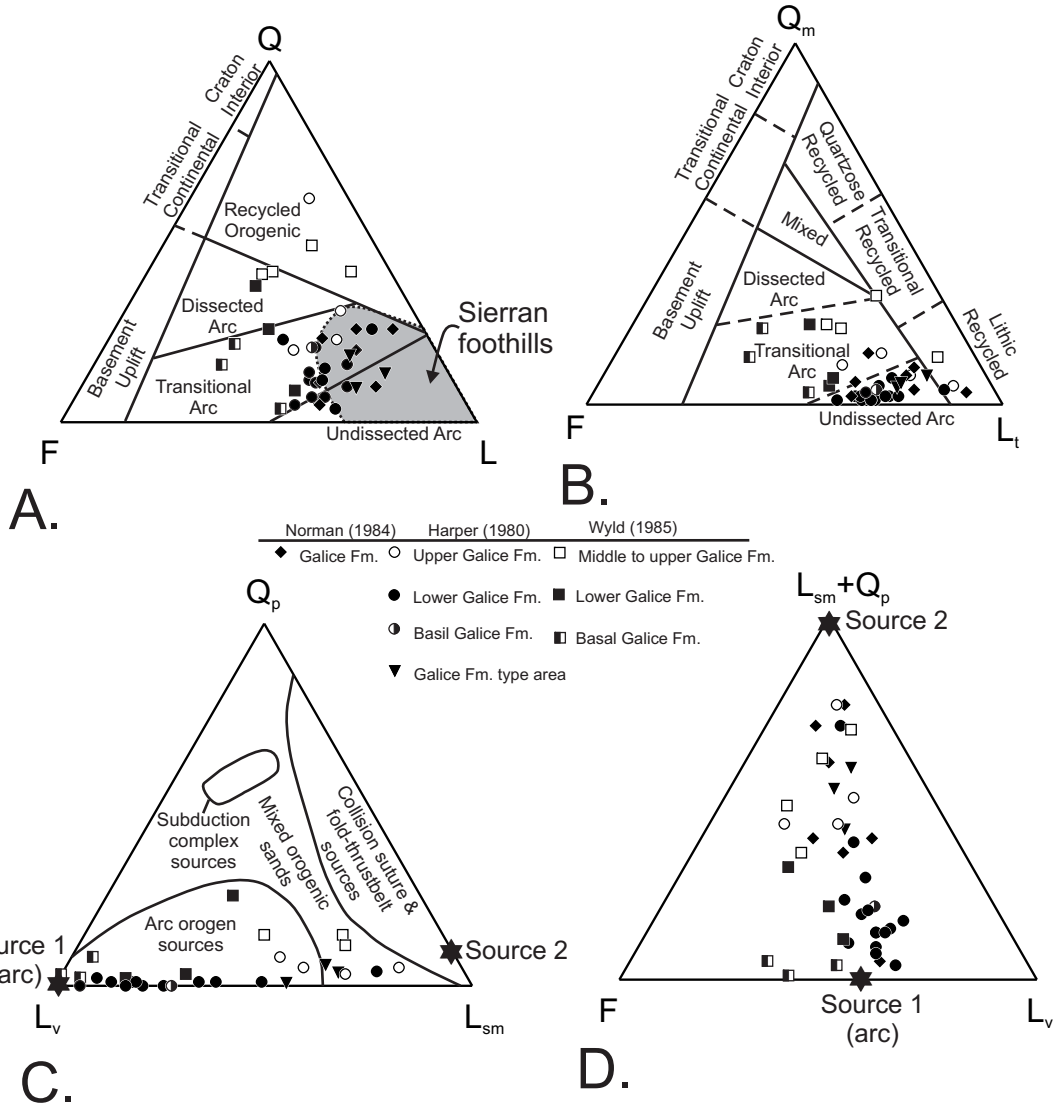
Q
Craton Interior
Transitional Continental
Recycled Orogenic
Dissected Arc
Basement Uplift
Transitional Arc
Sierran foothills
Undissected Arc
F
L
A.
Q_m
Transitional Continental
Craton Interior
Quartzose Recycled
Transitional Recycled
Lithic Recycled
Mixed
Basement Uplift
Dissected Arc
Transitional Arc
Undissected Arc
F
L_t
B.
Norman (1984)
Harper (1980)
Wyld (1985)
Galice Fm.
Upper Galice Fm.
Middle to upper Galice Fm.
Lower Galice Fm.
Lower Galice Fm.
Basil Galice Fm.
Basal Galice Fm.
Galice Fm. type area
Q_p
Subduction complex sources
Mixed orogenic sands
Collision suture & fold-thrustbelt sources
Arc orogen sources
Source 1 (arc)
Source 2
L_v
L_sm
C.
L_sm+Q_p
Source 2
F
Source 1 (arc)
L_v
D.

Figure 9. Conglomerate point count data for the Galice Formation and the Mariposa Formation in the central Sierran foothills illustrating provenance differences. I = igneous rocks, Q = quartz sandstone and quartzite, C = chert. Data from Wyld (1985) and Seiders (1991, and written comm., 1992).

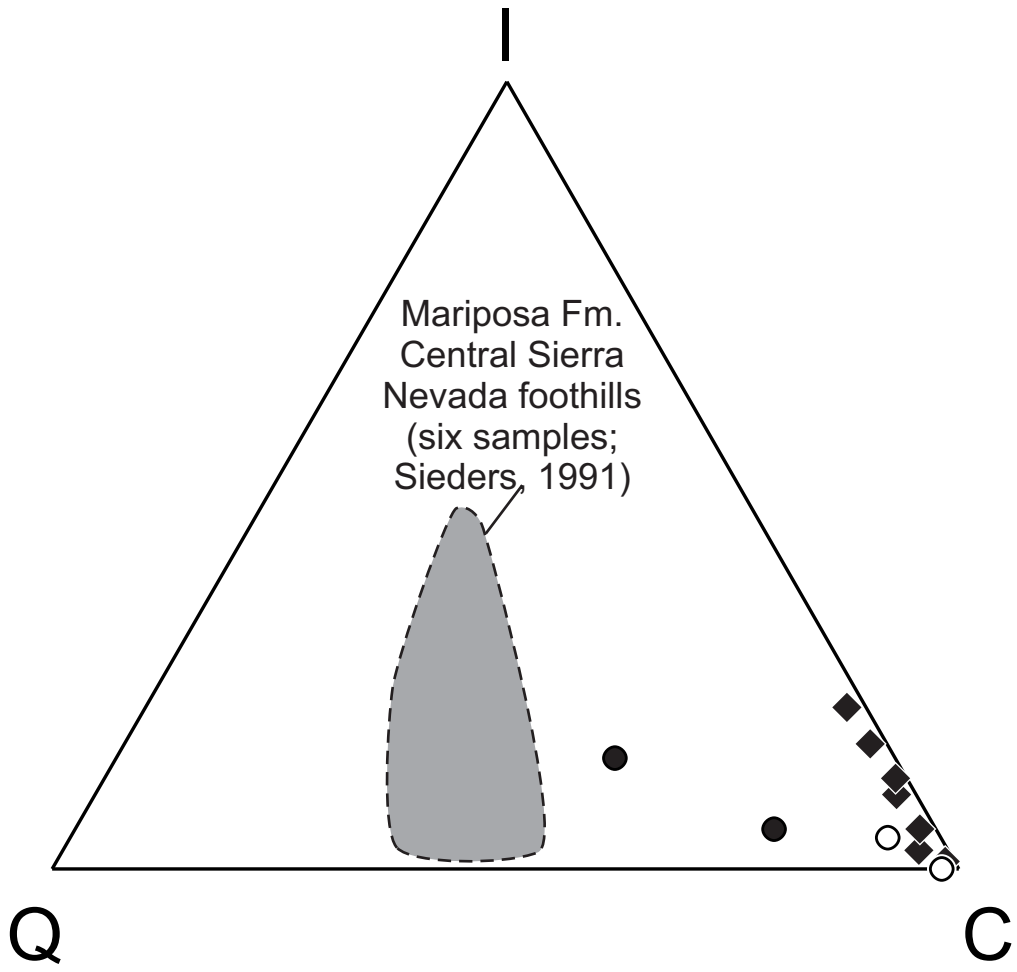

◆ Galice Formation conglomerate (Sieders, 1991 and pers. comm.) West-central Klamath Mtns.

● Lower Galice Formation conglomerate (Wyld, 1985). Southern Klamath Mtns.

○ Middle to upper Galice Formation conglomerate (Wyld, 1985). Southern Klamath Mtns.

Figure 10. Al_2O_3 verses TiO_2 diagram showing detrital Cr-spinels from an intra-pillow sandstone in the Josephine ophiolite and a turbidite sandstone of the Galice Formation. Fields are from Kamenetsky et al. (2001). This diagram is a good discriminator for tectonic setting as well as for distinguishing volcanic from peridotite spinels. OIB = ocean-island (within-plate) basalt; MORB = mid-ocean ridge basalt; SSZ = supra-subduction zone. Also shown is the field for spinels from the Trinity peridotite (Quick, 1981).

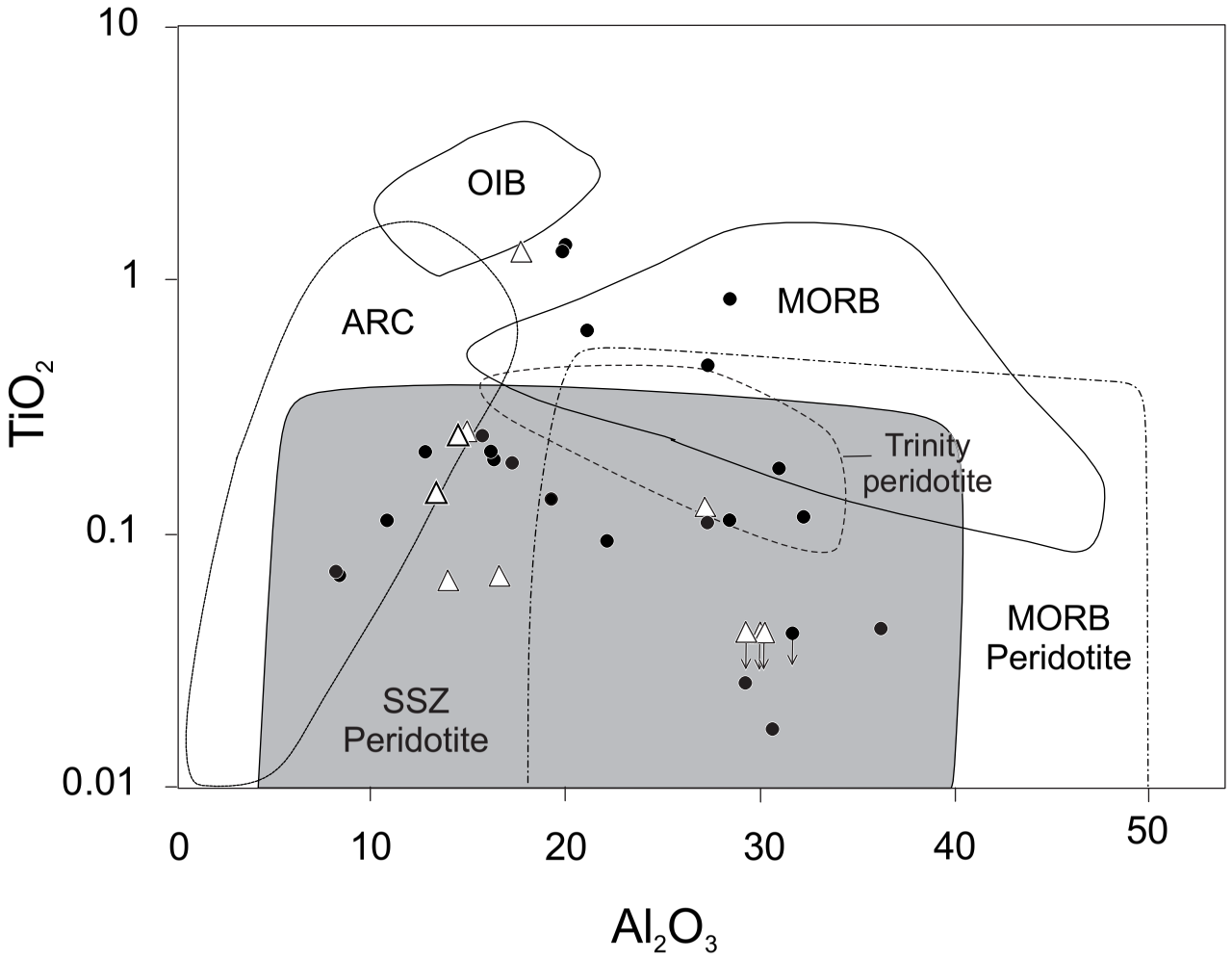

- lower turbidite sandstone
- △ sandstone in Josephine pillow basalts

Figure 11. Cr/(Cr+Al) versus Mg/(Mg+Fe^{2+}) diagram for detrital Cr-spinels from a sandstone within the pillow lavas of the Josephine ophiolite and a sandstone from the basal turbidite sequence overlying the ophiolite. Symbols are the same as in Figure 9. Field for Trinity peridotite from Quick (1981). Fields for MORB, SE Alaska intrusions, and abyssal peridotites (MORB residue) from Dick and Bullen (1984); field for back arc basin basalts from Dick and Bullen (1984), Hawkins and Mechoir (1985), Saunders and Tarney (1979; one sample); field for Hole 839 in the Lau Basin is from Allan (1994); field for low-Ca boninites is from Umino (1986); field for OIB from Kamenetsky et al. (2001); and field for supra-subduction zone peridotite is modified from Parkinson and Pearce (1998). Olivine isopleths are from Kamenetsky et al. (2001). A. Spinels derived from peridotite (as determined from Fig. 9). B. Spinels of volcanic origin (as determined from Fig. 9). C. Spinels that could be either volcanic or peridotitic origin (as determined from Fig. 9).

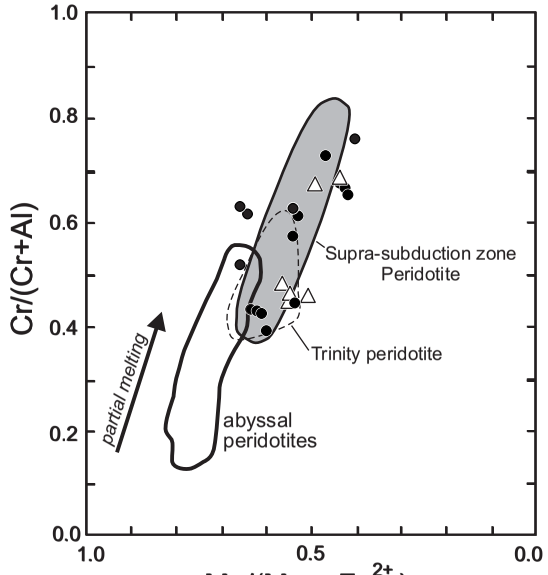

A.

Mantle peridotite spinels

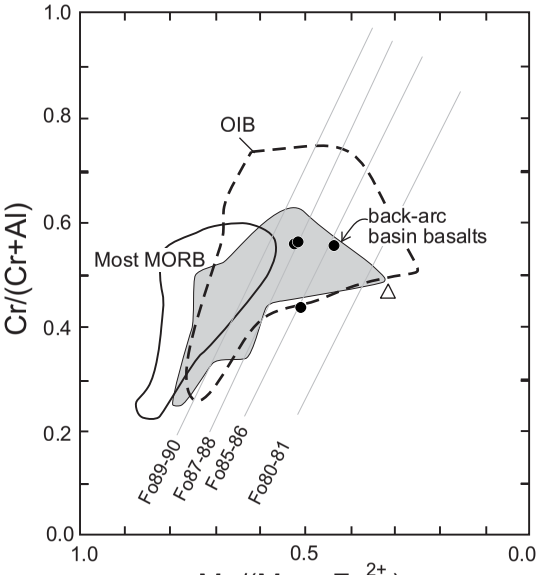

B.

Volcanic spinels

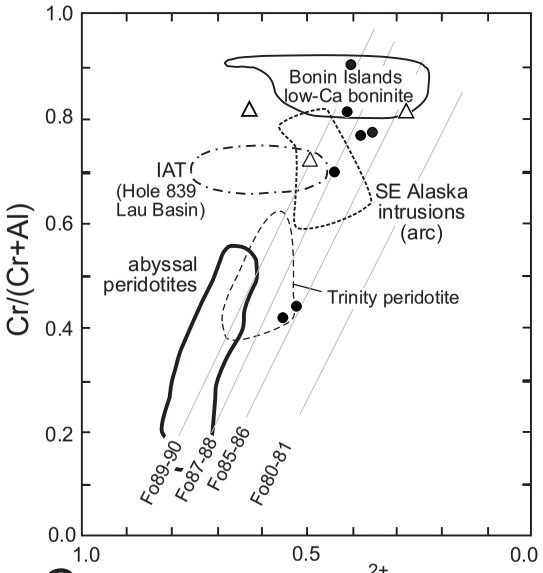

C.

Overlap mantle/volcanic spinels
From Figure Al_2O_3/TiO_2

Figure 12. Provenance discriminant-function diagram of Roser and Korsch (1988). Only samples from the Galice turbidite are plotted. Siliceous argillite and chert from the hemipelagic sequence and the Josephine ophiolite are not plotted because of their Fe-rich hemipelagic component. Also plotted are the average values for North American shale composite (NASC), post-Archean Australian shale composite (PAAS), upper continental crust (UC; Gromet et al., 1984; McLennan, 1989; McLennan, 2001), and fields for modern back arc basin turbidites (McLennan et al., 1990) and volcaniclastic sediments from the Lau back arc (Bednarz and Schmincke, 1994). Symbols are the same as in Figure 5.

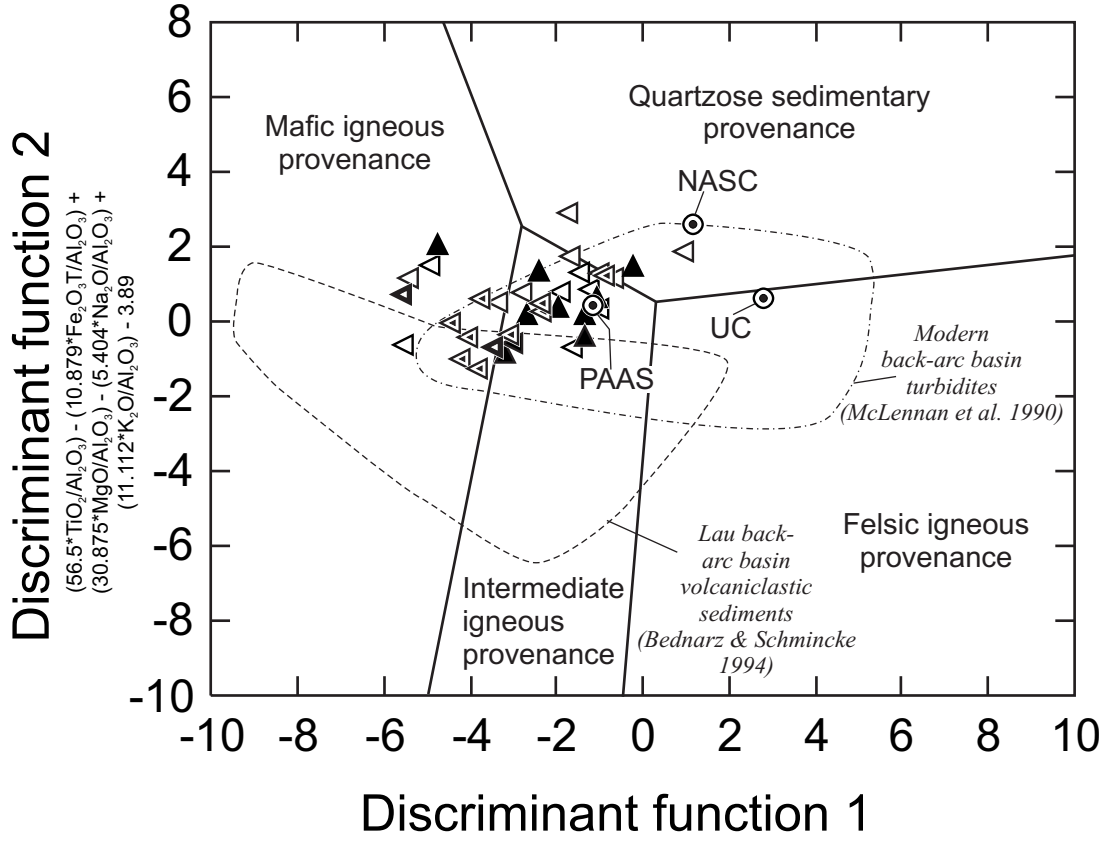
Discriminant function 2
(56.5*TiO2/Al2O3) - (10.879*Fe2O3T/Al2O3) +
(30.875*MgO/Al2O3) - (5.404*Na2O/Al2O3) +
(11.112*K2O/Al2O3) - 3.89
Discriminant function 1
(30.638*TiO2/Al2O3) - (12.541*Fe2O3T/Al2O3) +
(7.329*MgO/Al2O3) + 12.031*Na2O/Al2O3) +
(35.402*K2O/Al2O3) - 6.382
Mafic igneous provenance
Quartzose sedimentary provenance
Intermediate igneous provenance
Felsic igneous provenance
NASC
UC
PAAS
Modern back-arc basin turbidites (McLennan et al. 1990)
Lau back-arc basin volcaniclastic sediments (Bednarz & Schmincke 1994)

Figure 13. Th/Sc versus Zr/Sc plot modified from McLennan et al. (1993) by the addition of average upper continental crust (representing cratonic sources; McLennan, 2001), a modern island-arc tholeiite (representing mafic sources; Pearce et al., 1995), and the field for modern back arc basin turbidities (McLennan et al., 1990). Symbols are the same as in Figure 5.

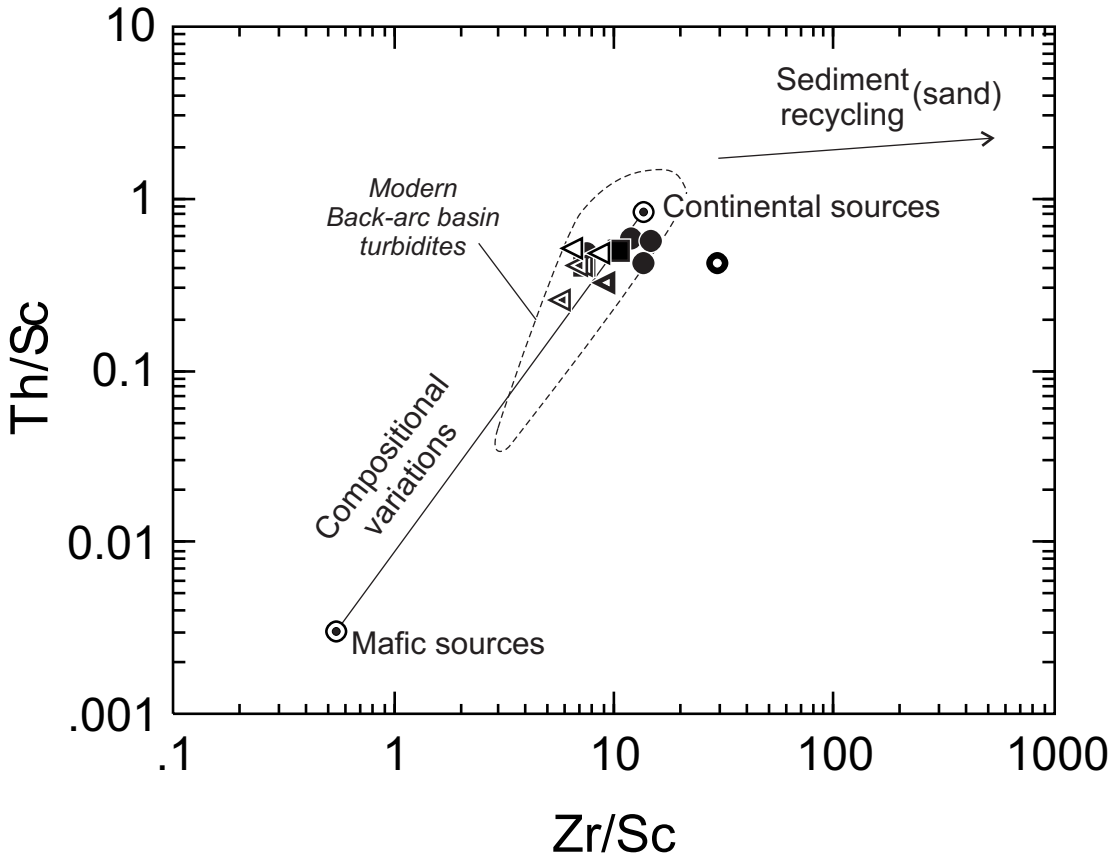
10
1
0.1
0.01
.001
Th/Sc
.1
1
10
100
1000
Zr/Sc
Sediment recycling (sand)
Modern Back-arc basin turbidites
Continental sources
Compositional variations
Mafic sources

Figure 14. Post-Archean Australian shale composite (PAAS) normalized diagrams. A. North American shale composite (NASC) from Gromet et al. (1984), Cyprus Umber from Ravizza et al. (1999), and Upper Continental crust value from McLennan (2001). B. Back arc basin sediments (Japan and Celebes Seas) from McLennan et al. (1990) and modern island arc tholeiite (IAT) from Pearce et al. (1995). C. Chert from the hemipelagic sequence and typical metalliferous and intra-pillow argillites. D. Typical slate and sandstone from the turbidite overlying the Josephine ophiolite, and a typical slate from the type area of the Galice Formation. Normalization values are from McLennan (1989).

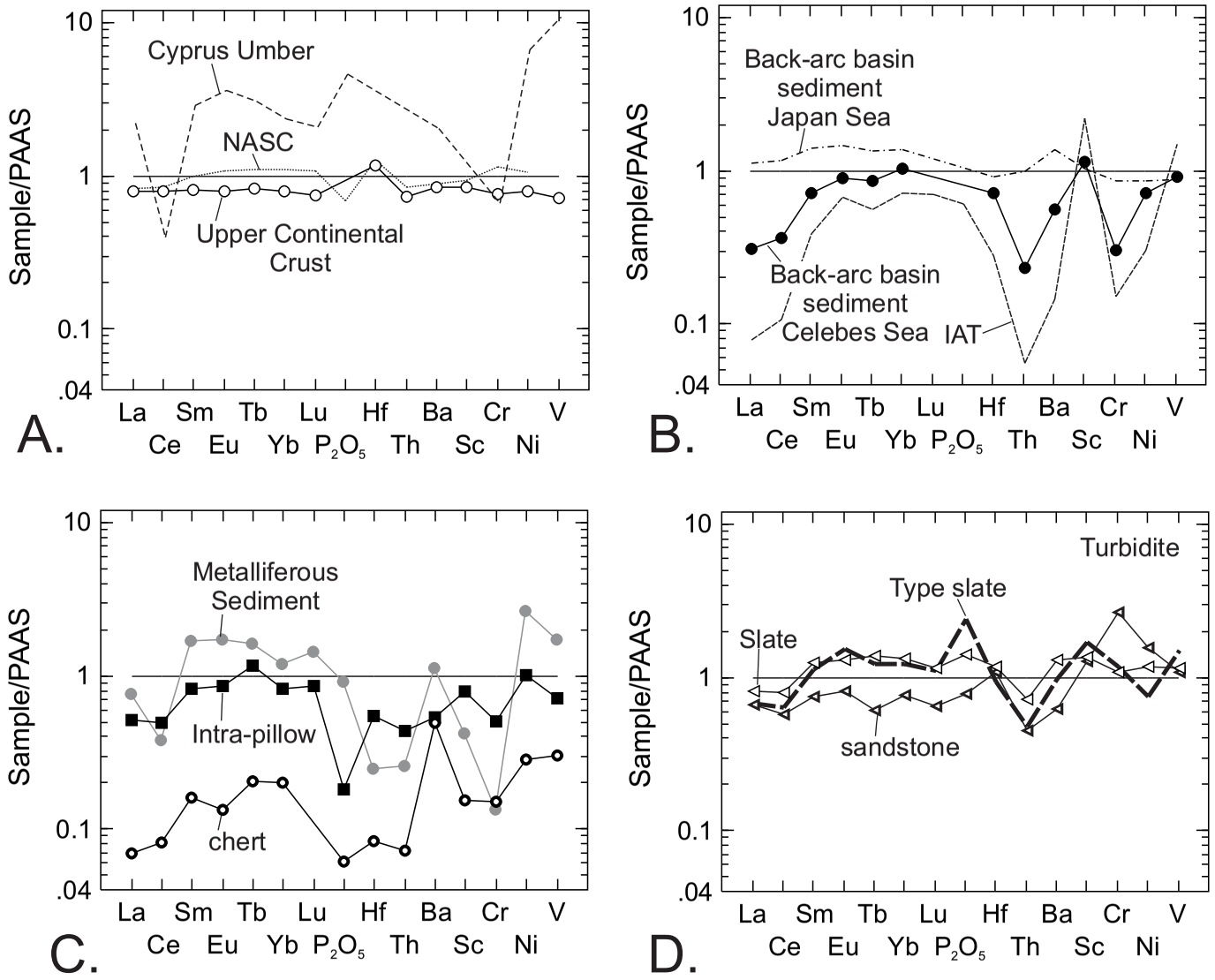
Sample/PAAS
10
1
0.1
.04
Cyprus Umber
NASC
Upper Continental Crust
La Sm Tb Lu Hf Ba Cr V
Ce Eu Yb P_2O_5 Th Sc Ni
A.
Back-arc basin sediment Japan Sea
Back-arc basin sediment Celebes Sea
IAT
B.
Metalliferous Sediment
Intra-pillow
chert
C.
Turbidite
Type slate
Slate
sandstone
D.

Figure 15. Tectonic model for the generation and emplacement of the Galice Formation and the underlying Josephine ophiolite. The inferred oblique subduction model is similar to the modern Andaman Sea. Arrows indicate probable paleocurrent flow directions. Modified from Harper and Wright (1984), Harper et al. (1985), Wyld and Wright (1988), and Harper et al. (1994). A. Paleogeography prior to deposition of Galice turbidite. B. Paleogeography during deposition of Galice turbidite.

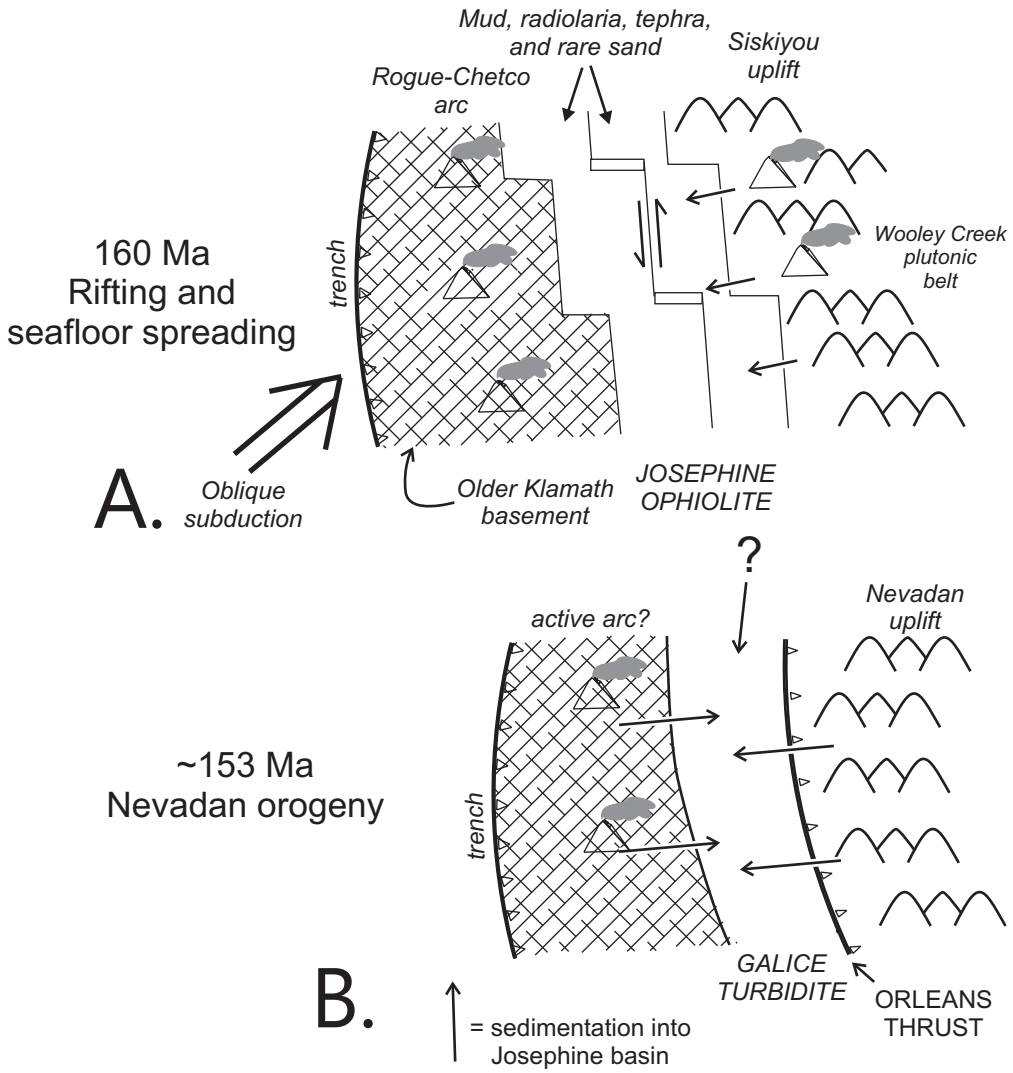
Mud, radiolaria, tephra, and rare sand
Siskiyou uplift
Rogue-Chetco arc
Wooley Creek plutonic belt
trench
160 Ma
Rifting and
seafloor spreading
A.
Oblique subduction
Older Klamath basement
JOSEPHINE OPHIOLITE
?
Nevadan uplift
active arc?
~153 Ma
Nevadan orogeny
trench
B.
GALICE TURBIDITE
ORLEANS THRUST
= sedimentation into Josephine basin

Figure 16. Location of Middle to Late Jurassic ophiolites of the North America Cordillera and older Rattlesnake Creek terrane. JO-DEO = Devils Elbow. Modified from Metzger et al. (2002).

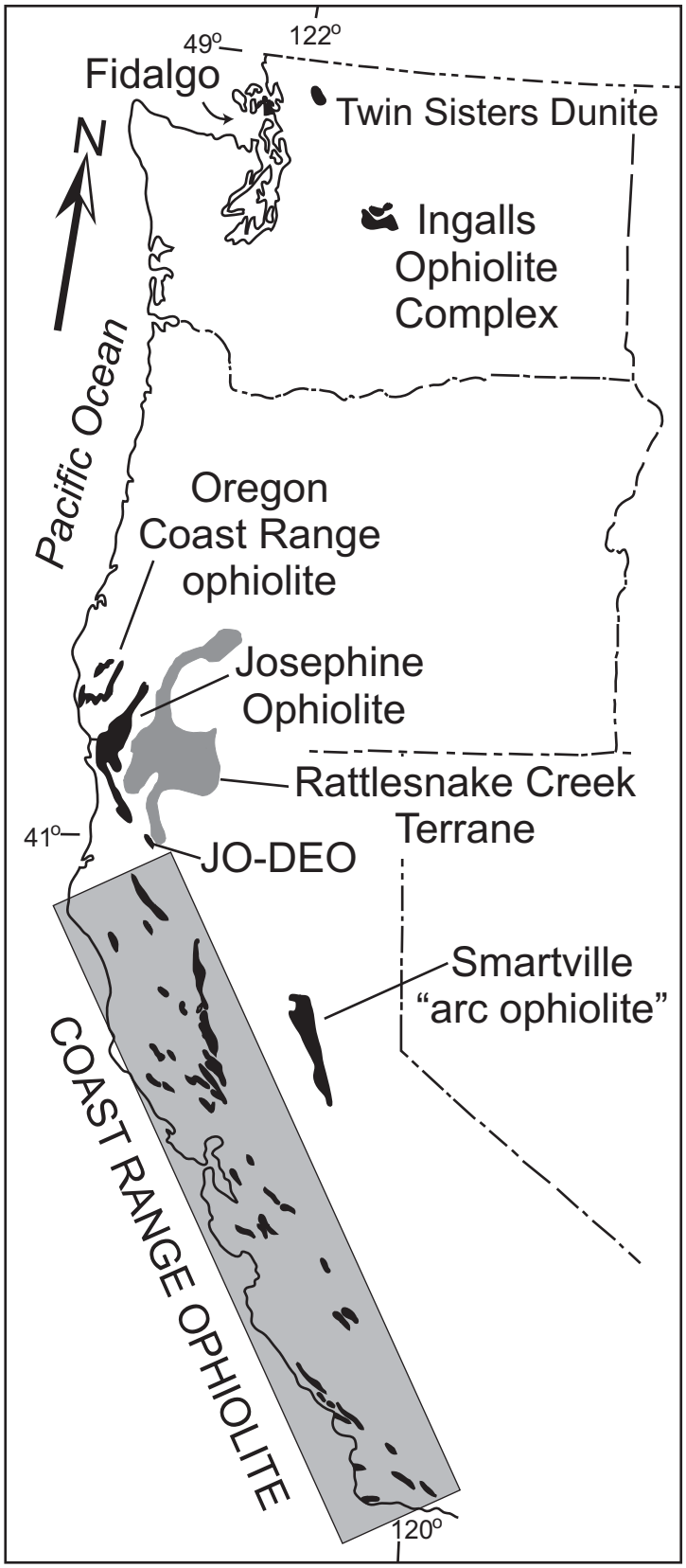
49°
122°
Fidalgo
Twin Sisters Dunite
N
Ingalls
Ophiolite
Complex
Pacific Ocean
Oregon
Coast Range
ophiolite
Josephine
Ophiolite
Rattlesnake Creek
Terrane
41°
JO-DEO
Smartville
“arc ophiolite”
COAST RANGE OPHIOLITE
120°

Figure 17. Map of the Ingalls ophiolite complex and surrounding units. EP = Esmeralda Peaks; NDFZ = Navaho Divide fault zone; I = Iron Mountain; S = Sheep Mountain. IAT = island-arc tholeiite; MORB = mid-ocean ridge basalt; WPB = within-plate basalt. Indicated Jurassic ages are based on Radiolaria in chert (E. Pessagno, 2002, personal communication to MacDonald et al. 2006).

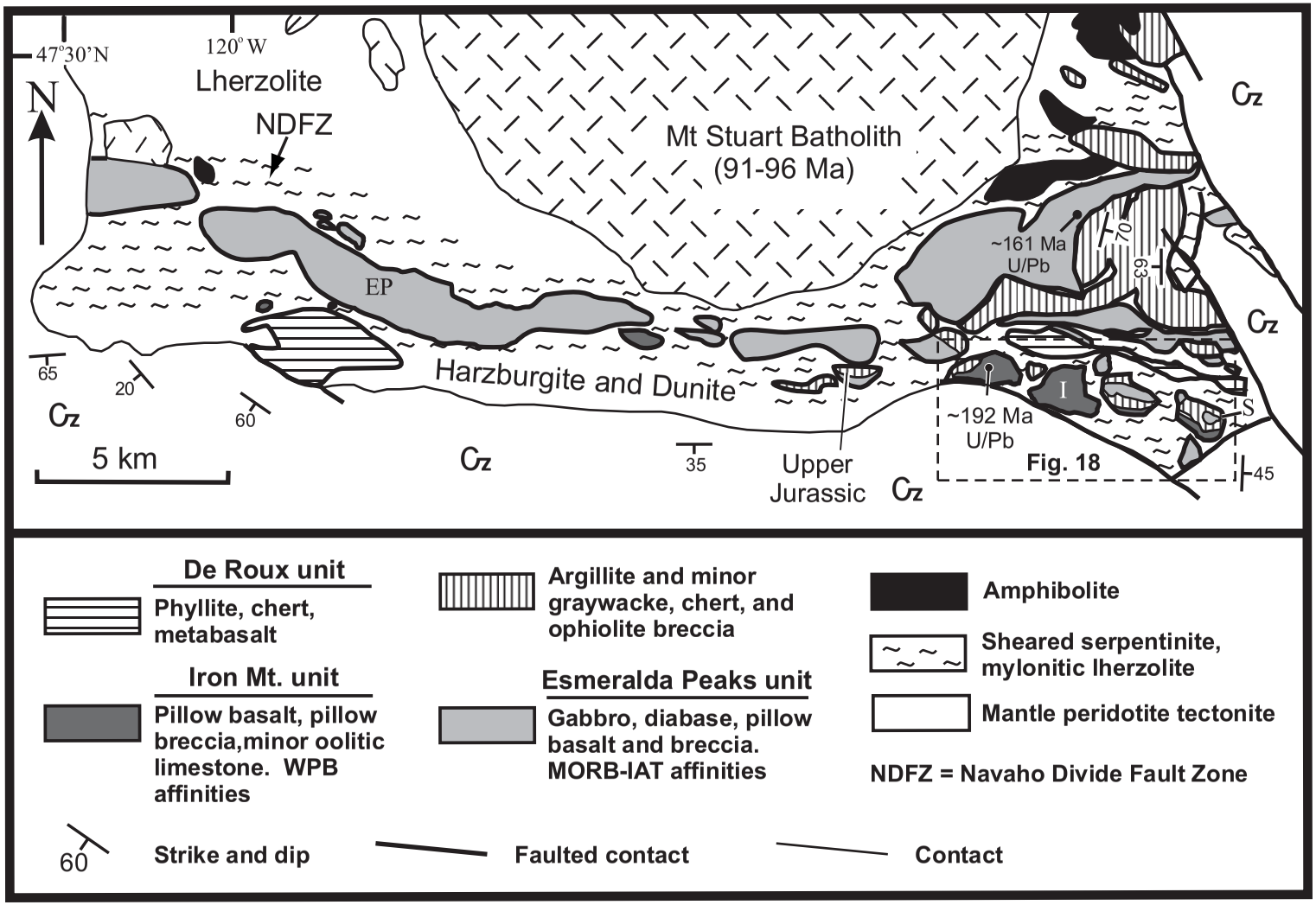
47°30'N
120° W
N
Lherzolite
NDFZ
Mt Stuart Batholith
(91-96 Ma)
Cz
~161 Ma
U/Pb
70
63
EP
65
20
60
Harzburgite and Dunite
Cz
5 km
Cz
35
Upper
Jurassic
Cz
I
S
~192 Ma
U/Pb
Fig. 18
45
De Roux unit
Phyllite, chert, metabasalt
Argillite and minor graywacke, chert, and ophiolite breccia
Amphibolite
Sheared serpentinite, mylonitic lherzolite
Iron Mt. unit
Pillow basalt, pillow breccia,minor oolitic limestone. WPB affinities
Esmeralda Peaks unit
Gabbro, diabase, pillow basalt and breccia. MORB-IAT affinities
Mantle peridotite tectonite
NDFZ = Navaho Divide Fault Zone
60
Strike and dip
Faulted contact
Contact

Figure 18. Geologic map of the southeastern part of the Ingalls Ophiolite Complex. Jurassic ages based on Radiolaria (Miller et al., 1993; C. Blome, personal communication, 1992; E. Pessagno, personal communication, 2002, 2004). Modified from Tabor and colleagues (1982, 1987, 1993, and 2000) and Harper et al. (2003).

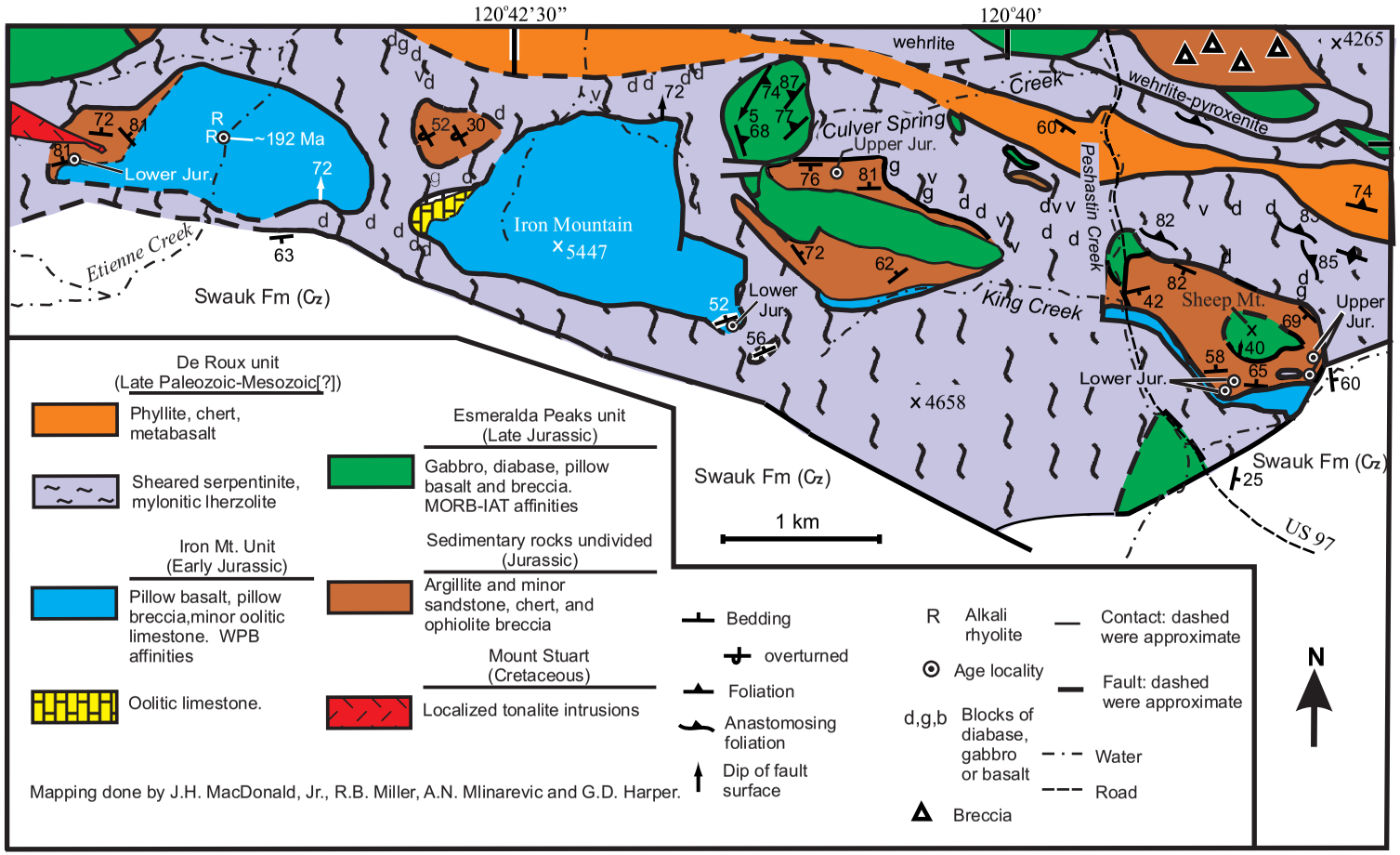
120°42'30"
120°40'
47°25'
wehrlite
wehrlite-pyroxenite
Creek
Culver Spring
Upper Jur.
Peshastin Creek
King Creek
Sheep Mt.
Upper Jur.
Lower Jur.
Iron Mountain
×5447
×4265
×4658
R
~192 Ma
Lower Jur.
Etienne Creek
Swauk Fm (Cz)
Swauk Fm (Cz)
Swauk Fm (Cz)
1 km
US 97
N
De Roux unit
(Late Paleozoic-Mesozoic[?])
Phyllite, chert, metabasalt
Sheared serpentinite, mylonitic lherzolite
Iron Mt. Unit
(Early Jurassic)
Pillow basalt, pillow breccia,minor oolitic limestone. WPB affinities
Oolitic limestone.
Esmeralda Peaks unit
(Late Jurassic)
Gabbro, diabase, pillow basalt and breccia. MORB-IAT affinities
Sedimentary rocks undivided
(Jurassic)
Argillite and minor sandstone, chert, and ophiolite breccia
Mount Stuart
(Cretaceous)
Localized tonalite intrusions
Bedding
overturned
Foliation
Anastomosing foliation
Dip of fault surface
R Alkali rhyolite
Age locality
d,g,b Blocks of diabase, gabbro or basalt
Breccia
Contact: dashed were approximate
Fault: dashed were approximate
Water
Road
Mapping done by J.H. MacDonald, Jr., R.B. Miller, A.N. Mlinarevic and G.D. Harper.

Figure 19. Stratigraphic section (synthesized from map; not measured) of Sheep Mountain, Iron Mountain, Negro creek and west of Negro creek. Radiolarian ages are from Miller et al. (1993), C. Blome (1992, personal communication) and E. Pessagno (1999, personal communication).

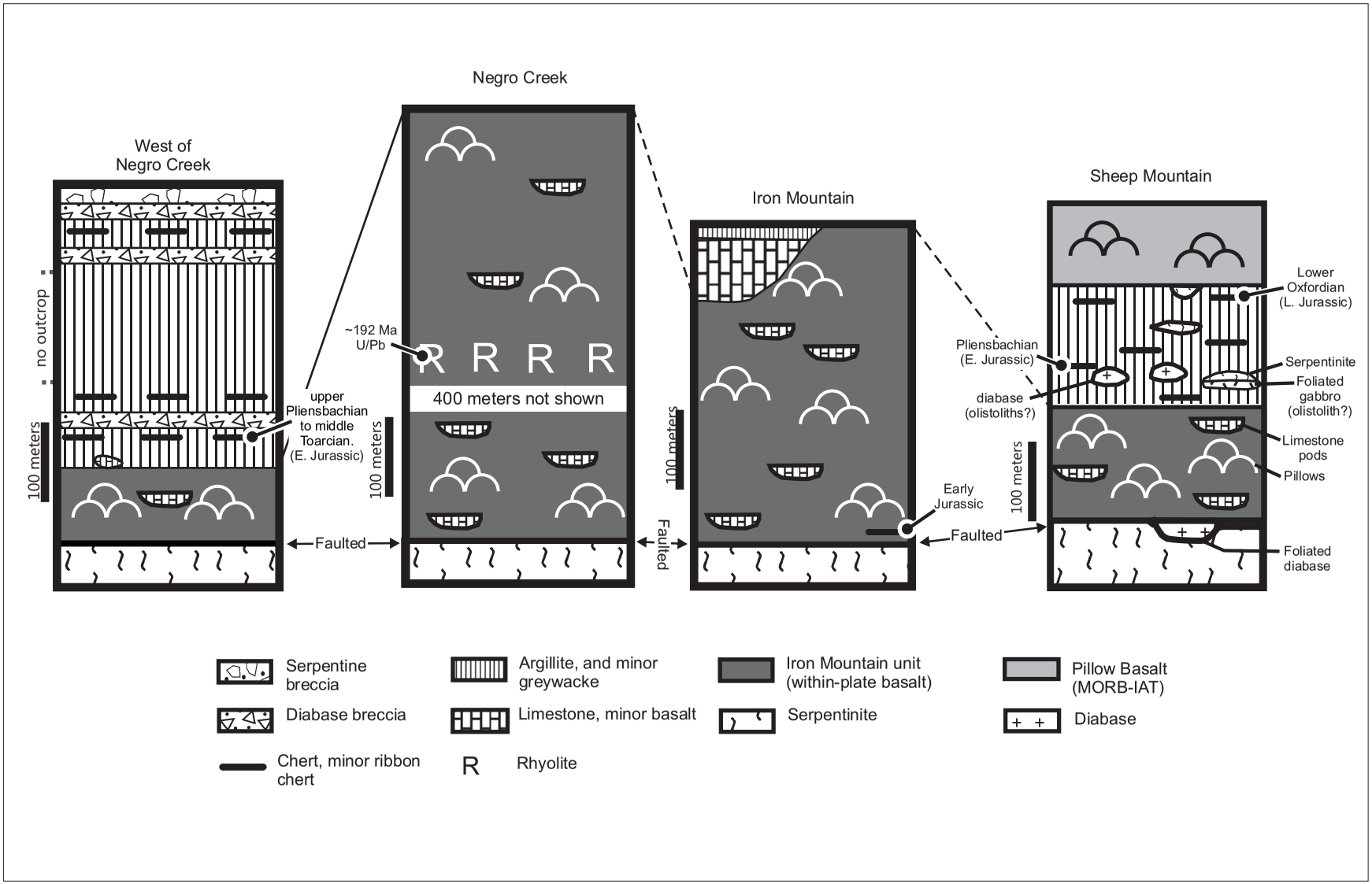
West of
Negro Creek
Negro Creek
Iron Mountain
Sheep Mountain
no outcrop
100 meters
upper
Pliensbachian
to middle
Toarcian.
(E. Jurassic)
~192 Ma
U/Pb
R R R R
400 meters not shown
100 meters
Faulted
Faulted
100 meters
Early
Jurassic
Faulted
Pliensbachian
(E. Jurassic)
diabase
(olistoliths?)
100 meters
Lower
Oxfordian
(L. Jurassic)
Serpentinite
Foliated
gabbro
(olistolith?)
Limestone
pods
Pillows
Foliated
diabase
Serpentine
breccia
Diabase breccia
Chert, minor ribbon
chert
Argillite, and minor
greywacke
Limestone, minor basalt
R
Rhyolite
Iron Mountain unit
(within-plate basalt)
Serpentinite
Pillow Basalt
(MORB-IAT)
Diabase

Figure 20. Chondrite-, MORB-normalized diagram. (A) Representative samples of different magma types including N-MORB, E-MORB, and WPB (Sun and McDonough, 1989), IAT (SSS5-4; Pearce et al., 1995), and within-plate granite (WPG; Pearce et al., 1984). Chondrite and MORB normalizing values are from Sun and McDonough (1989). (B) Ten basalt samples and one rhyolite from the Iron Mountain unit along with a shaded field for Esmeralda Peaks samples (boninite not plotted).

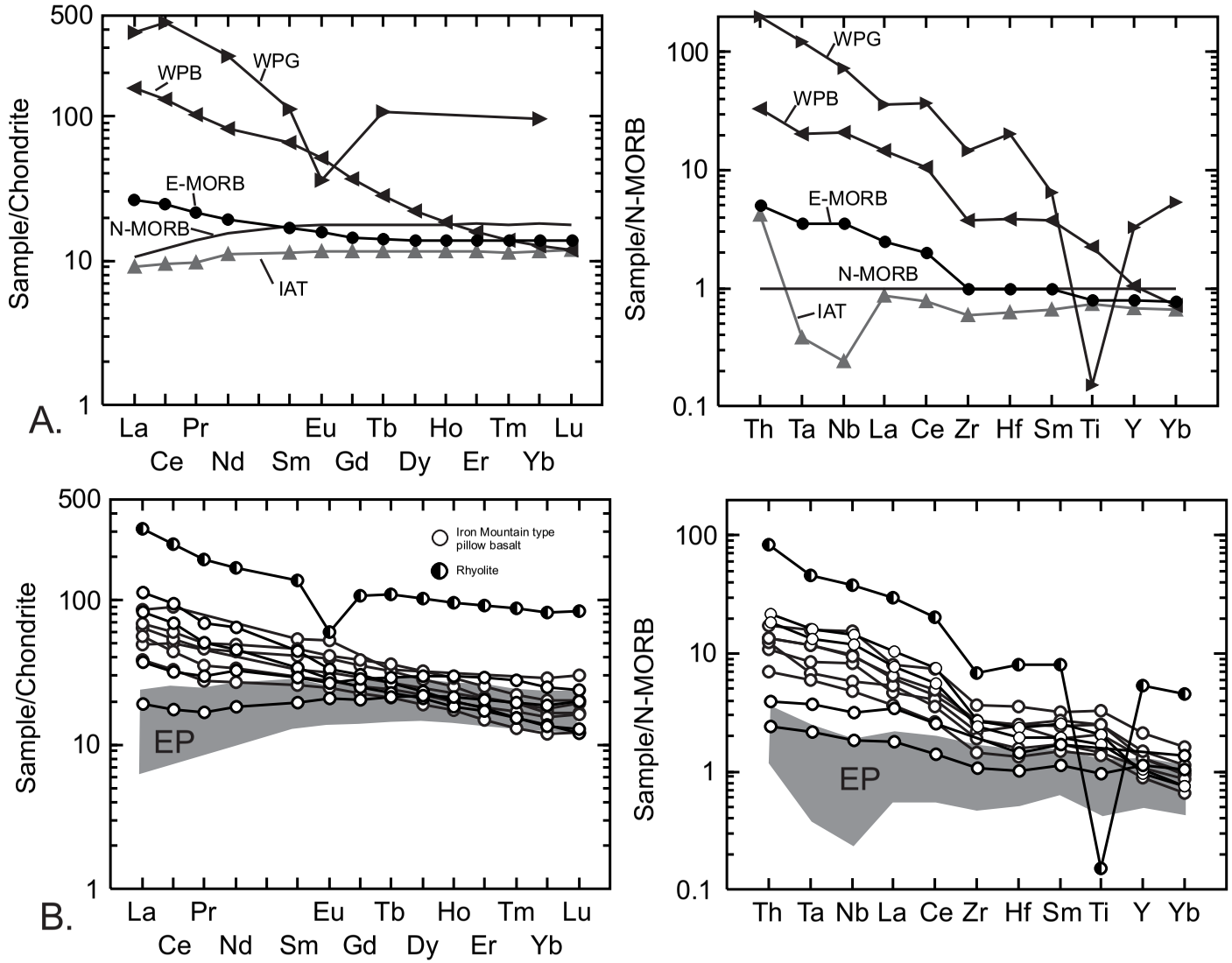
A.
Sample/Chondrite
500
100
10
1
WPB
WPG
E-MORB
N-MORB
IAT
La Pr Eu Tb Ho Tm Lu
Ce Nd Sm Gd Dy Er Yb
Sample/N-MORB
100
10
1
0.1
WPG
WPB
E-MORB
N-MORB
IAT
Th Ta Nb La Ce Zr Hf Sm Ti Y Yb
B.
Sample/Chondrite
500
100
10
1
Iron Mountain type pillow basalt
Rhyolite
EP
La Pr Eu Tb Ho Tm Lu
Ce Nd Sm Gd Dy Er Yb
Sample/N-MORB
100
10
1
0.1
EP
Th Ta Nb La Ce Zr Hf Sm Ti Y Yb

Figure 21. Th/Yb-Ta/Yb discriminant diagram (Pearce, 1982) for Iron Mountain basalts and rhyolite and a shaded field and a labeled boninite for the Esmeralda Peaks unit. N-MORB, E-MORB and WPB average values are from Sun and McDonough (1989). Within-plate granite (WPG) is from Pearce et al. (1984). Lau and Mariana back-arc basin field were compiled by Harper (2003). Symbols are the same as Figure 19.

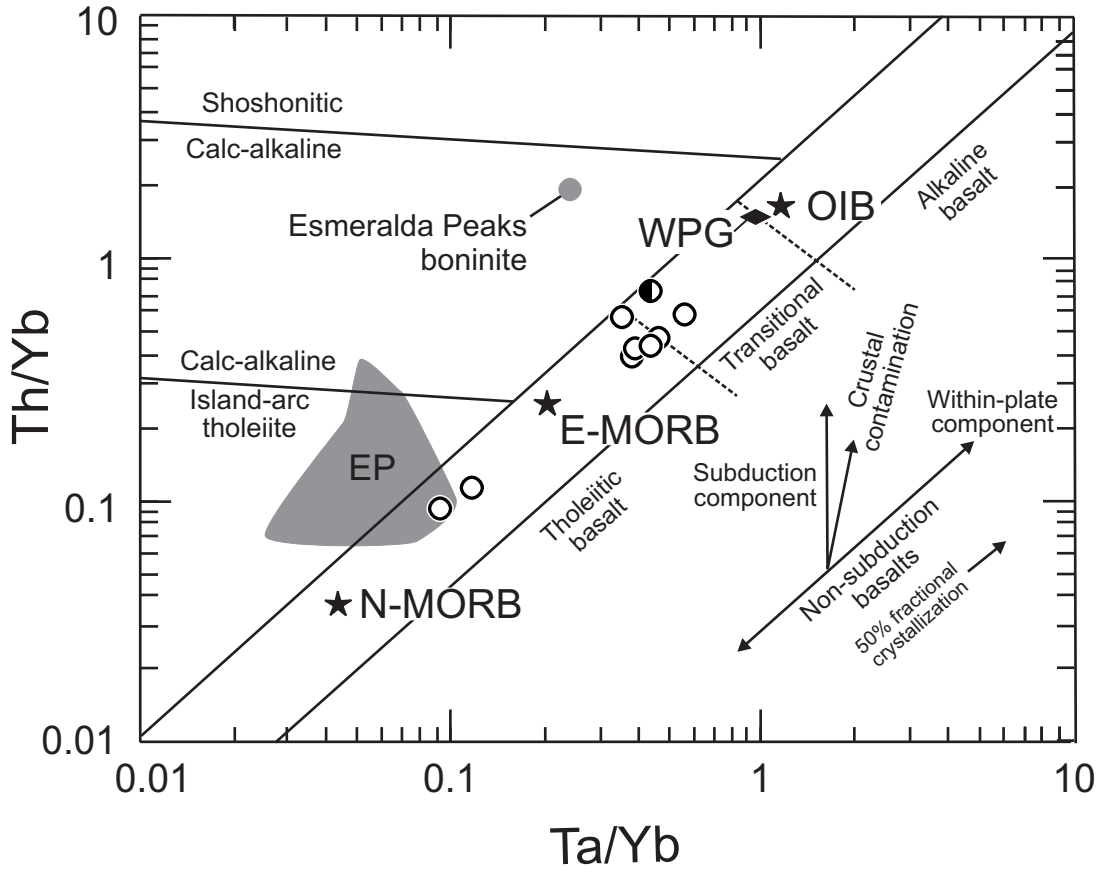
10
1
0.1
0.01
0.01
0.1
1
10
Th/Yb
Ta/Yb
Shoshonitic
Calc-alkaline
Esmeralda Peaks
boninite
WPG
OIB
Alkaline
basalt
Transitional
basalt
Crustal
contamination
Within-plate
component
Calc-alkaline
Island-arc
tholeiite
E-MORB
EP
Subduction
component
Tholeiitic
basalt
N-MORB
Non-subduction
basalts
50% fractional
crystallization

Figure 22. Photomicrograph of oolites in limestone within the Iron Mountain unit.

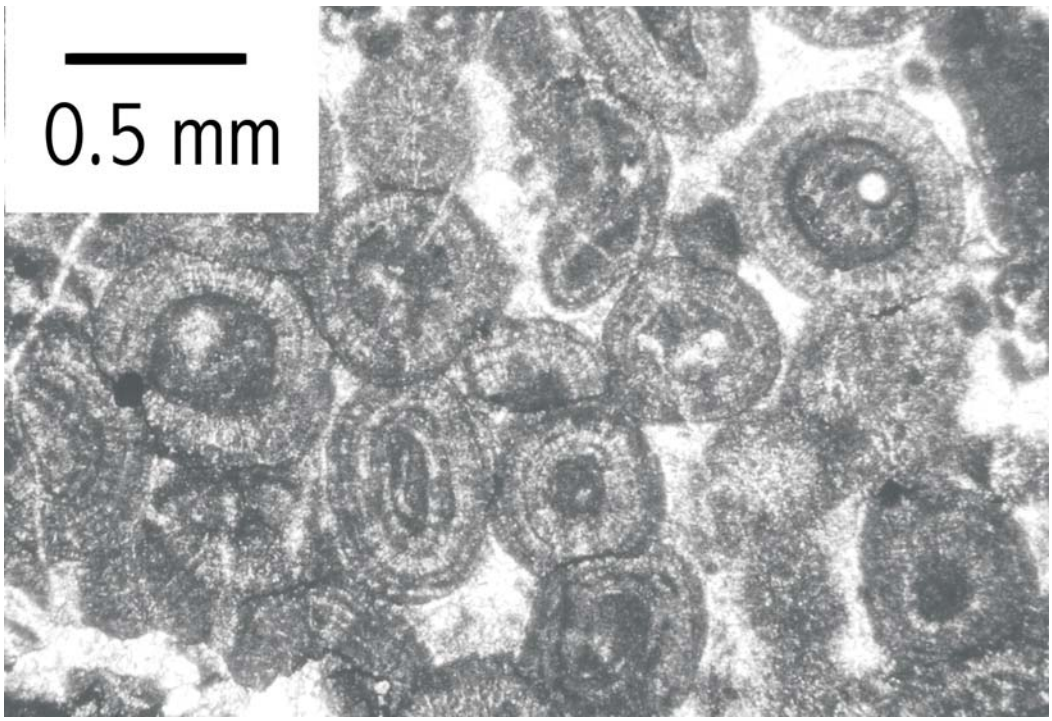
0.5 mm

Figure 23. Ti-Zr-Y discriminant diagram (Pearce and Cann, 1973) for basalts from the Iron Mountain unit along with a shaded field and a labeled boninite for the Esmeralda Peaks unit. Symbols are the same as Fig. 19.

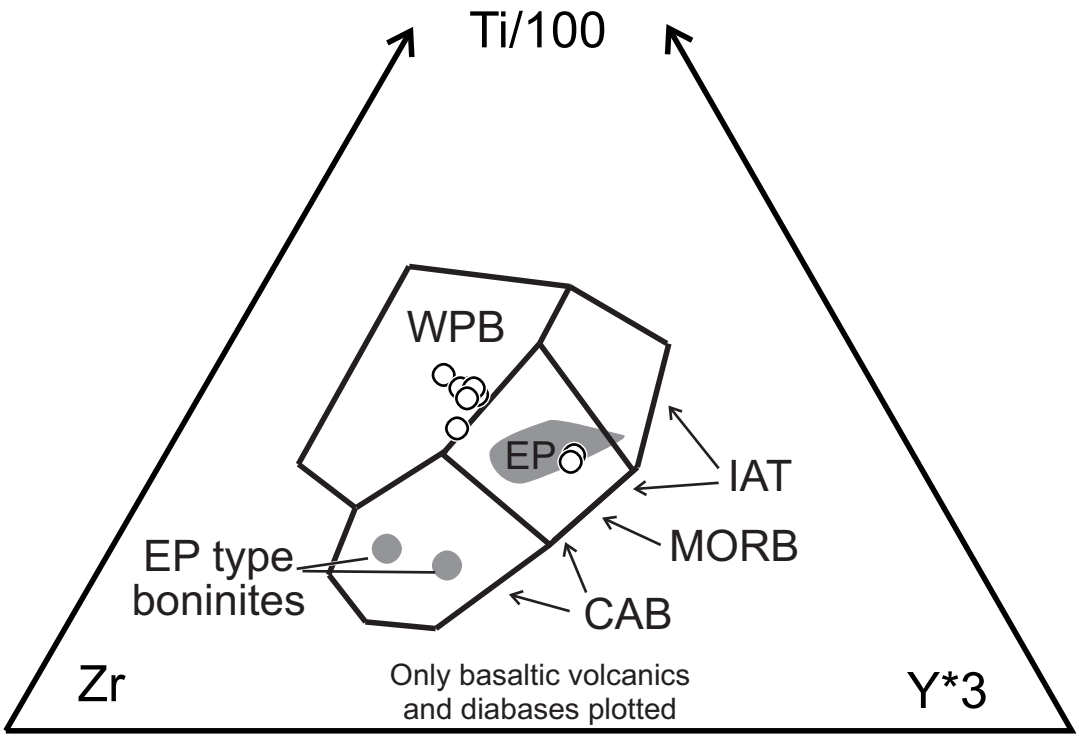
Ti/100
WPB
EP
IAT
MORB
CAB
EP type
boninites
Zr
Only basaltic volcanics
and diabases plotted
Y*3

Figure 24. Ti-V discriminant diagram (Shervais, 1982) for Iron Mountain basalts along with a shaded field for the Esmeralda Peaks unit. Only mafic rocks are shown. Calc-alkaline basalts are excluded because Ti-V changes with fractionation. The back-arc basin field was compiled by Harper et al. (2003) and the Hawaii field was compiled from the GEOROC geochemical database (http://georoc.mpch-mainz.gwdg.de/georoc/).

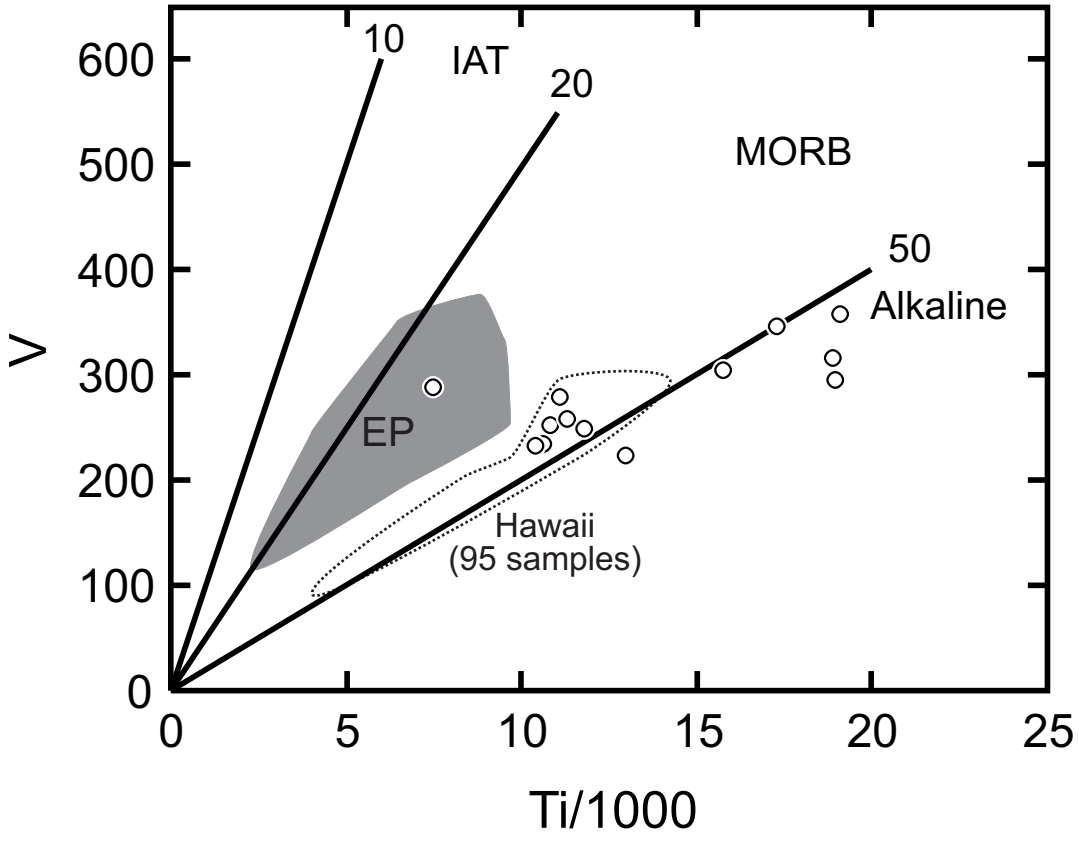
10
IAT
20
MORB
50
Alkaline
EP
Hawaii
(95 samples)
V
Ti/1000
600
500
400
300
200
100
0
0
5
10
15
20
25

Figure 25. Concordia diagram for a rhyolite (sample BL-150) from the Iron Mountain unit (see Table 4). Ellipses reflect 2-sigma error.

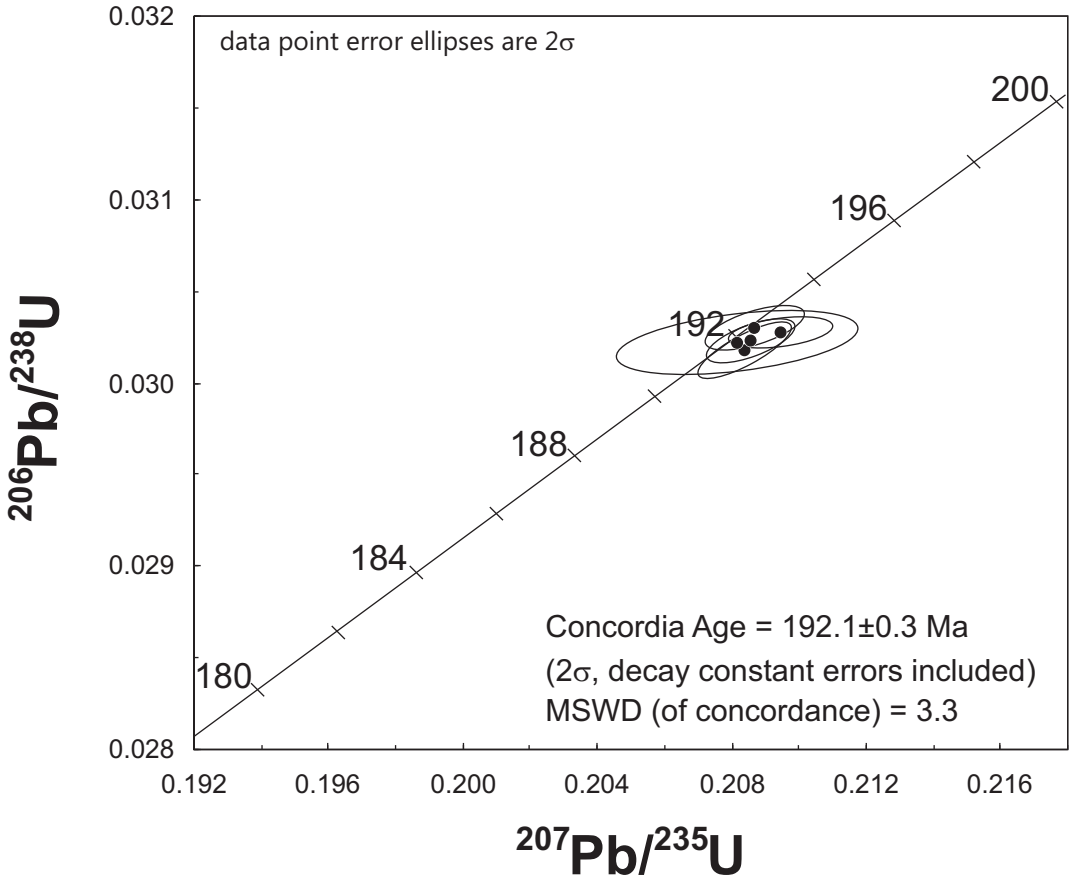
data point error ellipses are 2σ
200
196
192
188
184
180
Concordia Age = 192.1±0.3 Ma
(2σ, decay constant errors included)
MSWD (of concordance) = 3.3
0.032
0.031
0.030
0.029
0.028
0.192
0.196
0.200
0.204
0.208
0.212
0.216
206Pb/238U
207Pb/235U

Figure 26. Tectonic diagram for the Ingalls Ophiolite Complex. (A) Initial formation of the Iron Mountain unit as a seamount during the Early Jurassic. (B) Deposition of the Early Jurassic sediments. (C) Formation of the Esmeralda Peaks unit during the Late Jurassic by possible rifting of the older Iron Mountain unit. (D) Mélange formation that enclosed most units.

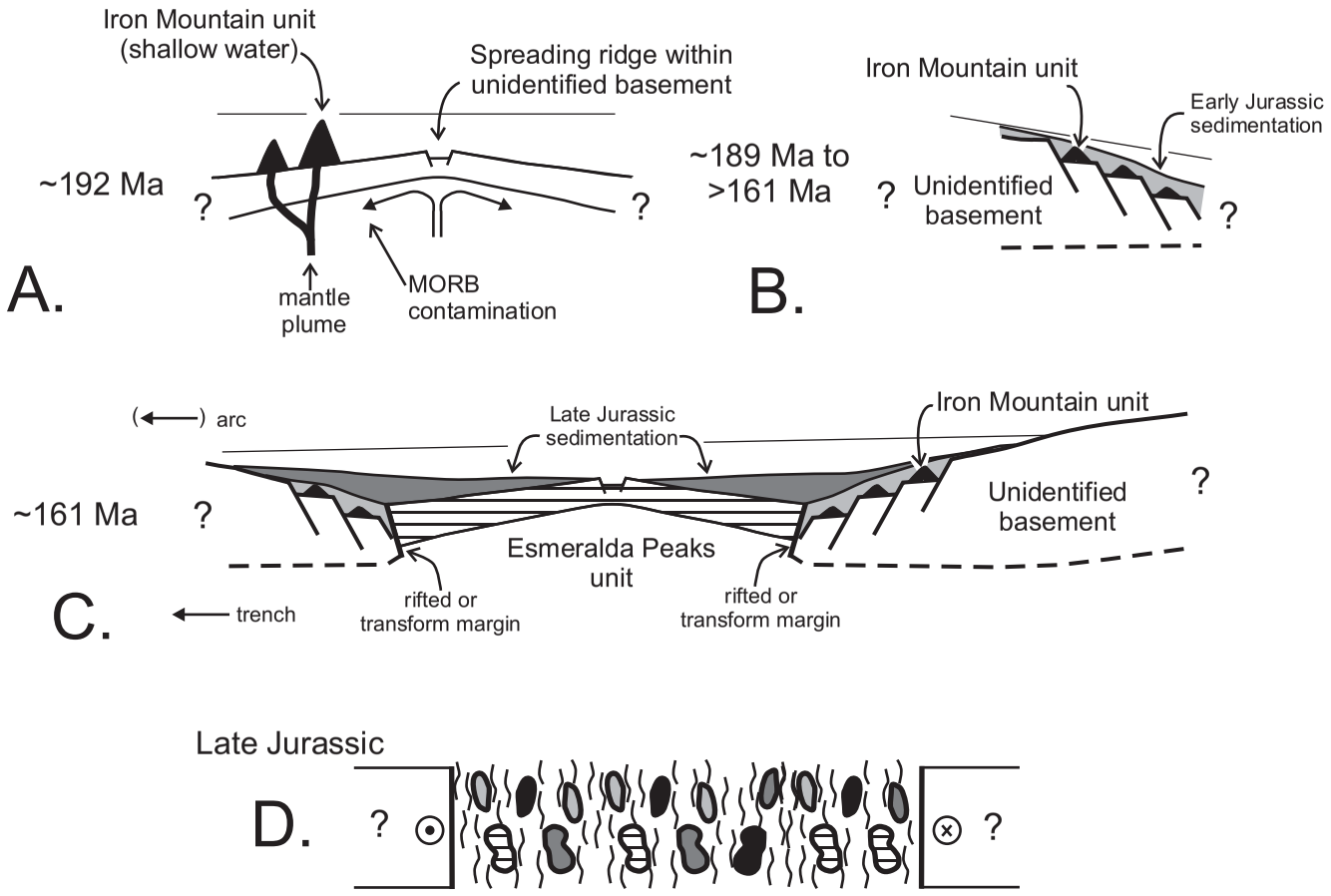
Iron Mountain unit
(shallow water)
Spreading ridge within
unidentified basement
~192 Ma
?
?
A.
mantle
plume
MORB
contamination
~189 Ma to
>161 Ma
Iron Mountain unit
Early Jurassic
sedimentation
?
Unidentified
basement
?
B.
(←) arc
Late Jurassic
sedimentation
Iron Mountain unit
~161 Ma
?
Unidentified
basement
?
Esmeralda Peaks
unit
C.
trench
rifted or
transform margin
rifted or
transform margin
Late Jurassic
D.
?
?

Figure 27. Location of the Middle to Late Jurassic North American Cordilleran ophiolites and the older Rattlesnake Creek terrane. Modified from Miller et al. (1993) and Metzger et al. (2002). Name of the Inlier containing the Late Jurassic arc complexes are, from north to south, Hicks Butte, Manastash and Rimrock Lake (Miller, 1989; Miller et al., 1993). JO-DEO = Devils Elbow ophiolite.

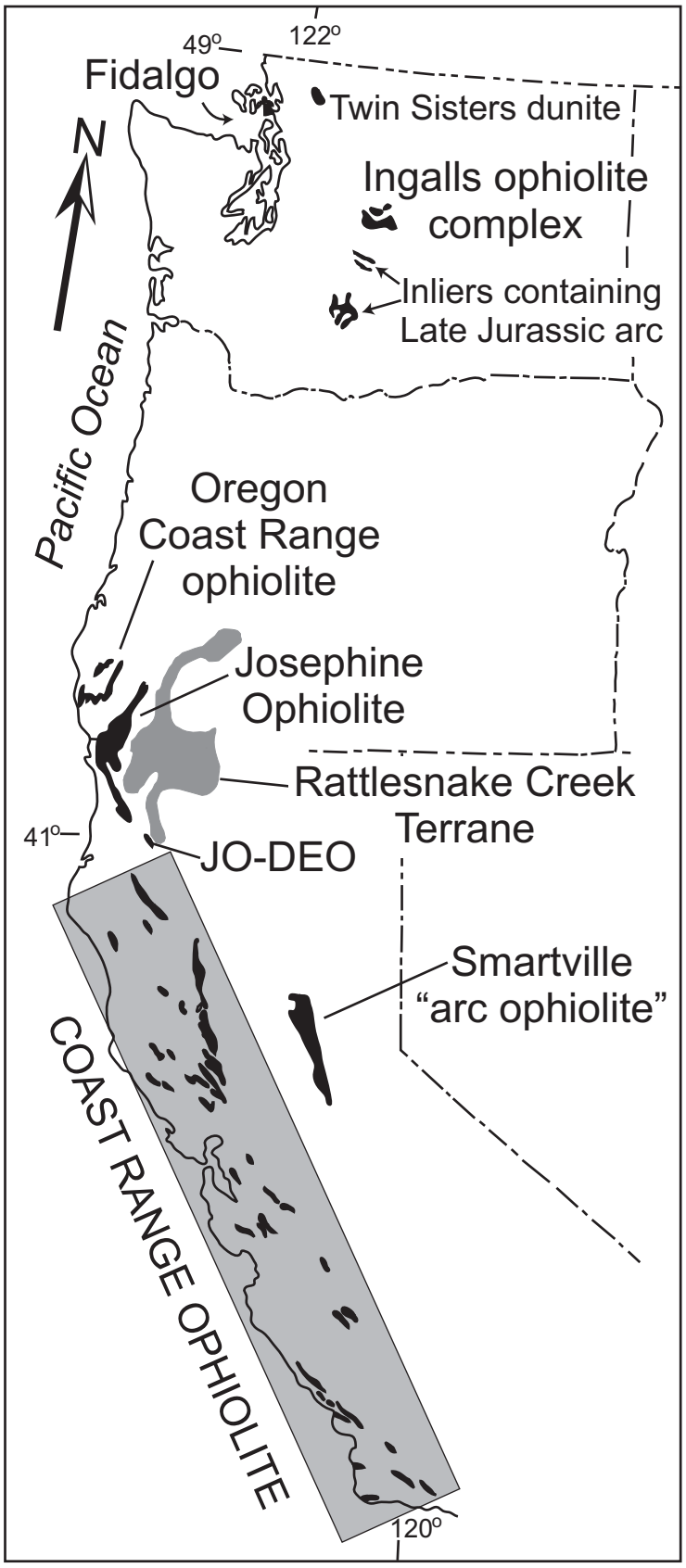
49°
122°
Fidalgo
Twin Sisters dunite
N
Ingalls ophiolite complex
Inliers containing Late Jurassic arc
Pacific Ocean
Oregon Coast Range ophiolite
Josephine Ophiolite
Rattlesnake Creek Terrane
41°
JO-DEO
Smartville "arc ophiolite"
COAST RANGE OPHIOLITE
120°

Figure 28. Map of the Ingalls ophiolite complex and surrounding units outlining major structures. Modified from Miller (1980) and Tabor and collaborators (1982, 1987, 1993, and 2000). CERFZ = Cle Elum Ridge fault zone; DPF = Deception Pass fault; LF = Leavenworth fault; NDFZ = Navaho Divide fault zone; WPT = Windy Pass thrust.

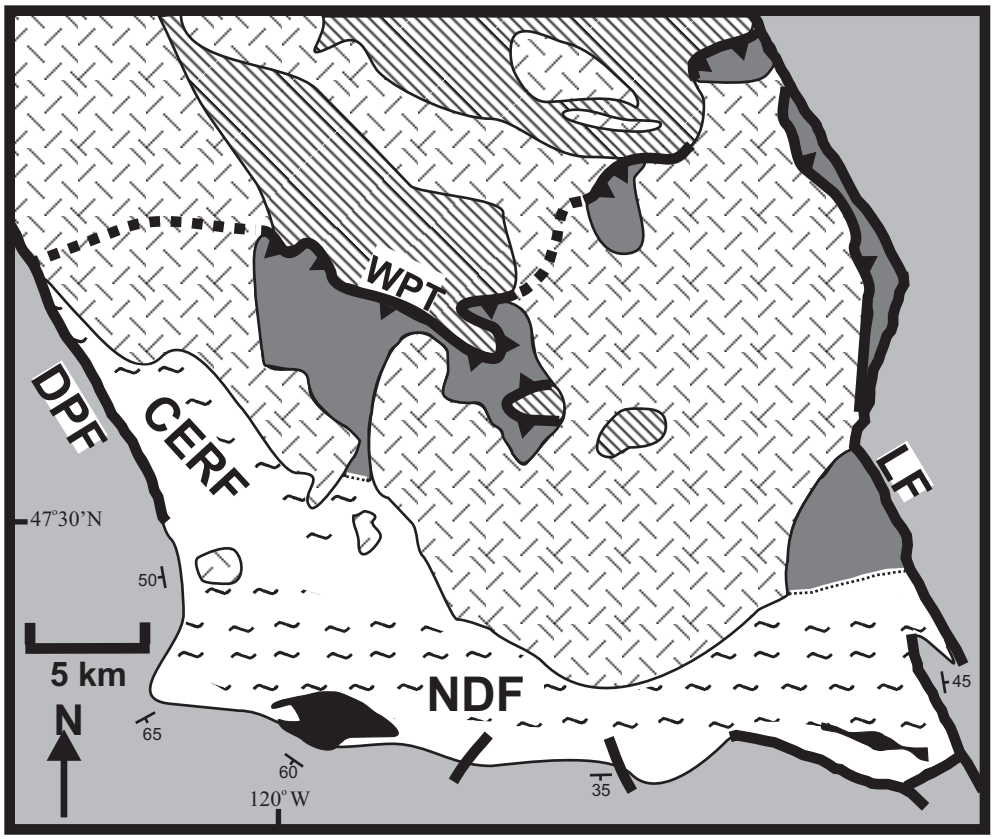

Swauk and Chumstick Formations (Eocene)

Mount Stuart batholith (Cretaceous (96.5-91

Ingalls Ophiolite Complex (Early to Late Jurassic)
Low-grade metamorphic facies

Ingalls Ophiolite Complex (Early to Late Jurassic)
Amphibolite facies metamorphism

Chiwaukum Schist (Late Jurassic (?))

De Roux Unit (Late Paleozoic-Mesozoic(?))

Figure 29. Map showing the mafic units of the Ingalls ophiolite complex and the unrelated De Roux unit. Modified from Tabor and collaborators (1982, 1987, 1993, and 2000) and Harper et al. (2003). EP = location of Esmeralda Peaks; I = location of Iron Mountain; S = location of Sheep Mountain.

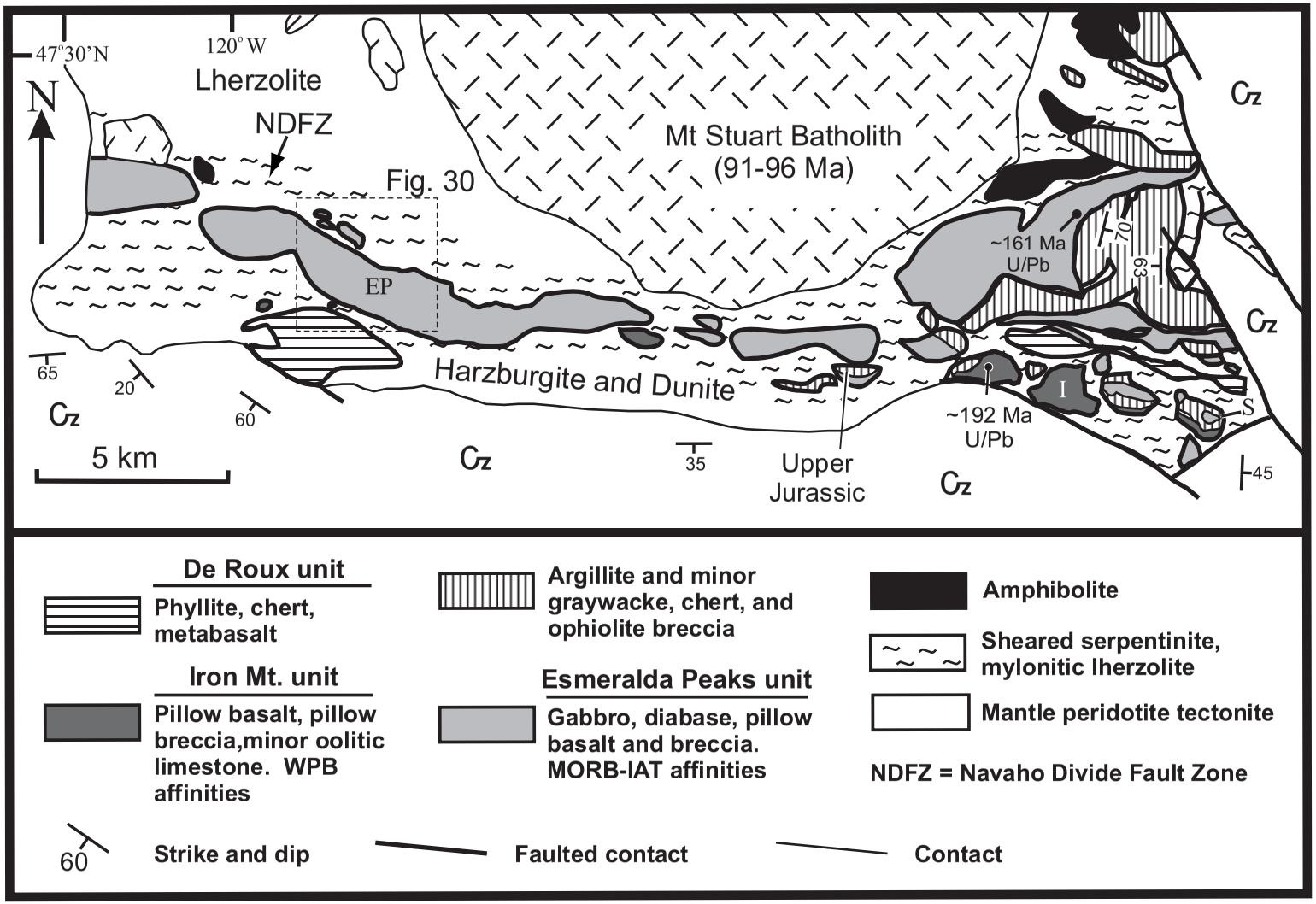
47°30'N
120° W
N
Lherzolite
NDFZ
Fig. 30
Mt Stuart Batholith
(91-96 Ma)
EP
~161 Ma
U/Pb
70
63
Cz
Harzburgite and Dunite
65
20
60
35
5 km
Cz
Cz
Upper
Jurassic
~192 Ma
U/Pb
I
S
45
De Roux unit
Phyllite, chert, metabasalt
Iron Mt. unit
Pillow basalt, pillow breccia,minor oolitic limestone. WPB affinities
Argillite and minor graywacke, chert, and ophiolite breccia
Esmeralda Peaks unit
Gabbro, diabase, pillow basalt and breccia. MORB-IAT affinities
Amphibolite
Sheared serpentinite, mylonitic lherzolite
Mantle peridotite tectonite
NDFZ = Navaho Divide Fault Zone
60
Strike and dip
Faulted contact
Contact

Figure 30. Geologic map of the Esmeralda Peaks and Longs Pass area of the Ingalls ophiolite complex. Mapping done by MacDonald, R. Miller and Harper. See Figure 29 for key and location.

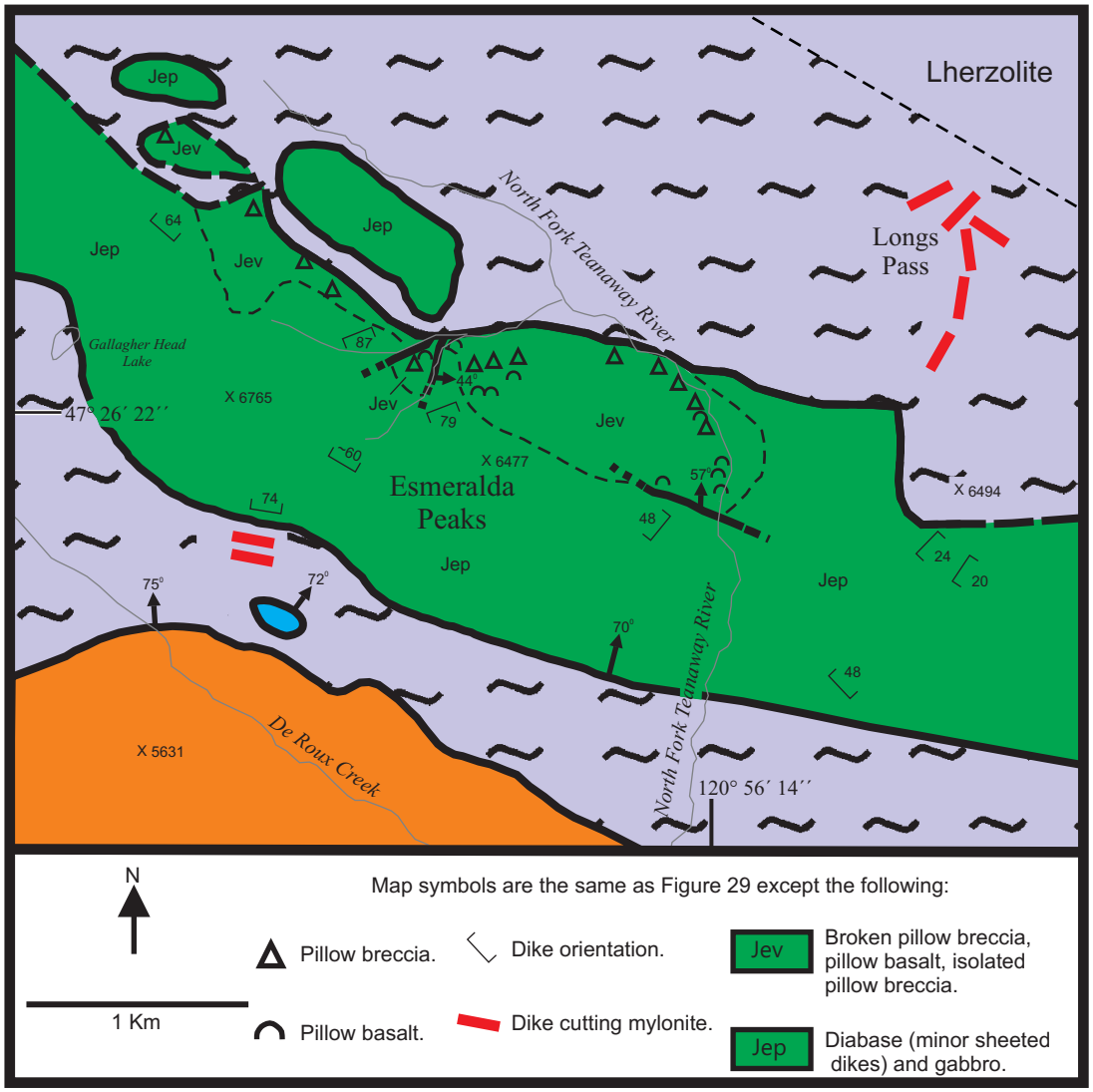
Lherzolite
Jep
Jev
Jep
Jep
Jev
64
North Fork Teanaway River
Longs
Pass
Gallagher Head
Lake
87
44°
X 6765
47° 26′ 22′′
Jev
79
Jev
60
X 6477
Esmeralda
Peaks
57°
X 6494
74
48
Jep
Jep
24
20
75°
72°
70°
48
De Roux Creek
X 5631
North Fork Teanaway River
120° 56′ 14′′
N
1 Km
Map symbols are the same as Figure 29 except the following:
Pillow breccia.
Pillow basalt.
Dike orientation.
Dike cutting mylonite.
Jev
Broken pillow breccia, pillow basalt, isolated pillow breccia.
Jep
Diabase (minor sheeted dikes) and gabbro.

Figure 31. Ti-V basalt discriminant diagram (Shervais, 1982) displaying mafic rocks from the Ingalls ophiolite complex that have basaltic compositions. Gabbros are excluded because many of them appear to be cumulates. Field for backarc basins is compiled by Metzger et al. (2002; references given in Fig. 6, p. 551) and Leat et al. (2000).

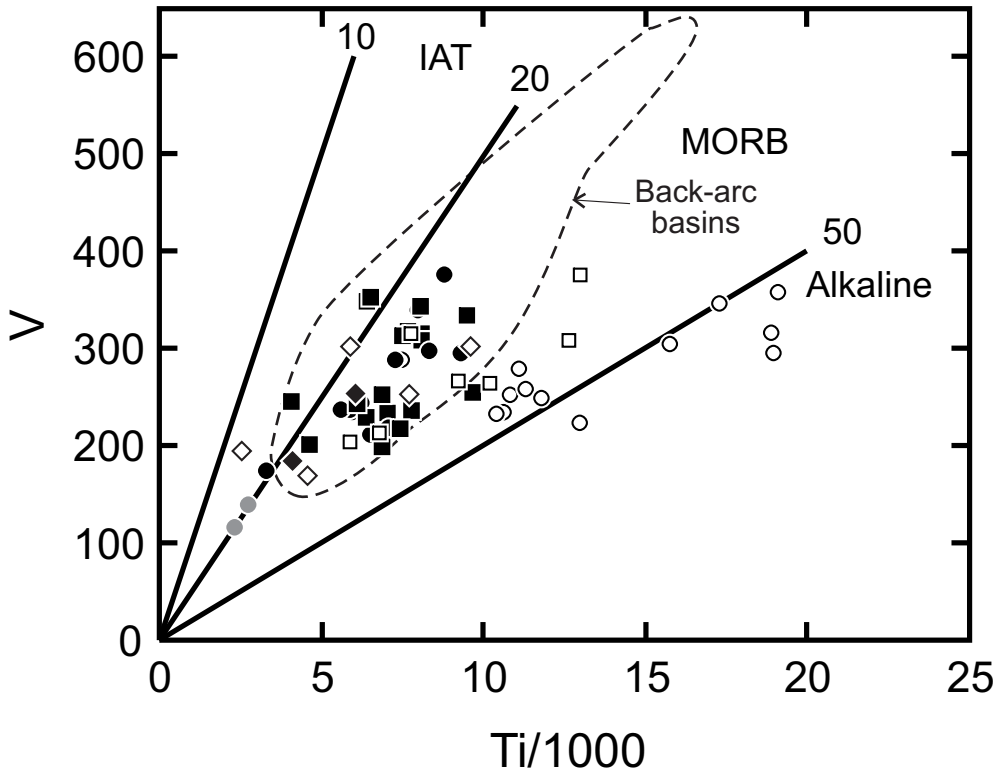

Esmeralda Peaks unit (Late Jurassic)		Iron Mountain unit (Early Jurassic)
● Boninite pillow basalt	□ Dike cutting mylonitic peridotite	○ Pillow basalt
● Pillow basalt	◆ Dike cutting amphibolite	
■ Diabase	◇ Amphibolite	

Figure 32. Th/Yb-Ta/Yb diagram from Pearce (1982) (see Fig. 31 for key to symbols). N-MORB, E-MORB and OIB normalizing values are from Sun and McDonough (1989). WPG = within-plate granite; from Harris (1983). Fields for Mariana, and Lau were compiled by Harper (2003a; Fig. 7, p. 219) and Scotia Sea is from Leat et al. (2000). Field for Hole 786 boninites is from Murton et al. (1992).

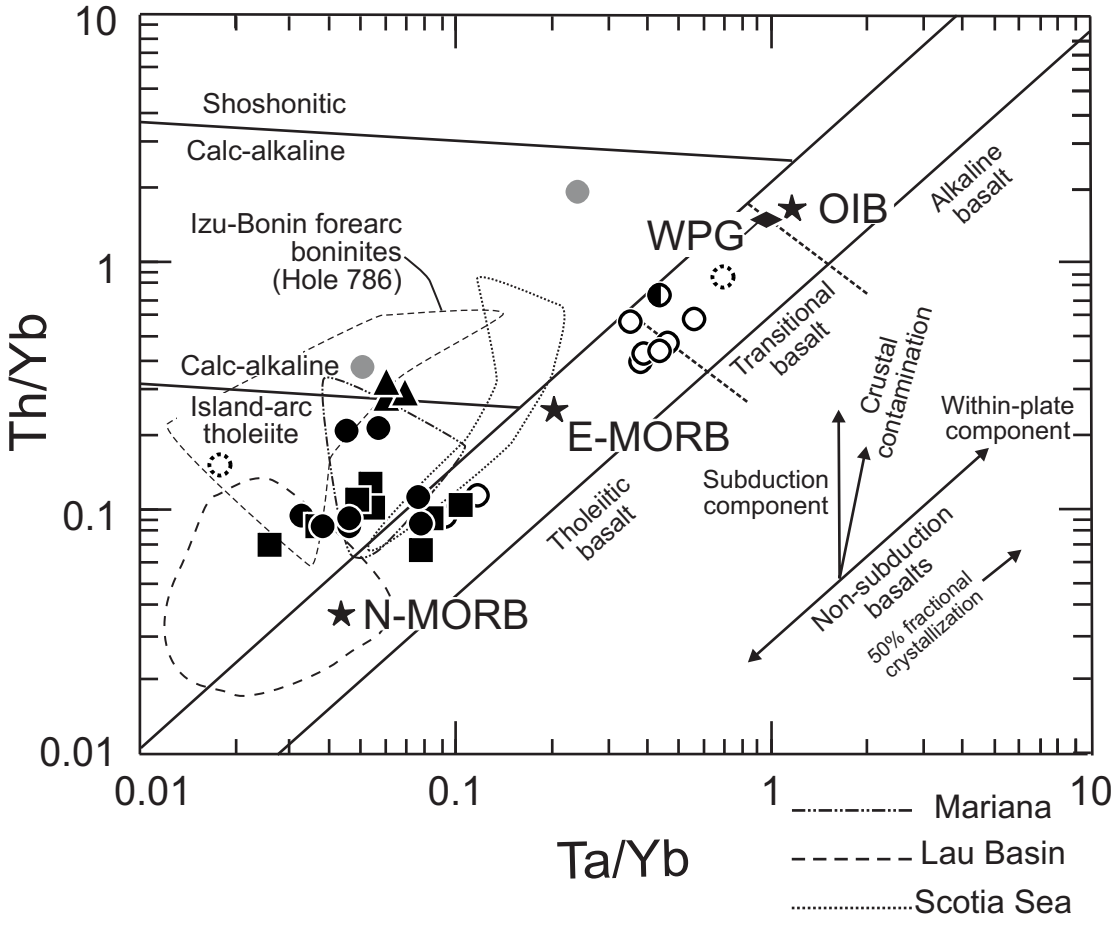
10
1
0.1
0.01
0.01
0.1
1
10
Th/Yb
Ta/Yb
Shoshonitic
Calc-alkaline
Izu-Bonin forearc
boninites
(Hole 786)
Calc-alkaline
Island-arc
tholeiite
WPG
OIB
Alkaline
basalt
Transitional
basalt
Crustal
contamination
Within-plate
component
E-MORB
Subduction
component
Tholeiitic
basalt
N-MORB
Non-subduction
basalts
50% fractional
crystallization
Mariana
Lau Basin
Scotia Sea

Figure 33. Chondrite- and N-MORB-normalized diagrams (see Fig. 31 for key to symbols). Chondrite and N-MORB normalized values are from Sun and McDonough (1989). Gabbros are not plotted due to their apparent cumulus geochemical affinities. A. Modern reference suite. OIG = WPG from Harris (1983); N-MORB, E-MORB, and OIB from Sun and McDonough (1989); IAT from Pearce et al. (1995); boninite from Pearce and Parkinson (1993). B. Iron Mountain unit basalts and rhyolite. C. Esmeralda Peaks unit basalts and diabase. D. Esmeralda Peaks unit felsic plutonic rocks (triangles) and boninites.

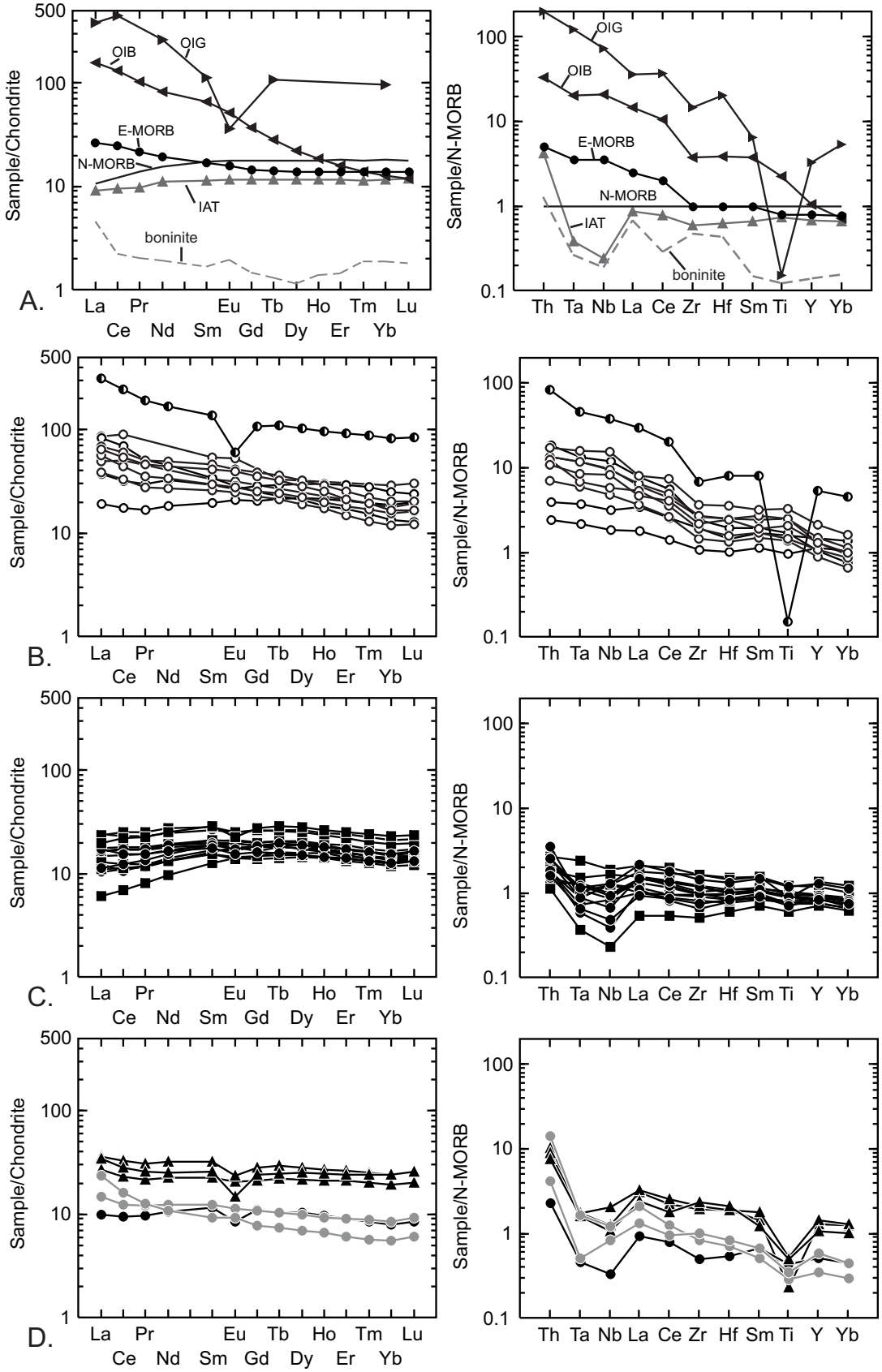
A.
B.
C.
D.
Sample/Chondrite
Sample/N-MORB
OIG
OIB
E-MORB
N-MORB
IAT
boninite
La Ce Pr Nd Sm Eu Gd Tb Dy Ho Er Tm Yb Lu
Th Ta Nb La Ce Zr Hf Sm Ti Y Yb

Figure 34. Cr-Y discriminant diagram (Pearce, 1982) (see Fig. 31 for key to symbols). Arrows A, B, and C represent crystallization paths for magmas fractionating Cr-spinel + olivine + pyroxene for MORB, IAT and boninites respectively. See Figure 31 and 32 for references to fields. Only basaltic compositions are plotted on the diagram and gabbros are excluded.

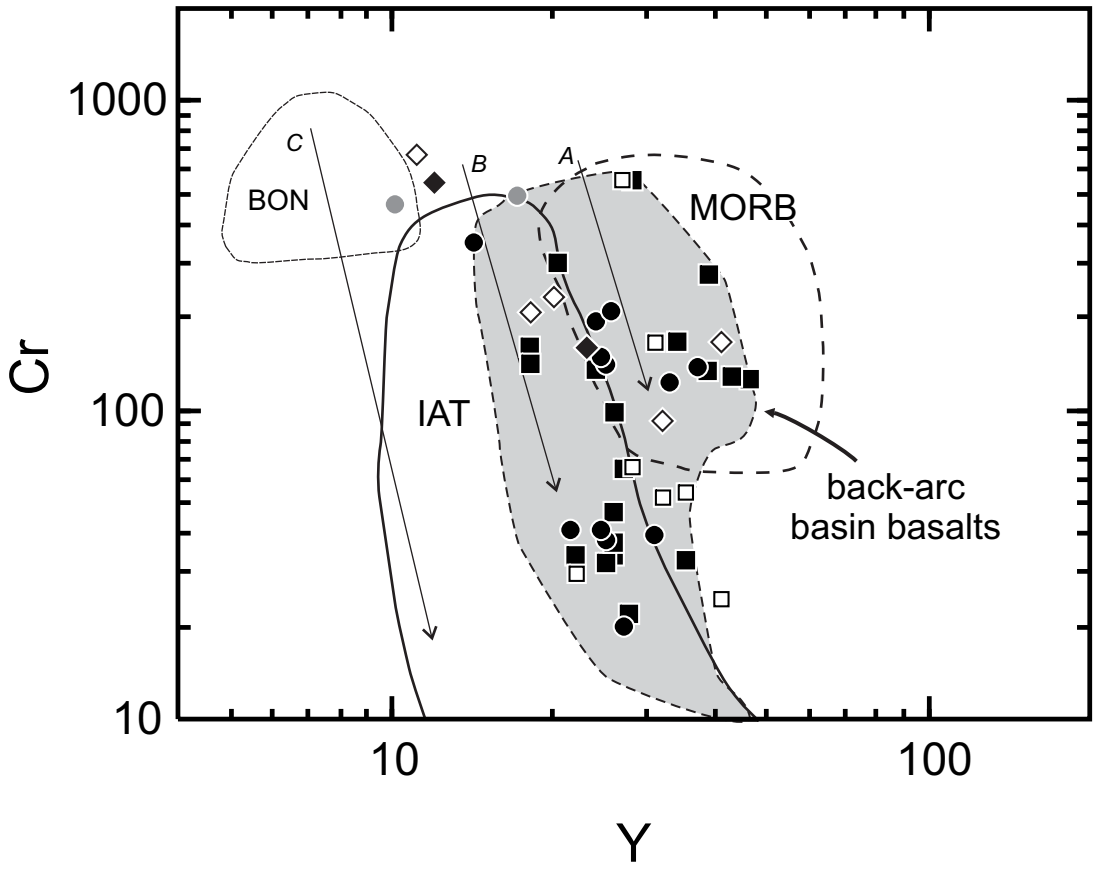
1000
100
10
Cr
10
100
Y
C
B
A
BON
IAT
MORB
back-arc
basin basalts

Figure 35. Cr-Yb diagram for melt and residue compositions (Pearce and Parkinson, 1995) (see Fig. 31 for key to symbols). Field for Hole 786 boninites is from Murton et al. (1992). Only basaltic composition Ingalls ophiolite samples are plotted and gabbros are excluded. FMM = fertile-MORB-mantle.

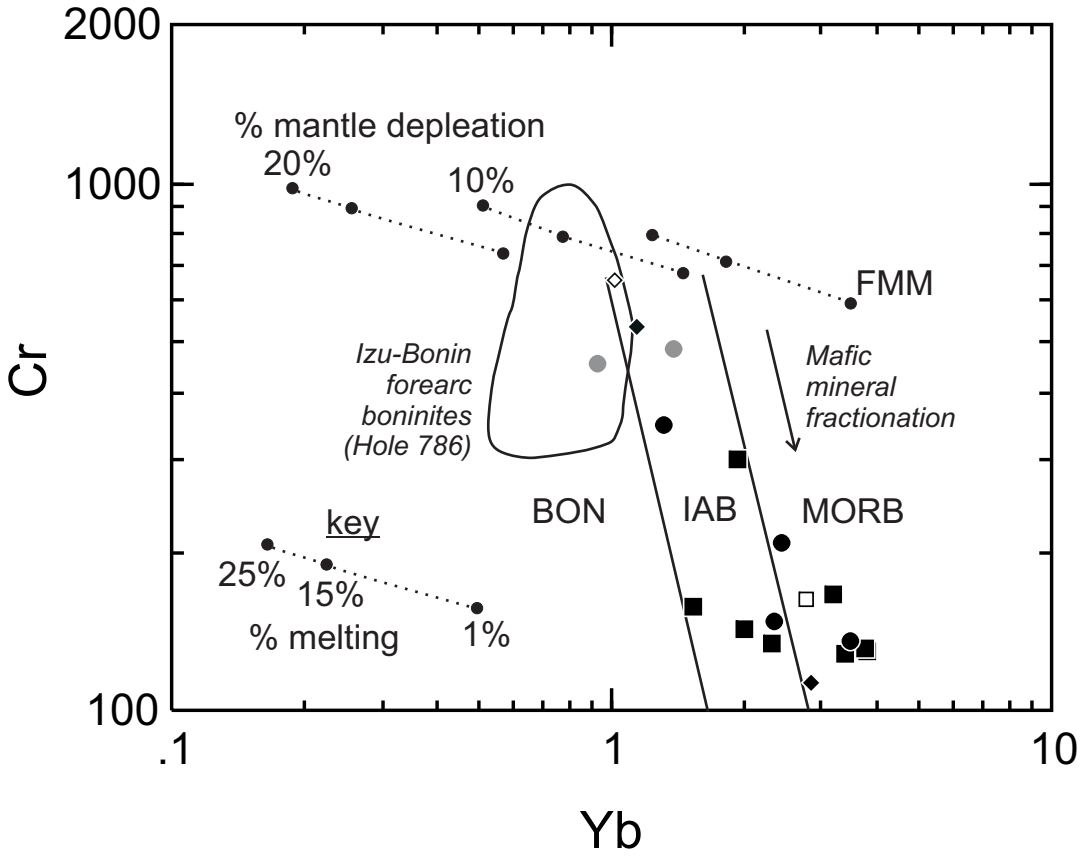
2000
1000
100
.1
1
10
Cr
Yb
% mantle depleation
20%
10%
FMM
Izu-Bonin
forearc
boninites
(Hole 786)
Mafic
mineral
fractionation
BON
IAB
MORB
key
25%
15%
% melting
1%

Figure 36. Fertile-MORB-mantle-normalized diagrams (Pearce and Parkinson, 1995) for Ingalls ophiolite complex mafic samples. Esmeralda Peaks unit basalts and diabases are shown as the shaded field. Hole 786 boninites are from Murton et al. (1992). A. Esmeralda Peaks boninites. B. Dikes that cut mylonitic peridotite and dikes that cut amphibolites. See Figure 31 for key to symbols.

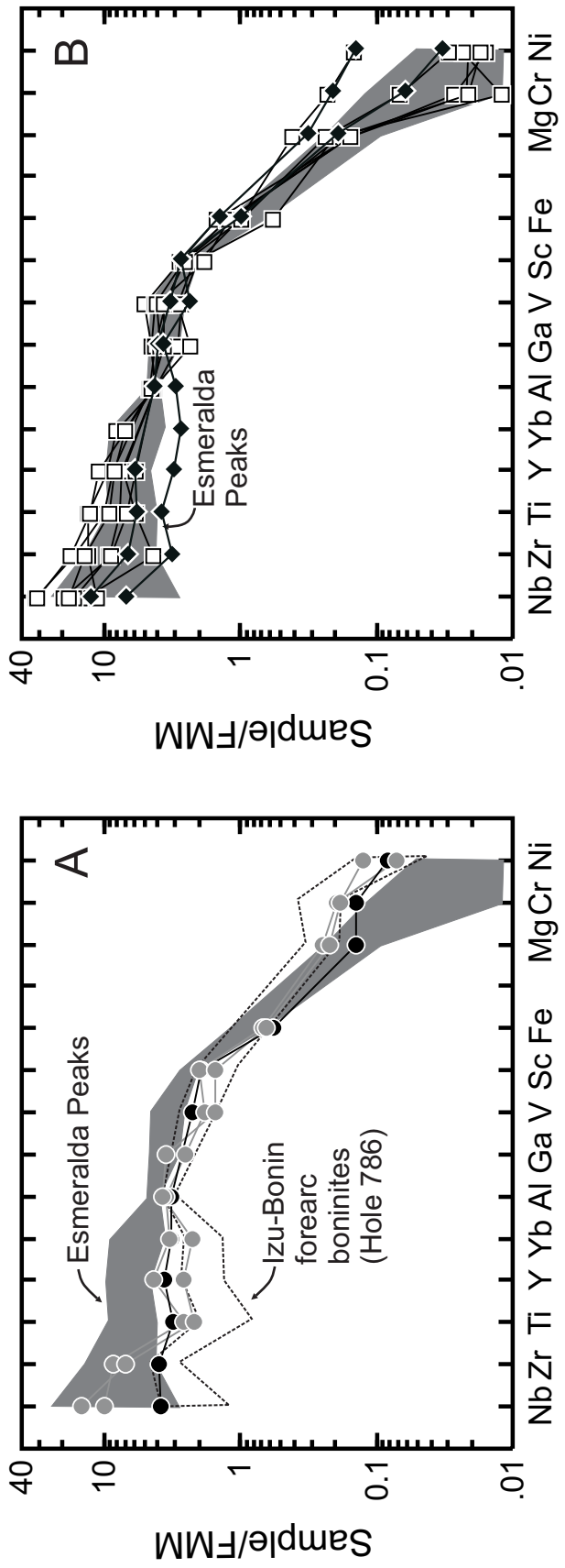
A
B
Esmeralda Peaks
Izu-Bonin forearc boninites (Hole 786)
Sample/FMM
40
10
1
0.1
.01
Nb Zr Ti Y Yb Al Ga V Sc Fe Mg Cr Ni

Figure 37. A. Dike, on right side of the sample, cutting an amphibolite that was originally a gabbro. B. Two small dikes, right one showing a propagating tip, cutting a foliated amphibolite from the same locality as in A.

B
dike
dike
Foliated Ambhibolite

A
dike
Ambhibolite

Figure 38. Tectonostratigraphy of the Ingalls ophiolite complex, Devils Elbow remnant of the Josephine ophiolite and underlying Rattlesnake Creek terrane (RCT), and the Josephine ophiolite. See text for discussion of fossil and U/Pb zircon ages and chemical affinities. Devils Elbow remnant and Josephine ophiolite modified from Harper et al. (1994) and Wright and Wyld (1994).

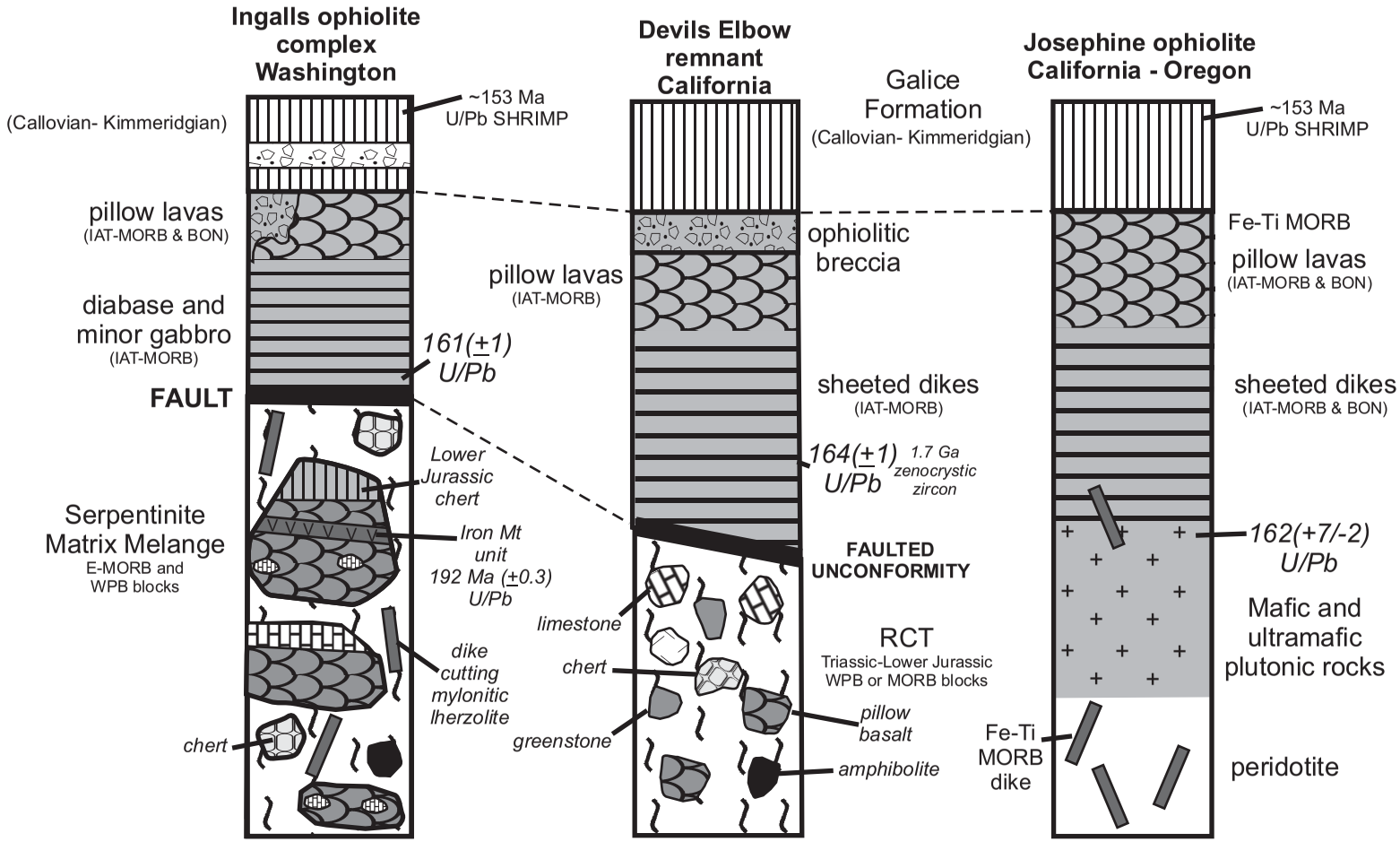
Ingalls ophiolite complex Washington
Devils Elbow remnant California
Galice Formation
(Callovian- Kimmeridgian)
Josephine ophiolite California - Oregon
(Callovian- Kimmeridgian)
~153 Ma U/Pb SHRIMP
~153 Ma U/Pb SHRIMP
pillow lavas
(IAT-MORB & BON)
diabase and minor gabbro
(IAT-MORB)
161(±1) U/Pb
FAULT
Serpentinite Matrix Melange
E-MORB and WPB blocks
Lower Jurassic chert
Iron Mt unit 192 Ma (±0.3) U/Pb
dike cutting mylonitic lherzolite
chert
pillow lavas
(IAT-MORB)
ophiolitic breccia
sheeted dikes
(IAT-MORB)
164(±1) U/Pb
1.7 Ga zenocrystic zircon
FAULTED UNCONFORMITY
limestone
chert
greenstone
RCT
Triassic-Lower Jurassic
WPB or MORB blocks
pillow basalt
amphibolite
Fe-Ti MORB
pillow lavas
(IAT-MORB & BON)
sheeted dikes
(IAT-MORB & BON)
162(+7/-2) U/Pb
Mafic and ultramafic plutonic rocks
Fe-Ti MORB dike
peridotite

Figure 39. Ta-Hf-Th discriminant diagram of Wood (1980). A. Ingalls ophiolite samples and field (see Fig. 31 for key to symbols) for backarc basins (see Fig. 31 for compilation). Esmeralda Peaks gabbros (sideways triangles) are plotted because fractionation and crystal accumulation does not significantly change the ratios of these elements. B. Rattlesnake Creek terrane (Wright and Wyld, 1994). C. Josephine ophiolite (references given in text). D. Coast Range ophiolite (references given in text).

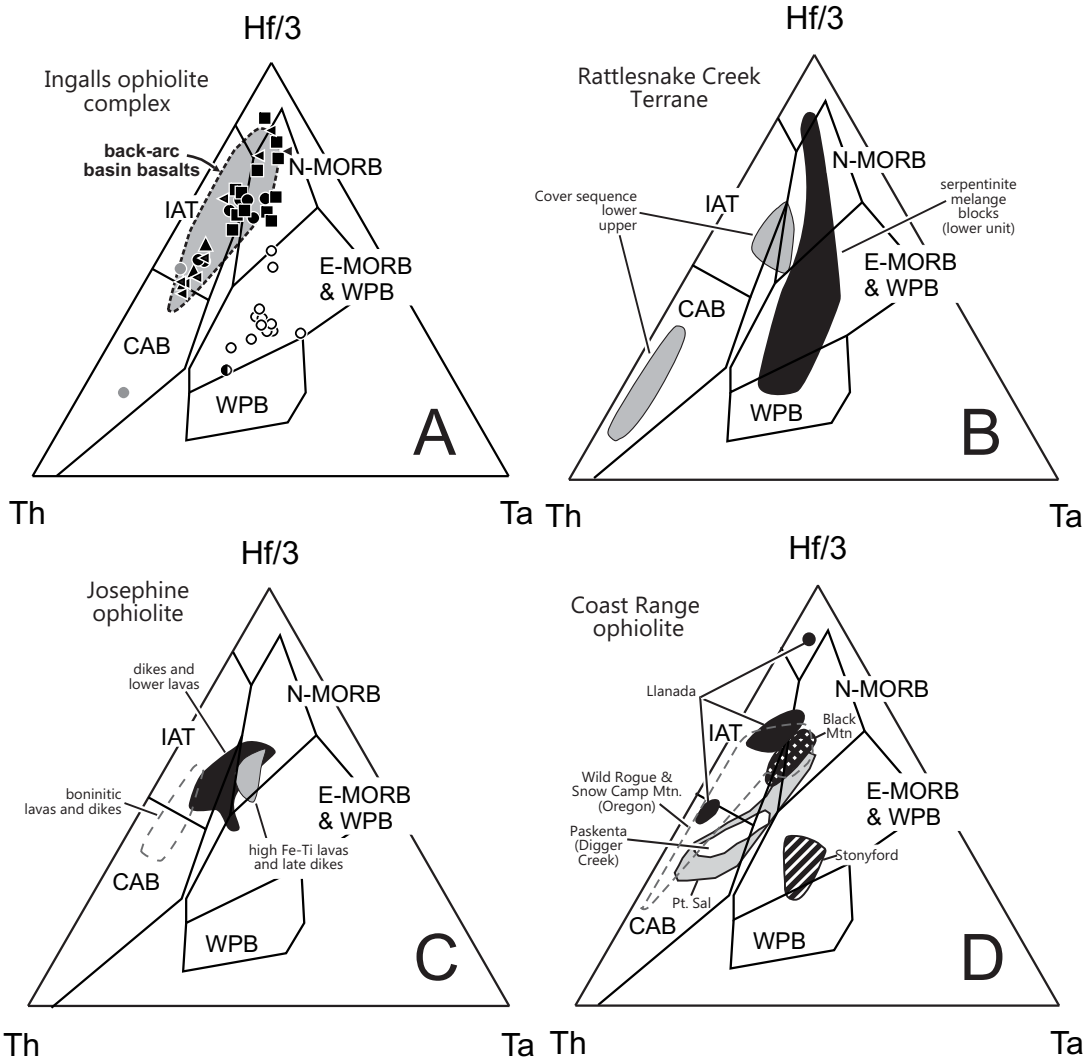
Hf/3
Ingalls ophiolite complex
back-arc basin basalts
N-MORB
IAT
E-MORB & WPB
CAB
WPB
A
Th
Ta
Hf/3
Rattlesnake Creek Terrane
Cover sequence
lower
upper
IAT
N-MORB
serpentinite melange blocks (lower unit)
E-MORB & WPB
CAB
WPB
B
Th
Ta
Hf/3
Josephine ophiolite
dikes and lower lavas
N-MORB
IAT
boninitic lavas and dikes
E-MORB & WPB
high Fe-Ti lavas and late dikes
CAB
WPB
C
Th
Ta
Hf/3
Coast Range ophiolite
Llanada
N-MORB
IAT
Black Mtn
Wild Rogue & Snow Camp Mtn. (Oregon)
E-MORB & WPB
Paskenta (Digger Creek)
Stonyford
Pt. Sal
CAB
WPB
D
Th
Ta

Figure 40. Map showing the Ingalls ophiolite complex, the De Roux unit, and surrounding geology. Inset map shows the position of the ophiolite within Washington state. Also shown on the map are the locations of the sedimentary serpentinite localities. Modified from Tabor and collaborators (1982, 1987, 1993, and 2000) and Harper et al. (2003). EP = location of Esmeralda Peaks; I = location of Iron Mountain; ND = Navaho Divide; S = location of Sheep Mountain.

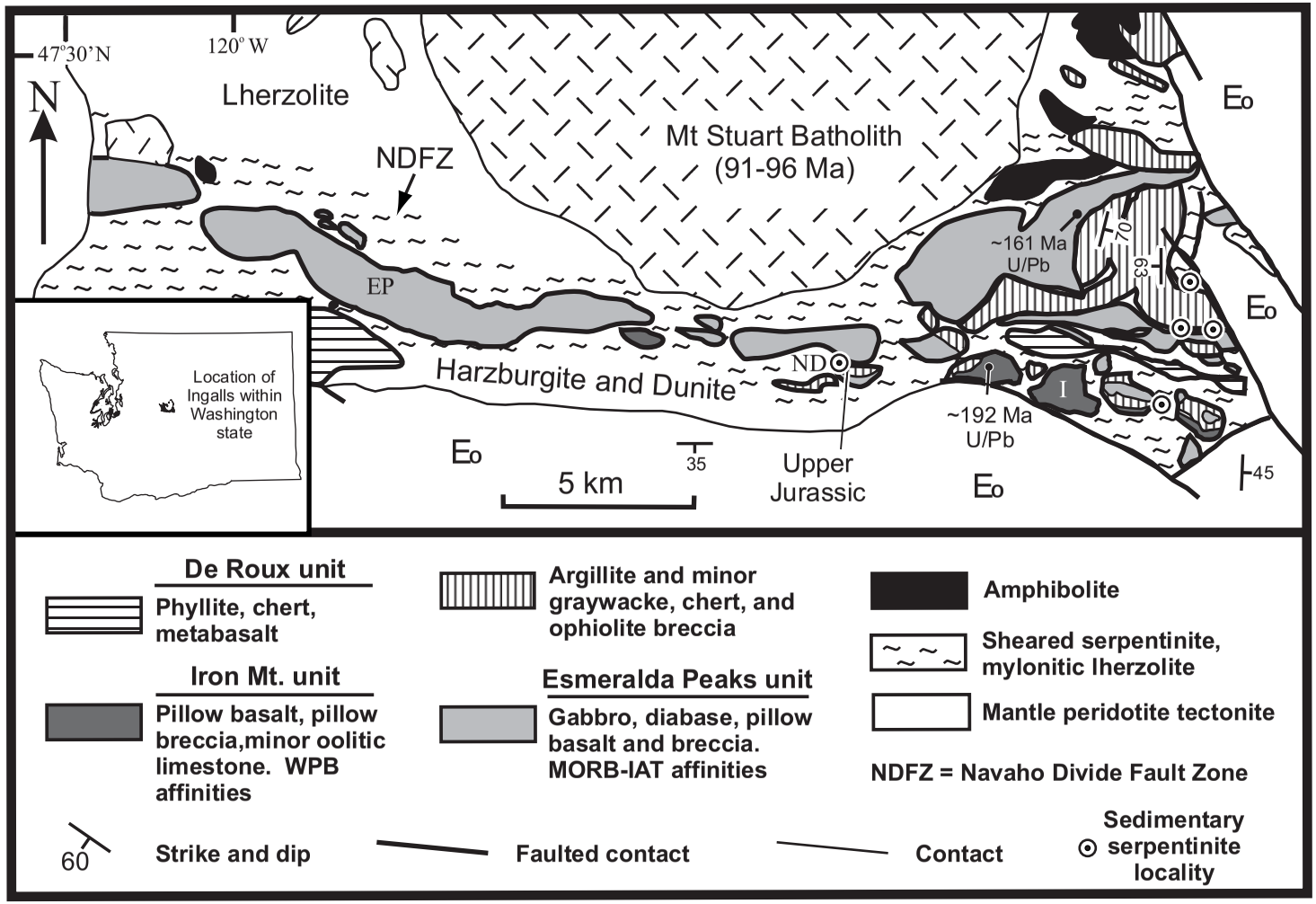
47°30'N
120° W
N
Lherzolite
NDFZ
Mt Stuart Batholith
(91-96 Ma)
Eo
~161 Ma
U/Pb
70
63
EP
Eo
Location of
Ingalls within
Washington
state
Harzburgite and Dunite
ND
I
~192 Ma
U/Pb
Eo
35
5 km
Upper
Jurassic
Eo
45
De Roux unit
Phyllite, chert,
metabasalt
Argillite and minor
graywacke, chert, and
ophiolite breccia
Amphibolite
Sheared serpentinite,
mylonitic lherzolite
Iron Mt. unit
Pillow basalt, pillow
breccia,minor oolitic
limestone. WPB
affinities
Esmeralda Peaks unit
Gabbro, diabase, pillow
basalt and breccia.
MORB-IAT affinities
Mantle peridotite tectonite
NDFZ = Navaho Divide Fault Zone
60
Strike and dip
Faulted contact
Contact
Sedimentary
serpentinite
locality

Figure 41. Cr/(Cr+Al) versus Mg/(Mg+Fe^{2+}) diagram for detrital Cr-spinels from three sedimentary serpentinites of the Ingalls ophiolite complex. See inset for symbol key. A. displaying fields for Cr-spinels from various magma types. Fields for SE Alaska intrusions and abyssal peridotites (MORB residue) from Dick and Bullen (1984); field for Hole 839 in the Lau Basin is from Allan (1994); field for low-Ca boninites is from Umino (1986); field for high-Ca boninites from Cameron (1985); and field for supra-subduction zone peridotite is modified from Parkinson and Pearce (1998). B. Plot for detrital Cr-spinels from Ingalls sedimentary serpentinites. Fields for Ingalls peridotite from Miller and Mogk (1987).

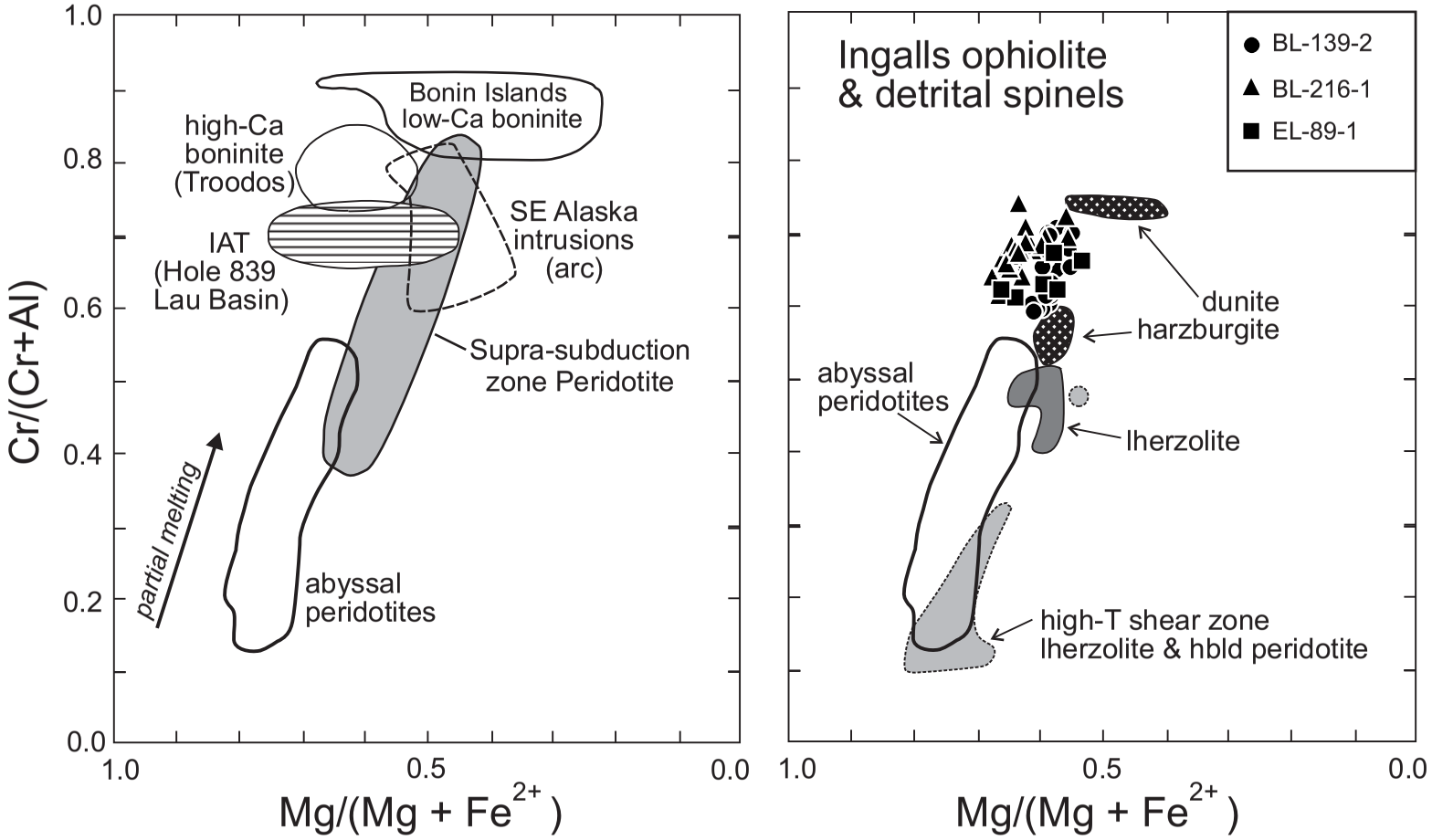
Cr/(Cr+Al)
1.0
0.8
0.6
0.4
0.2
0.0
1.0
0.5
0.0
Mg/(Mg + Fe2+)
Bonin Islands
low-Ca boninite
high-Ca
boninite
(Troodos)
IAT
(Hole 839
Lau Basin)
SE Alaska
intrusions
(arc)
Supra-subduction
zone Peridotite
partial melting
abyssal
peridotites
Ingalls ophiolite
& detrital spinels
BL-139-2
BL-216-1
EL-89-1
dunite
harzburgite
abyssal
peridotites
lherzolite
high-T shear zone
lherzolite & hbld peridotite

Figure 42. A. Gabbro block within argillite, interpreted as a huge olistolith (block in submarine landslide). B. Gabbro boulder in argillite, interpreted as an olistolith. Other smaller clasts of diabase and gabbro are located within this outcrop.

A.

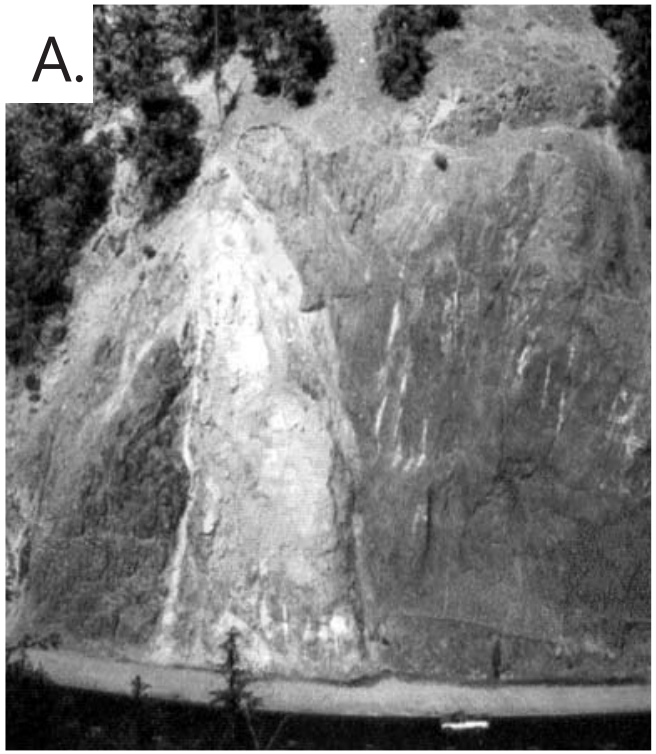

B.

Figure 43. A. Ti/V discriminant diagram (Shervais, 1982) for mafic clasts from the Ingalls ophiolitic breccias. Shaded field is for Esmeralda Peaks unit (Metzger et al., 2002; MacDonald et al., submitted). Only mafic rocks are shown, and gabbros are excluded, as many of them appear to be cumulates. Calc-alkaline basalts are not plotted because this diagram is not useful for distinguishing them (Ti/V changes with fractionation). B. Ta-Hf-Th discriminant diagram of Wood (1980) for all clasts from the Ingalls ophiolitic breccias, and a large gabbro olistolith (Fig. 3A; empty triangle). Shaded field is for Esmeralda Peaks samples (Metzger et al., 2002; MacDonald et al., submitted). All rock compositions are plotted on this diagram because fractionation and crystal accumulation does not significantly change the ratios of these elements.

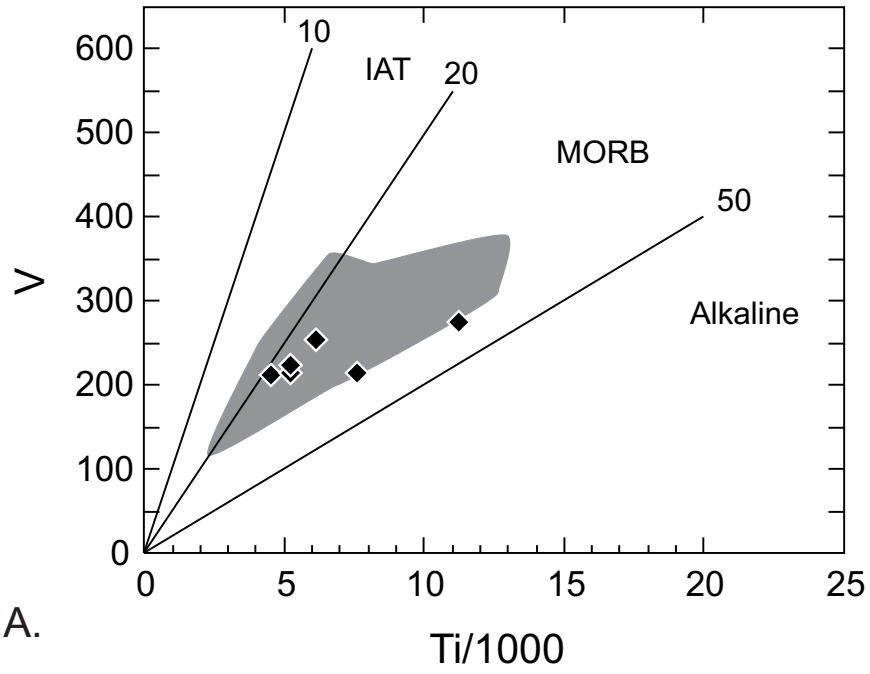
10
IAT
20
MORB
50
Alkaline
V
600
500
400
300
200
100
0
0
5
10
15
20
25
Ti/1000

A.

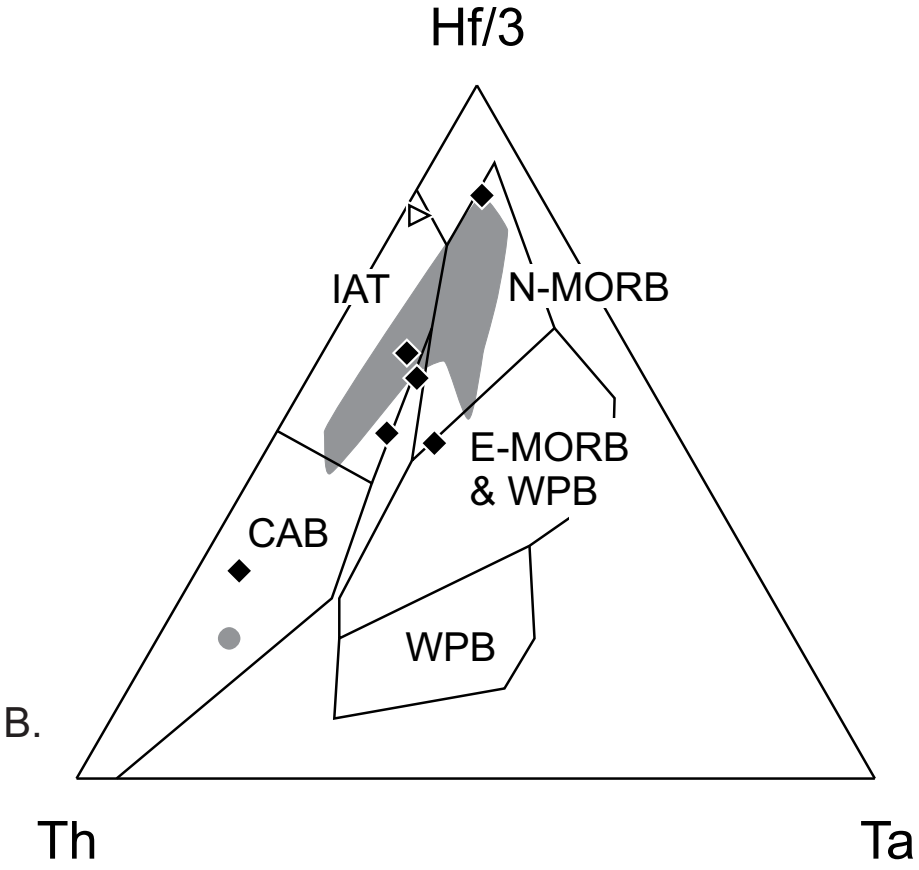
Hf/3
IAT
N-MORB
E-MORB
& WPB
CAB
WPB
Th
Ta

B.

Figure 44. A. Photomicrograph of poorly sorted sedimentary serpentinite (BL-139-1). Note angular to subangular clasts. B. Photomicrograph of a graded bed of sedimentary serpentinite (EL-89-1). Note angular clasts and grading.

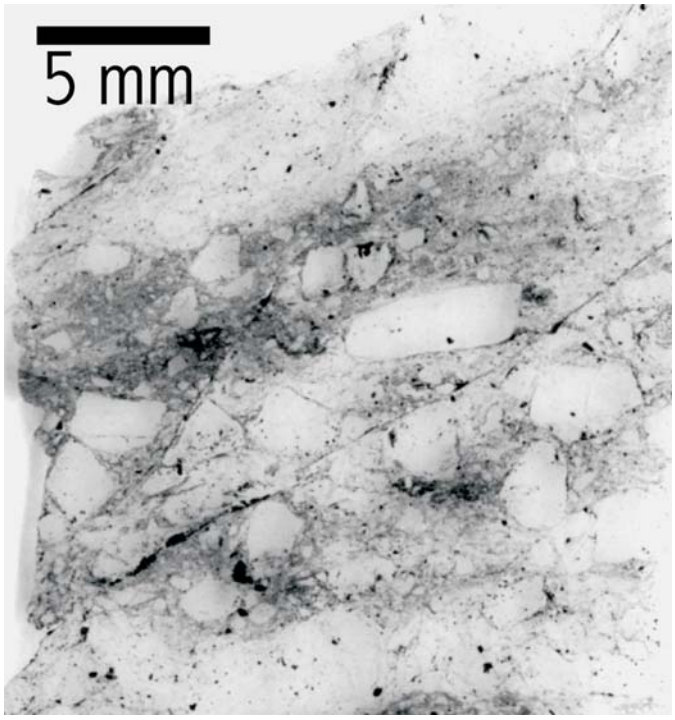

A.

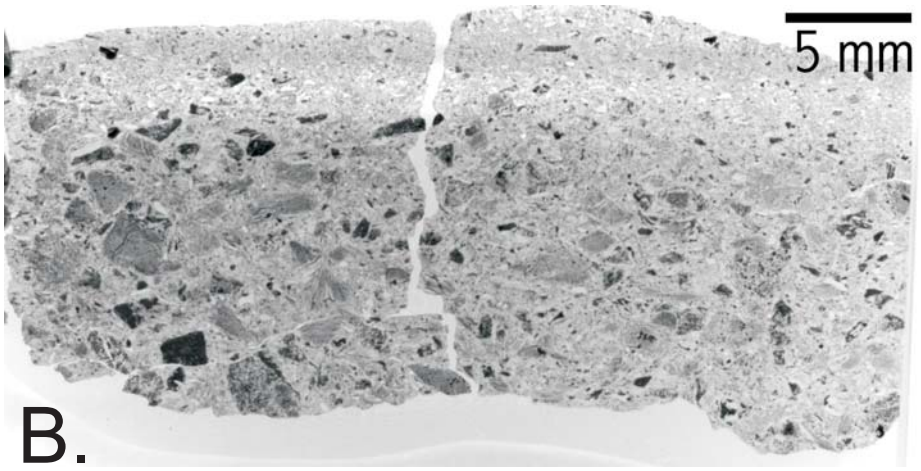

B.

Figure 45. Photo of sedimentary serpentinite (sample EL-216).

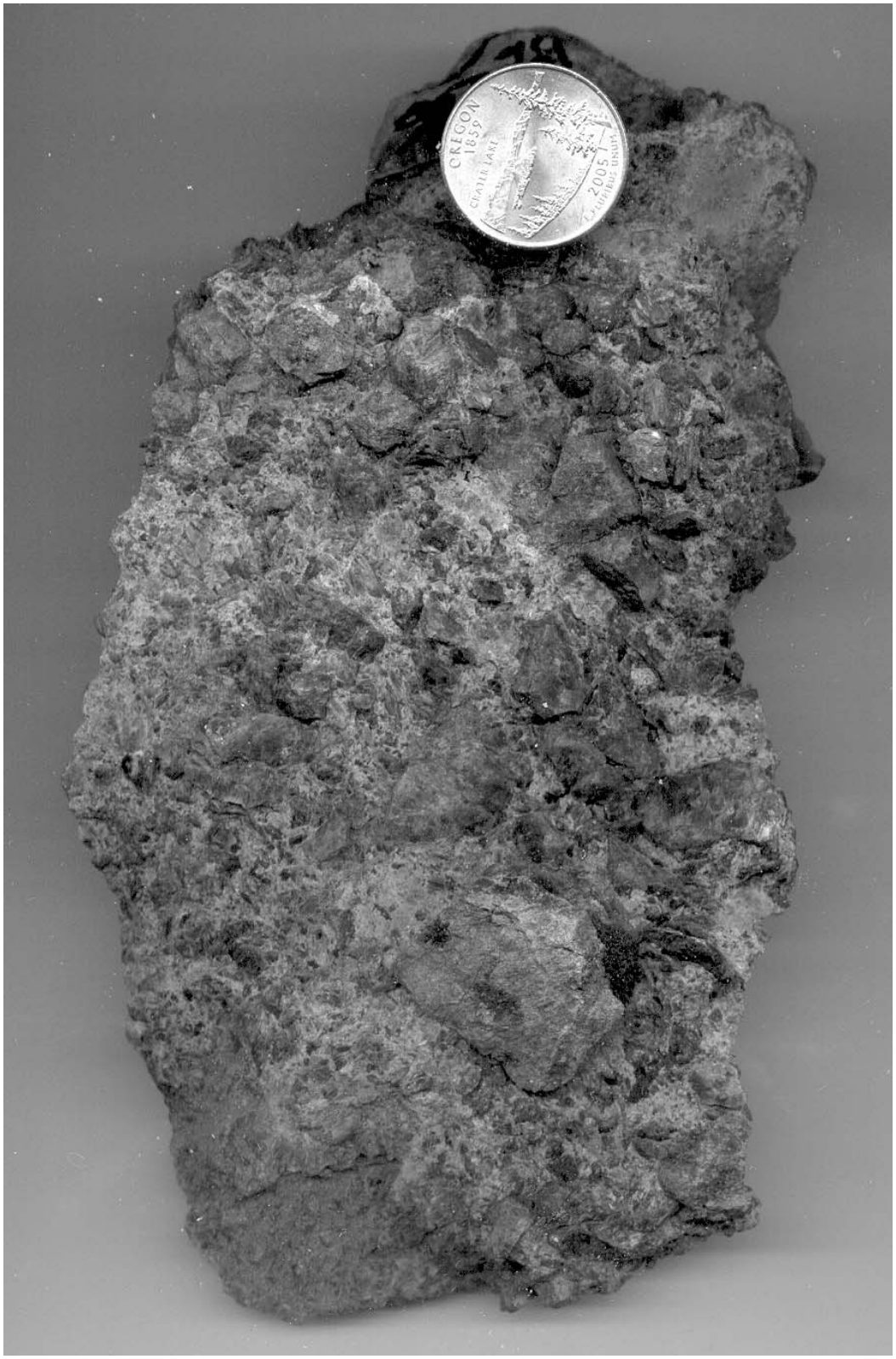
OREGON
1859
CRATER LAKE
2005

Figure 46. Annotated photo looking north from Navaho Divide. Contact between the Esmeralda Peaks unit basalt and Navaho Divide fault zone is faulted. All other contacts appear conformable; however internal faulting within the argillite cannot be ruled out. Large gabbro bodies are interpreted as olistoliths. The tree within the photo is ~ 4 meters tall.

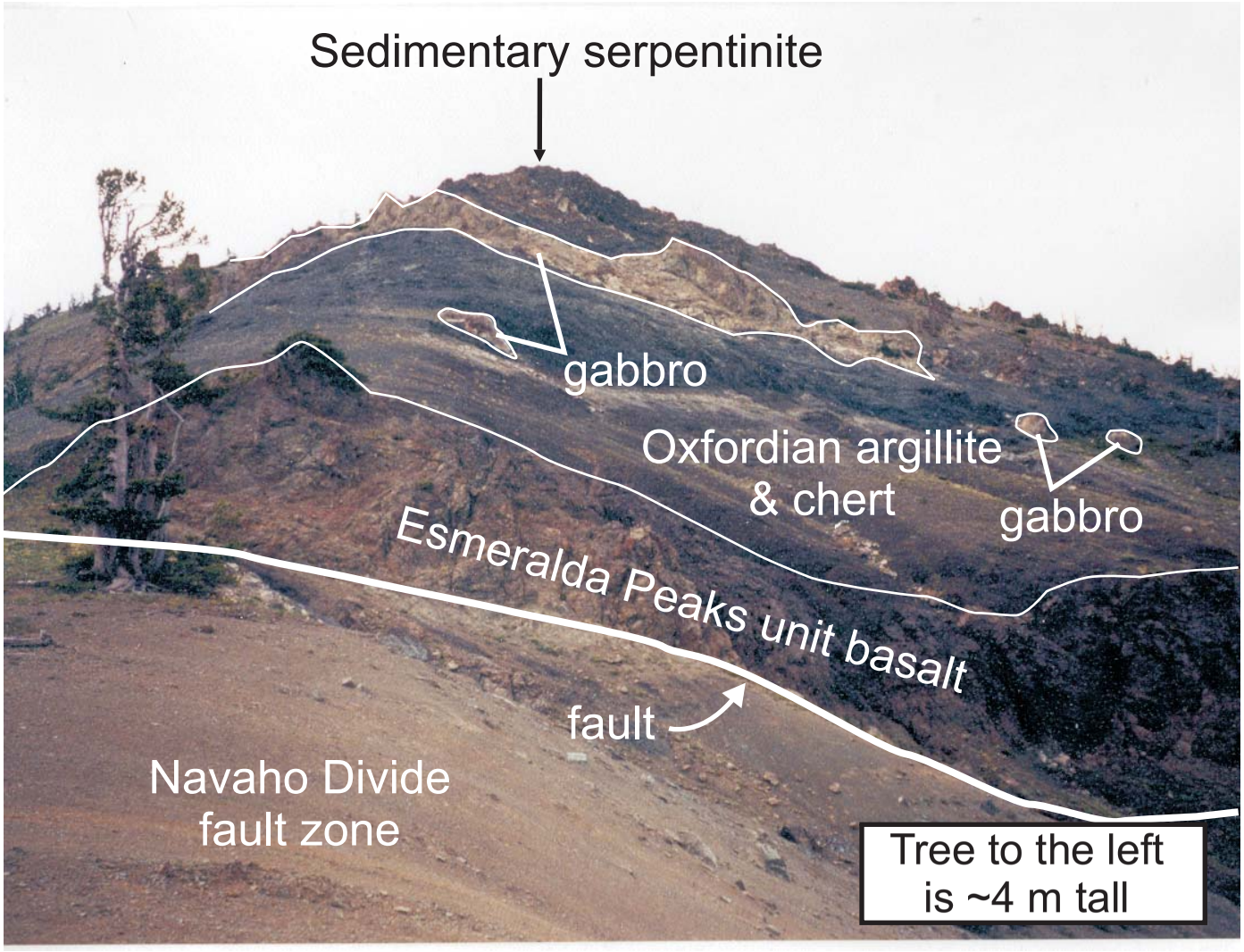
Sedimentary serpentinite
gabbro
Oxfordian argillite
& chert
gabbro
Esmeralda Peaks unit basalt
fault
Navaho Divide
fault zone
Tree to the left
is ~4 m tall

Figure 47. Al_2O_3 verses TiO_2 diagram showing detrital Cr-spinels from three sedimentary serpentinites of the Ingalls ophiolite complex. Inset shows key to symbols. Fields are from Kamenetsky et al. (2001). This diagram is a good discriminator for tectonic setting and distinguishing volcanic from peridotite spinels. MORB = mid-ocean ridge basalt; SSZ = supra-subduction zone. Also shown are the fields for spinels from the Ingalls peridotites (Miller and Mogk, 1987).

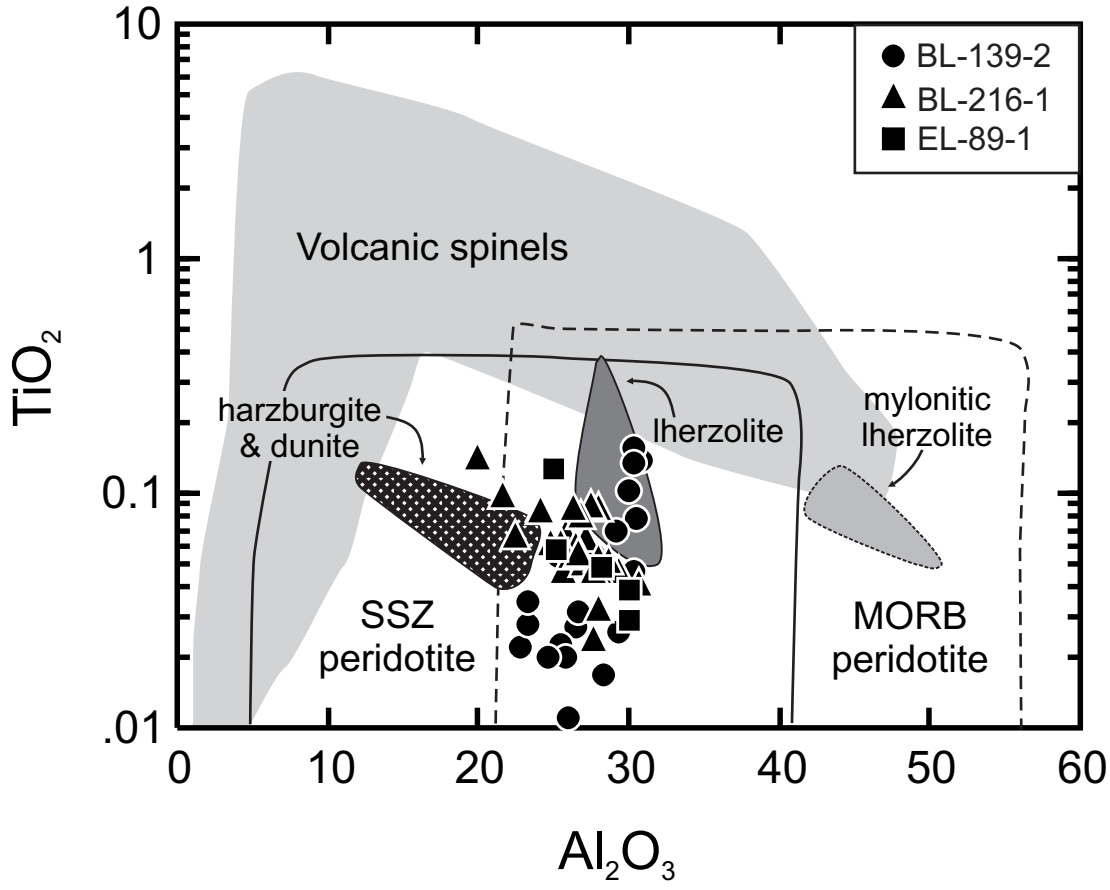
10
1
0.1
.01
0
10
20
30
40
50
60
TiO2
Al2O3
BL-139-2
BL-216-1
EL-89-1
Volcanic spinels
harzburgite
& dunite
lherzolite
mylonitic
lherzolite
SSZ
peridotite
MORB
peridotite

Figure 48. Backscatter electron image of a well zoned detrital spinel from sample EL-89-1. Core is rich in Cr and Al, while rim is rich in Fe and contains Si. Si is most likely from an intergrown silicate phase as a result of serpentinization (Burkhard, 1993).

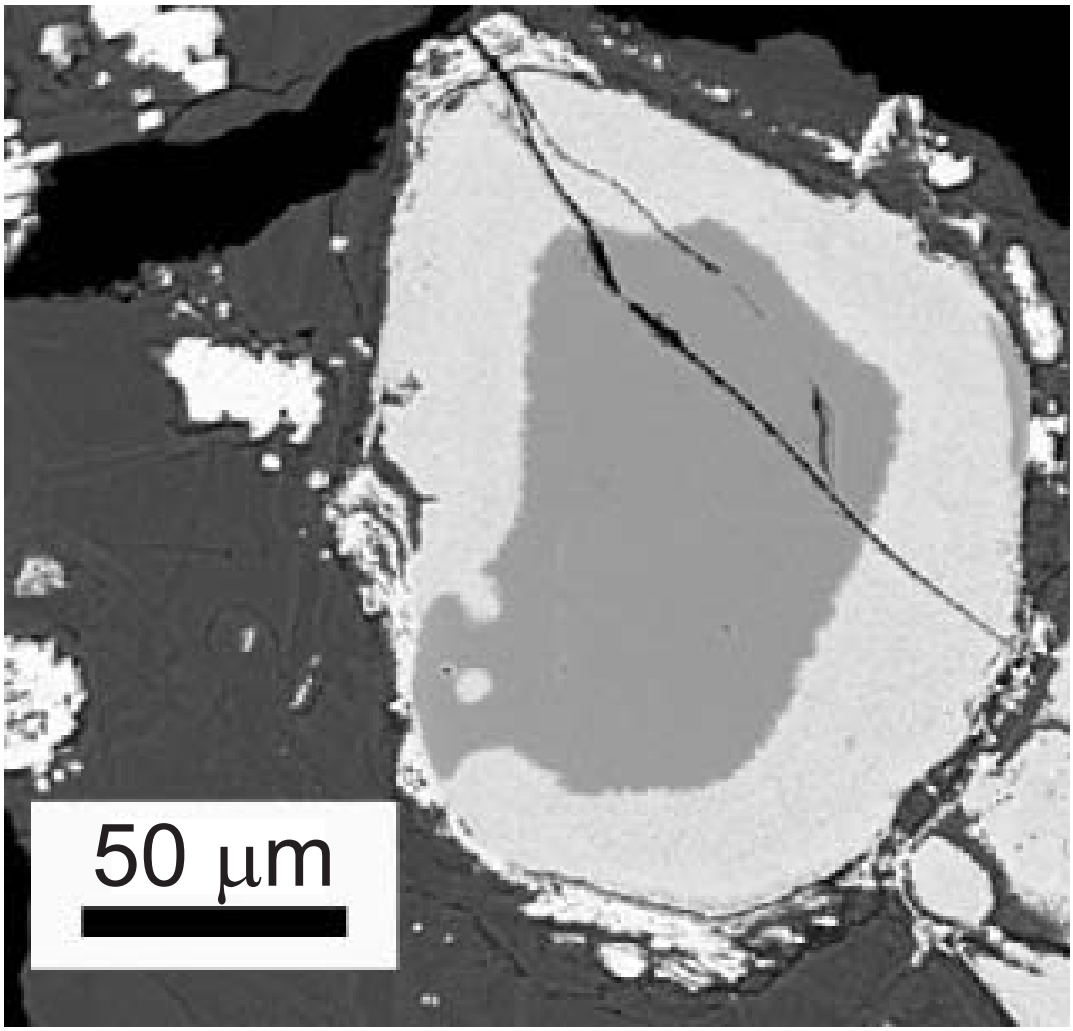
50 μm

Figure 49. Al-Cr-Fe^{3+} diagram from Burkhard (1993) for detrital spinels from Ingalls sedimentary serpentinites. See inset for symbol key. Serpentinite alteration trend displays first the loss of Al and then Cr relative to an increase in Fe^{3+}. Two core-rim (C = core; R = rim) pairs are connected with dashed lines.

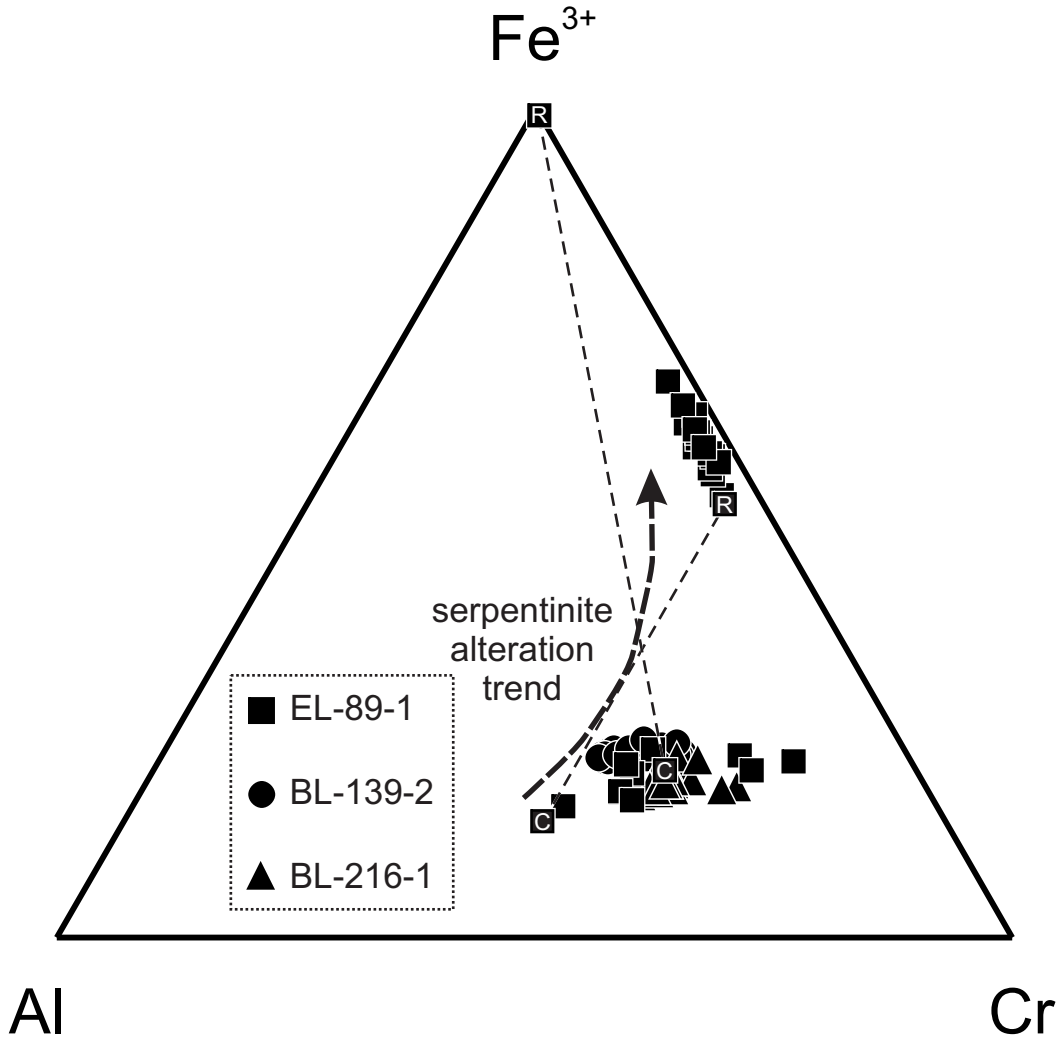
Fe3+
R
R
serpentinite
alteration
trend
EL-89-1
BL-139-2
BL-216-1
C
C
Al
Cr

Figure 50. Tectonic model for the formation of the ophiolitic breccia and sedimentary serpentinite in a Late Jurassic fracture zone setting. Argillite is far greater than ophiolitic debris, therefore this cartoon represents a time before much of the argillite was deposited. Note the source areas of the Esmeralda Peaks and harzburgite and dunite units.

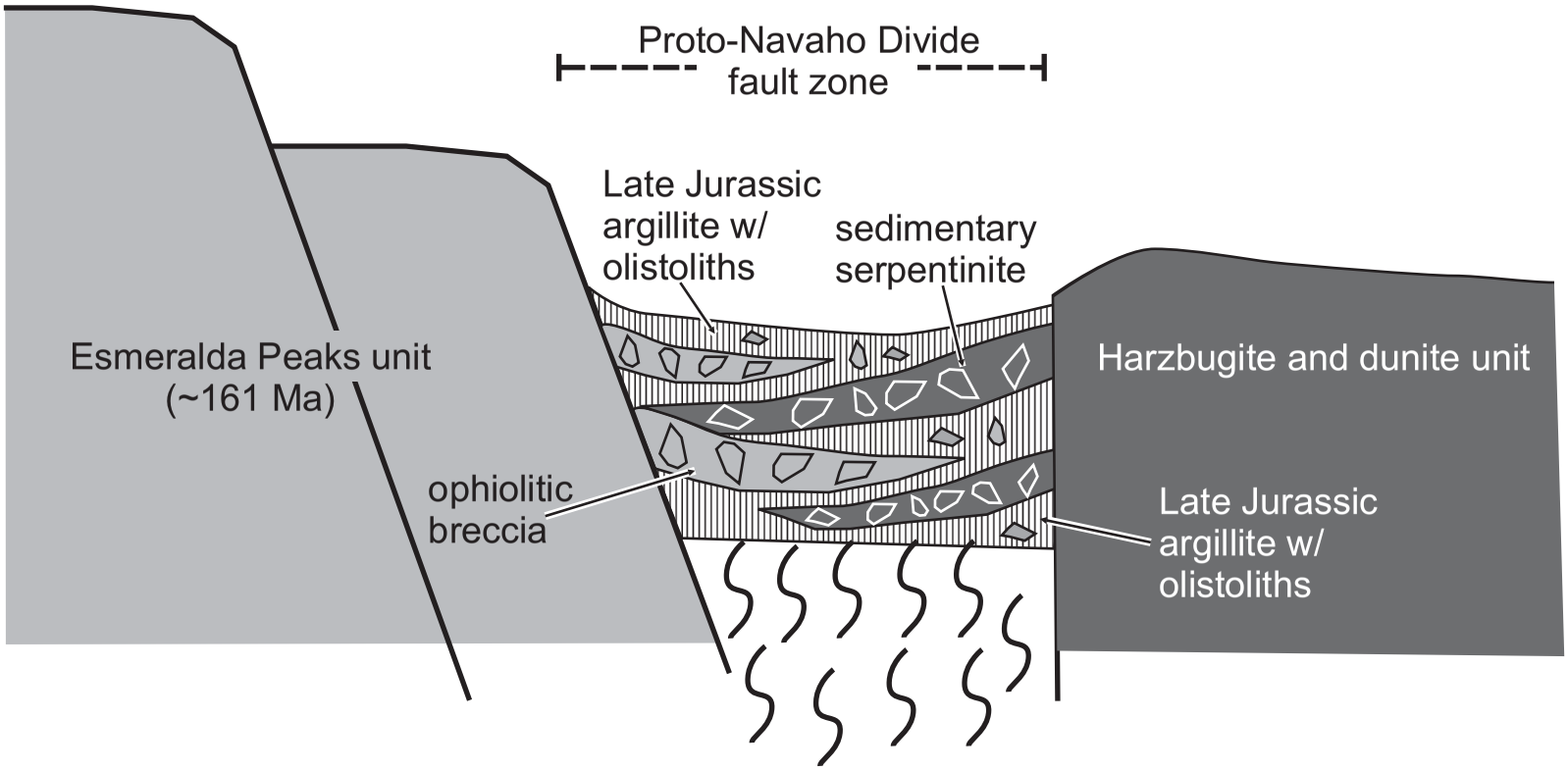
Proto-Navaho Divide
fault zone
Late Jurassic
argillite w/
olistoliths
sedimentary
serpentinite
Esmeralda Peaks unit
(~161 Ma)
Harzbugite and dunite unit
ophiolitic
breccia
Late Jurassic
argillite w/
olistoliths

Figure 51. Simplified geologic map showing the tectonic elements of the central and northwest Cascades. HHM = Helena-Haystack mélange; NWCS = Northwest Cascade System; WEMB = western and eastern mélange belts. Area of figure 52 is also shown on the map. Modified from Tabor et al. (1989), Miller et al. (1993), and Tabor (1994).

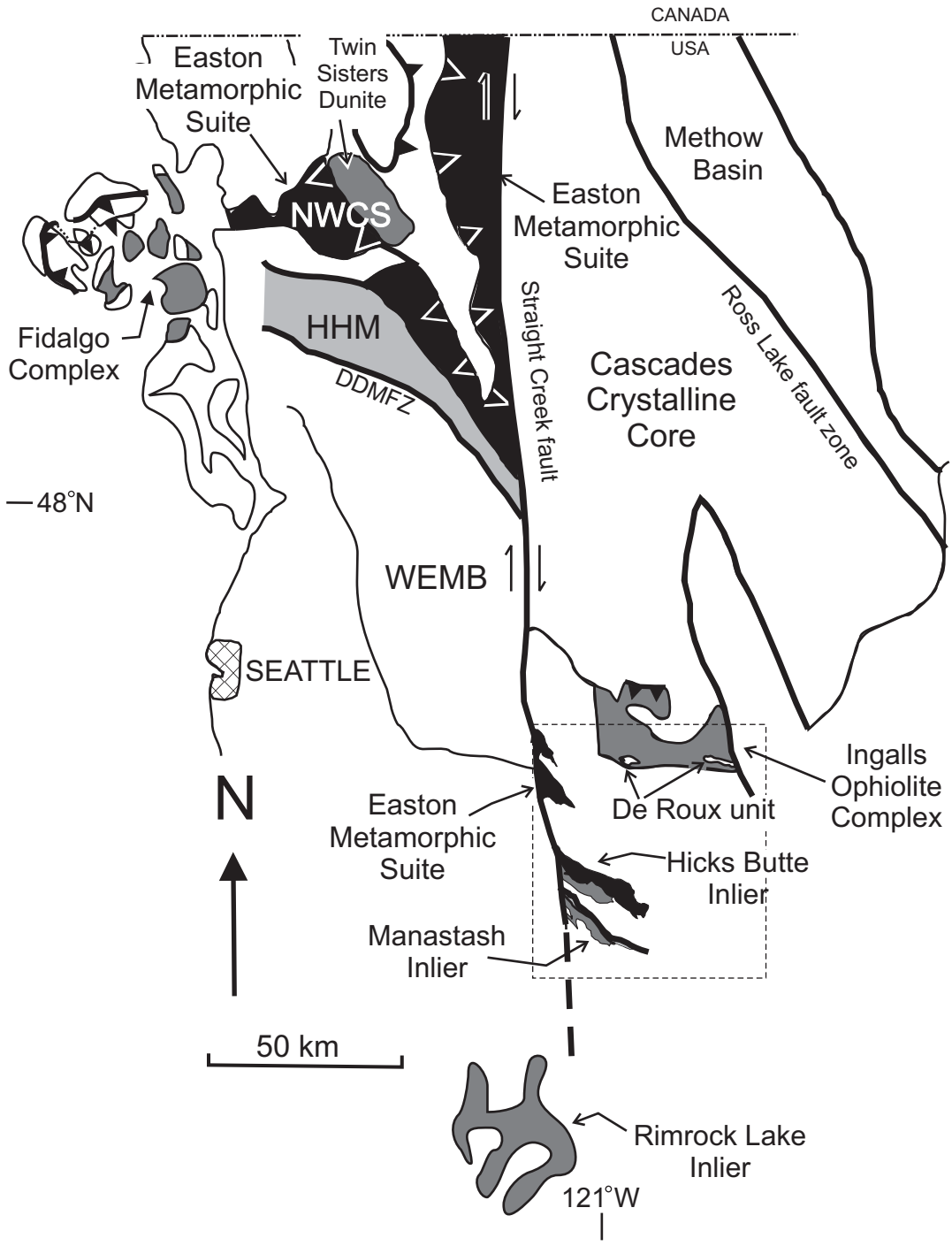
CANADA
USA
Easton
Metamorphic
Suite
Twin
Sisters
Dunite
NWCS
Methow
Basin
Easton
Metamorphic
Suite
Fidalgo
Complex
HHM
DDMFZ
Straight Creek fault
Ross Lake fault zone
Cascades
Crystalline
Core
48°N
WEMB
SEATTLE
N
Ingalls
Ophiolite
Complex
De Roux unit
Easton
Metamorphic
Suite
Hicks Butte
Inlier
Manastash
Inlier
50 km
Rimrock Lake
Inlier
121°W

Figure 52. Simplified geologic map displaying the tectonic elements east of the Straight Creek fault and south of the Cascades Crystalline Core. The northern-most Easton Metamorphic suite on this map is equal to the Kachess Lake inlier of Ashleman (1979). Modified from Tabor and colleagues (1982, 1987, 1993, 2000), Miller (1985, 1989), and Miller et al. (1993).

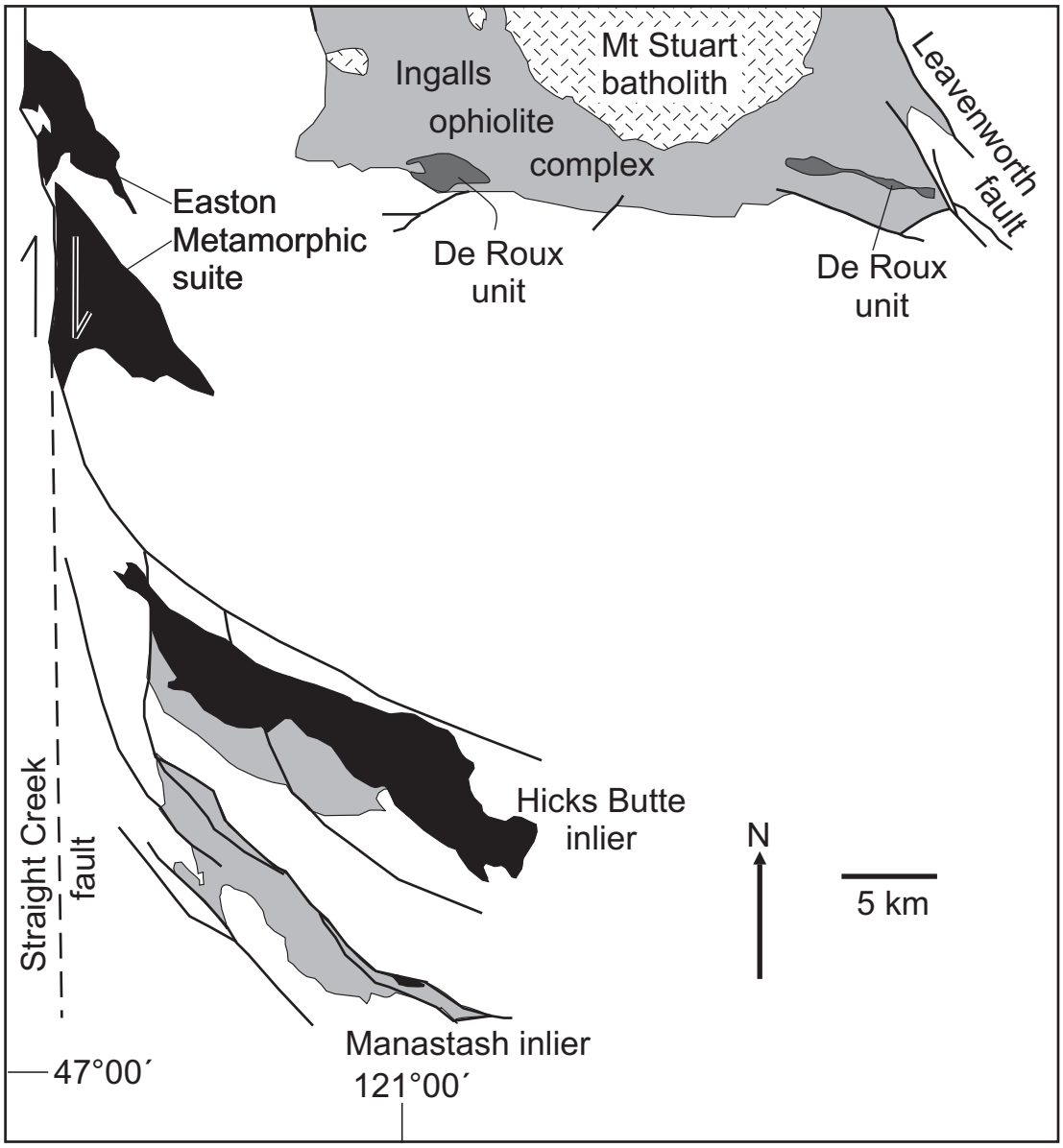
Mt Stuart
batholith
Ingalls
ophiolite
complex
Leavenworth
fault
Easton
Metamorphic
suite
De Roux
unit
De Roux
unit
Straight Creek
fault
Hicks Butte
inlier
N
5 km
Manastash inlier
47°00´
121°00´

Figure 53. Location of the Ingalls ophiolite complex, inliers east of the Straight Creek fault, Blue Mountains Provance, Klamath Mountains, and Northern Sierra terrane. Modified from Miller et al. (1993) and Metzger et al. (2002).

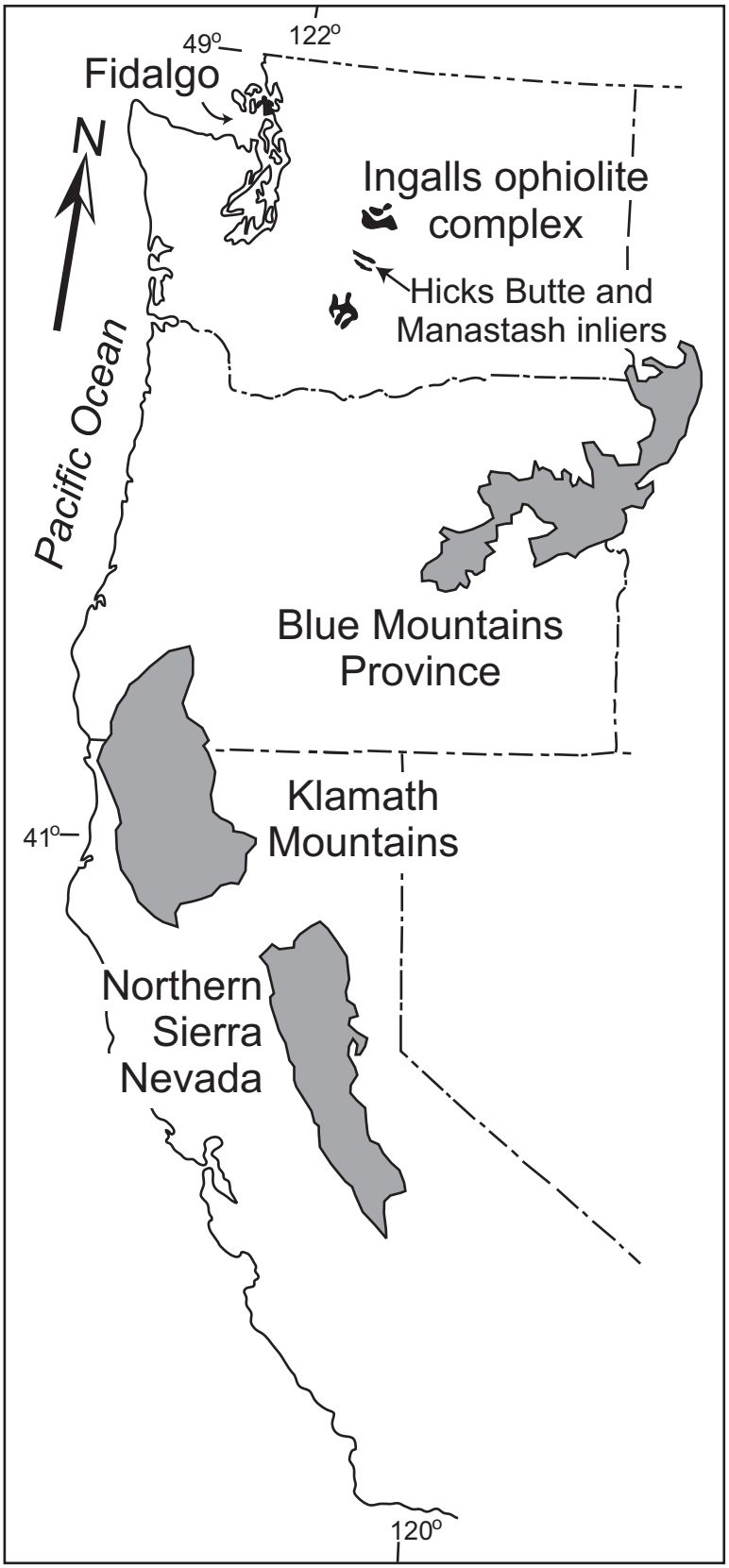
49°
122°
Fidalgo
N
Ingalls ophiolite
complex
Hicks Butte and
Manastash inliers
Pacific Ocean
Blue Mountains
Province
Klamath
Mountains
41°
Northern
Sierra
Nevada
120°

Figure 54. Structural stacking of terranes within the northwest Cascades, Washington state. Modified from Tabor (1994).

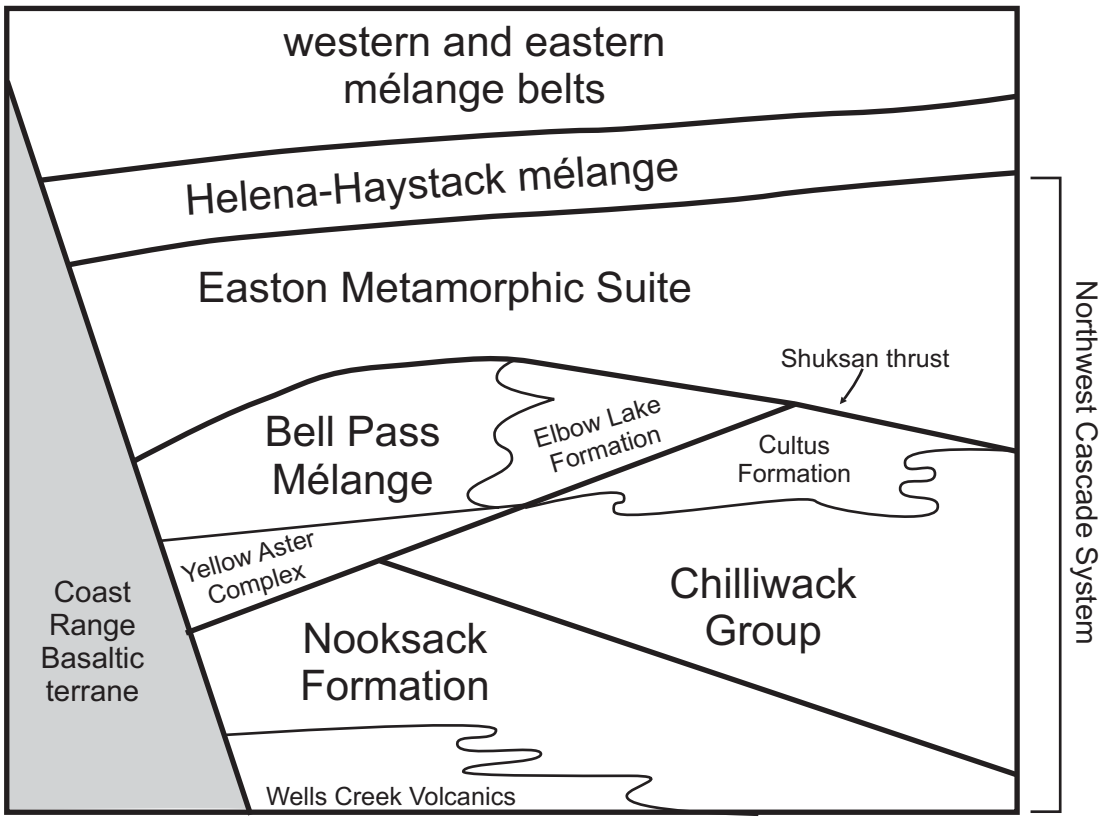
western and eastern
mélange belts
Helena-Haystack mélange
Easton Metamorphic Suite
Shuksan thrust
Bell Pass
Mélange
Elbow Lake
Formation
Cultus
Formation
Yellow Aster
Complex
Chilliwack
Group
Coast
Range
Basaltic
terrane
Nooksack
Formation
Wells Creek Volcanics
Northwest Cascade System

Figure 55. Detailed geologic map of the Hick Butte and Manastash inliers displaying geochronological localities. DDMFZ = Darrington-Devils Mountain fault zone. Modified from Goetsch (1978), Tabor et al. (1982, 2000), Treat (1987), Miller et al. (1993) and new mapping by J. MacDonald.

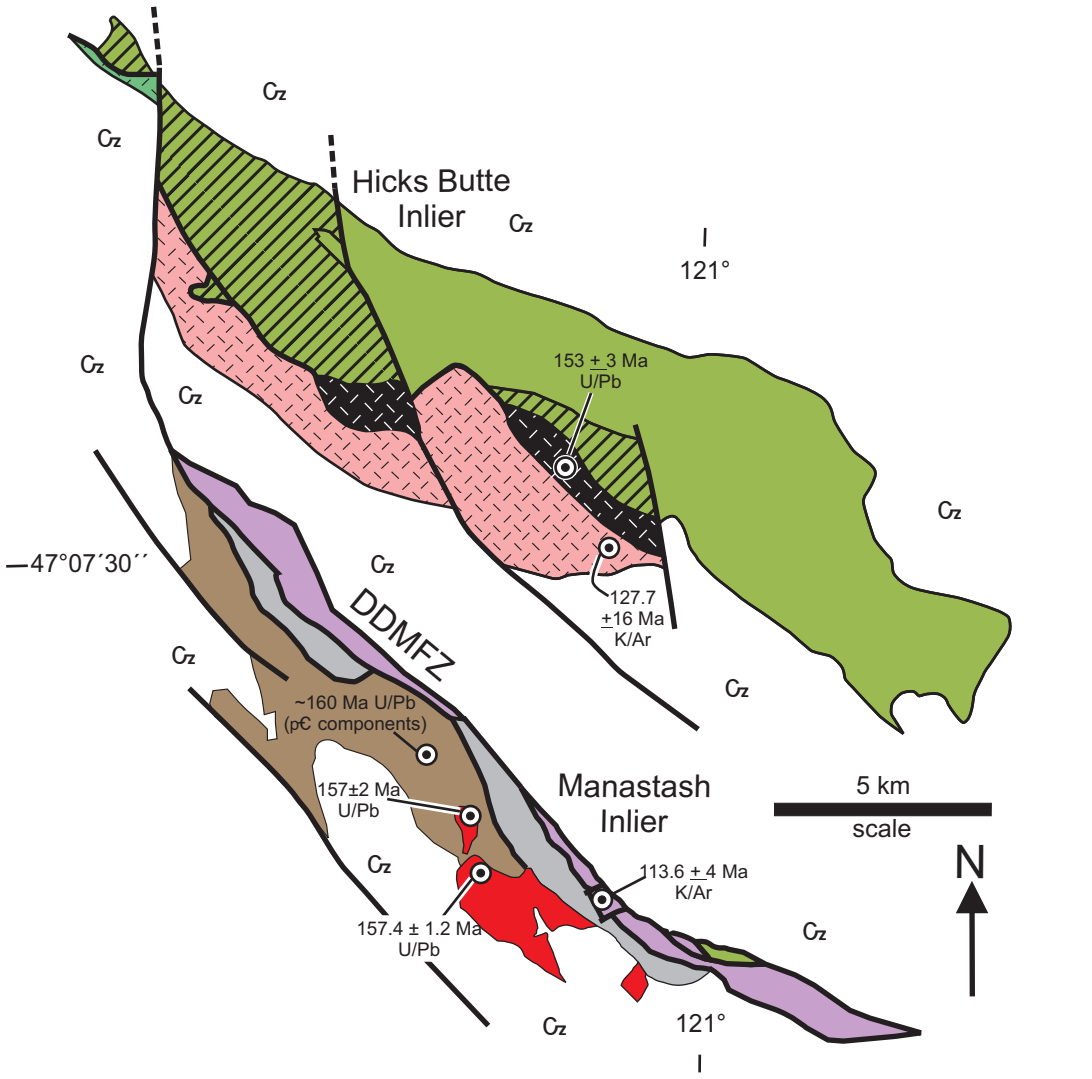
Cz
Hicks Butte
Inlier
121°
153 ± 3 Ma
U/Pb
127.7
±16 Ma
K/Ar
47°07′30″
DDMFZ
~160 Ma U/Pb
(p€ components)
157±2 Ma
U/Pb
Manastash
Inlier
5 km
scale
N
113.6 ± 4 Ma
K/Ar
157.4 ± 1.2 Ma
U/Pb
Tectonic complex of Stout (1964) (= Helena-Haystack melange; pre-Tertiary)
Easton Metamorphic Suite
Darrington Phyllite (Early Cretaceous)
Shuksan Greenschist (Early Cretaceous)
Hicks Butte complex (Late Jurassic)
Tectonic zone (Late Jurassic-Early Cretaceous?)
Quartz Mountain stock (Late Jurassic)
Lookout Mountain Formation (Late Jurassic)
Hereford Meadow Amphibolite (pre-Late Jurassic)
Modified from Tabor et al. (1982; 2000) and Miller et al. (1993).

Figure 56. Th/Yb-Ta/Yb discrimination diagram for Hereford Meadow samples (Pearce, 1982). N-MORB, E-MORB and OIB normalizing values are from Sun and McDonough (1989). N-MORB = normal-mid-ocean ridge basalt; E-MORB = enriched-mid-ocean ridge basalt; OIB = ocean island basalt (= within-plate basalt). Field for backarc basins was compiled by Harper (2003; Fig. 7, p. 219) from Mariana and Lau backarc basins.

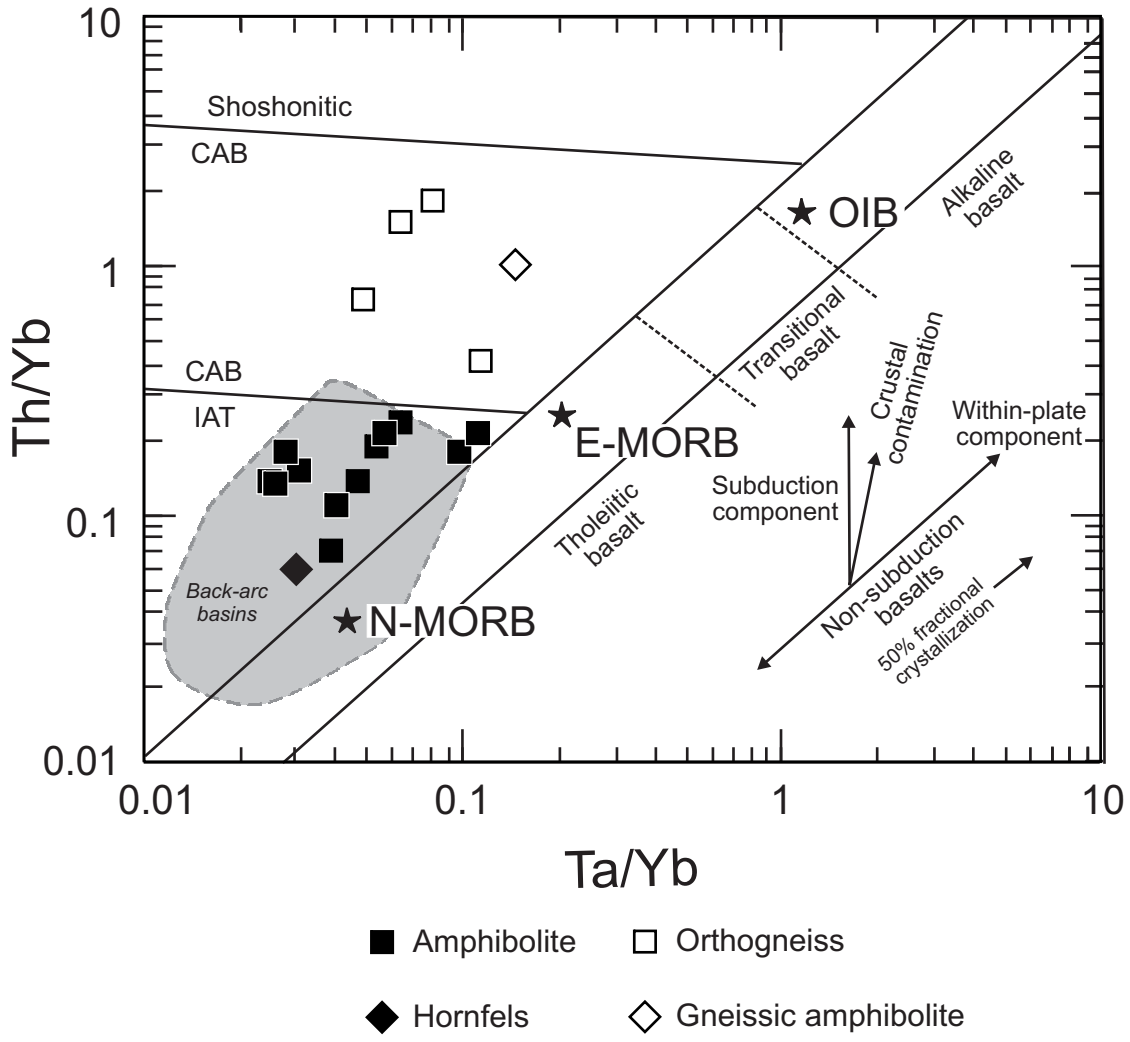
10
1
0.1
0.01
0.01
0.1
1
10
Th/Yb
Ta/Yb
Shoshonitic
CAB
CAB
IAT
OIB
Alkaline basalt
Transitional basalt
E-MORB
Tholeiitic basalt
Crustal contamination
Within-plate component
Subduction component
Non-subduction basalts
50% fractional crystallization
Back-arc basins
N-MORB
Amphibolite
Orthogneiss
Hornfels
Gneissic amphibolite

Figure 57. Chondrite- and N-MORB-normalized diagrams (see Fig. 56 for key to symbols). Chondrite and N-MORB normalized values are from Sun and McDonough (1989). A and B. Modern reference suite. N-MORB, E-MORB, and OIB from Sun and McDonough (1989); IAT and CAB from Pearce et al. (1995). C. Chondrite-normalized IAT affinity Hereford Meadow amphibolites. D. N-MORB-normalized IAT affinity Hereford Meadow amphibolites. E. Chondrite-normalized diagram for orthogneiss and gneissic amphibolite. F. N-MORB-normalized diagram for orthogneiss and gneissic amphibolite.

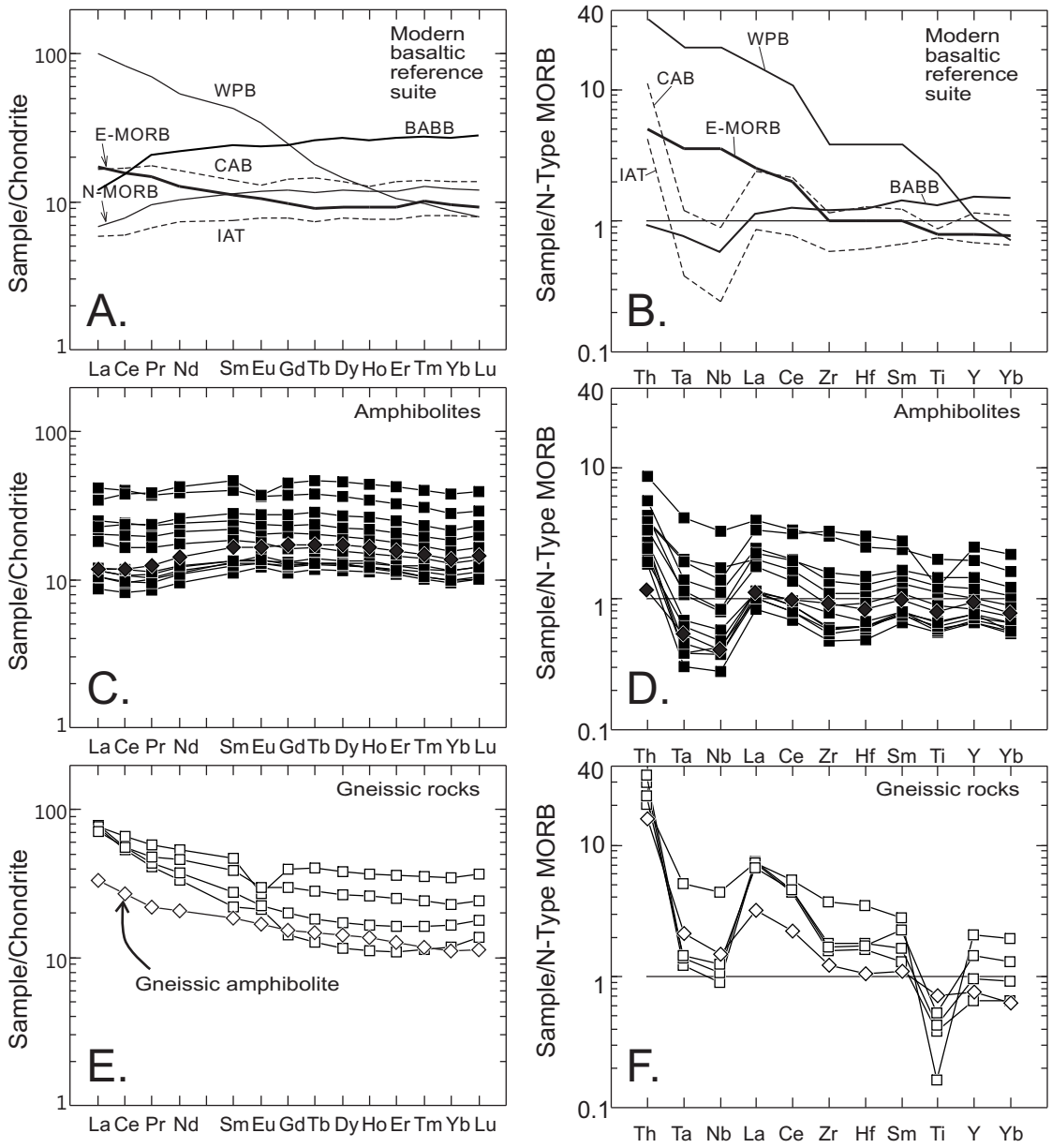
Modern basaltic reference suite
WPB
E-MORB
N-MORB
CAB
BABB
IAT
Sample/Chondrite
Sample/N-Type MORB
A.
B.
Amphibolites
C.
D.
Gneissic rocks
Gneissic amphibolite
E.
F.
La Ce Pr Nd Sm Eu Gd Tb Dy Ho Er Tm Yb Lu
Th Ta Nb La Ce Zr Hf Sm Ti Y Yb

Figure 58. Ti-V basalt discriminant diagram (Shervais, 1982) displaying mafic rocks from the Hereford Meadow amphibolite that have mafic compositions. See figure 56 for key to symbols. Field for backarc basins is compiled by Metzger et al. (2002; references given in Fig. 6, p. 551) and Leat et al. (2000).

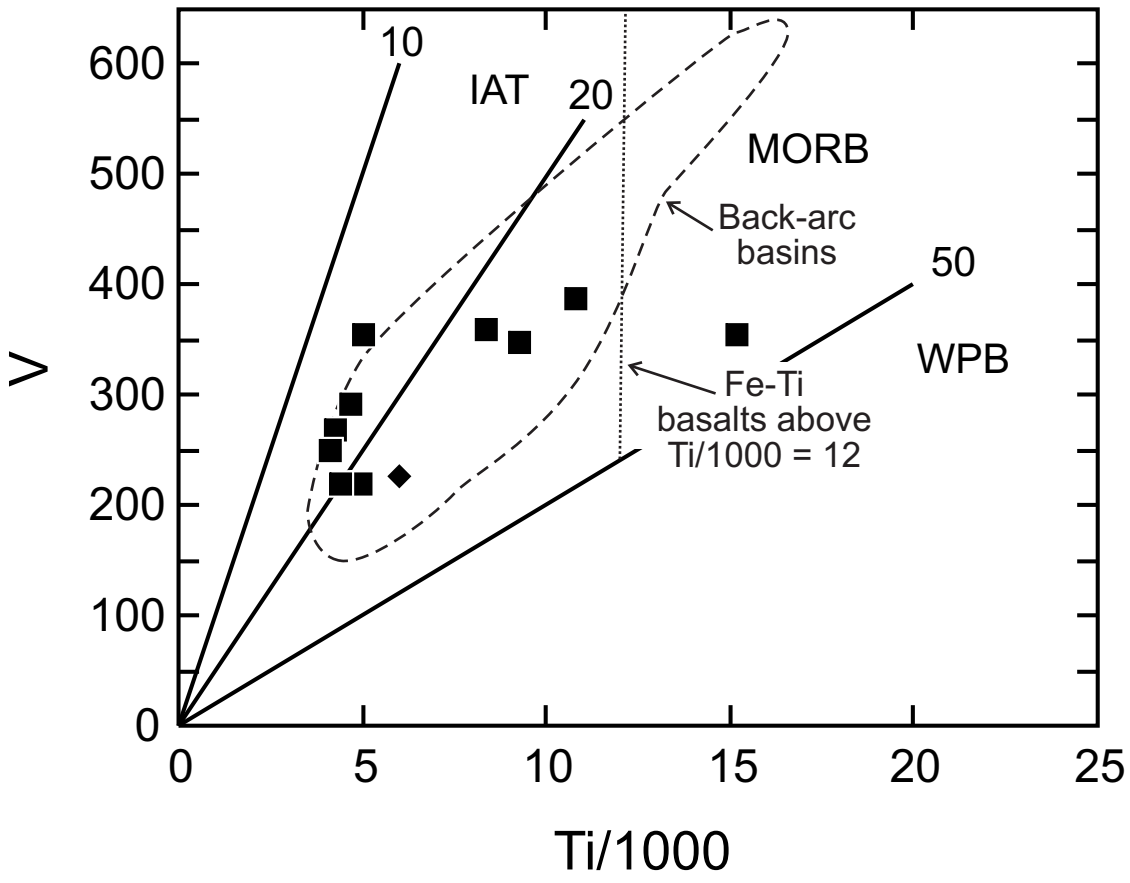
10
IAT
20
MORB
Back-arc
basins
50
WPB
Fe-Ti
basalts above
Ti/1000 = 12
600
500
400
300
200
100
0
V
0
5
10
15
20
25
Ti/1000

Figure 59. Cr-Y basalt discriminant diagram (Pearce, 1982) (see Fig. 56 for key to symbols). Arrows A, B, and C represent crystallization paths for magmas fractionating Cr-spinel + olivine + pyroxene for MORB, IAT, and boninite respectively. Field for backarc basins is compiled by Metzger et al. (2002; references given in Fig. 6, p. 551) and Leat et al. (2000). Field for Fe-Ti basalts is from Harper (2003b). Only basaltic compositions are plotted on the diagram.

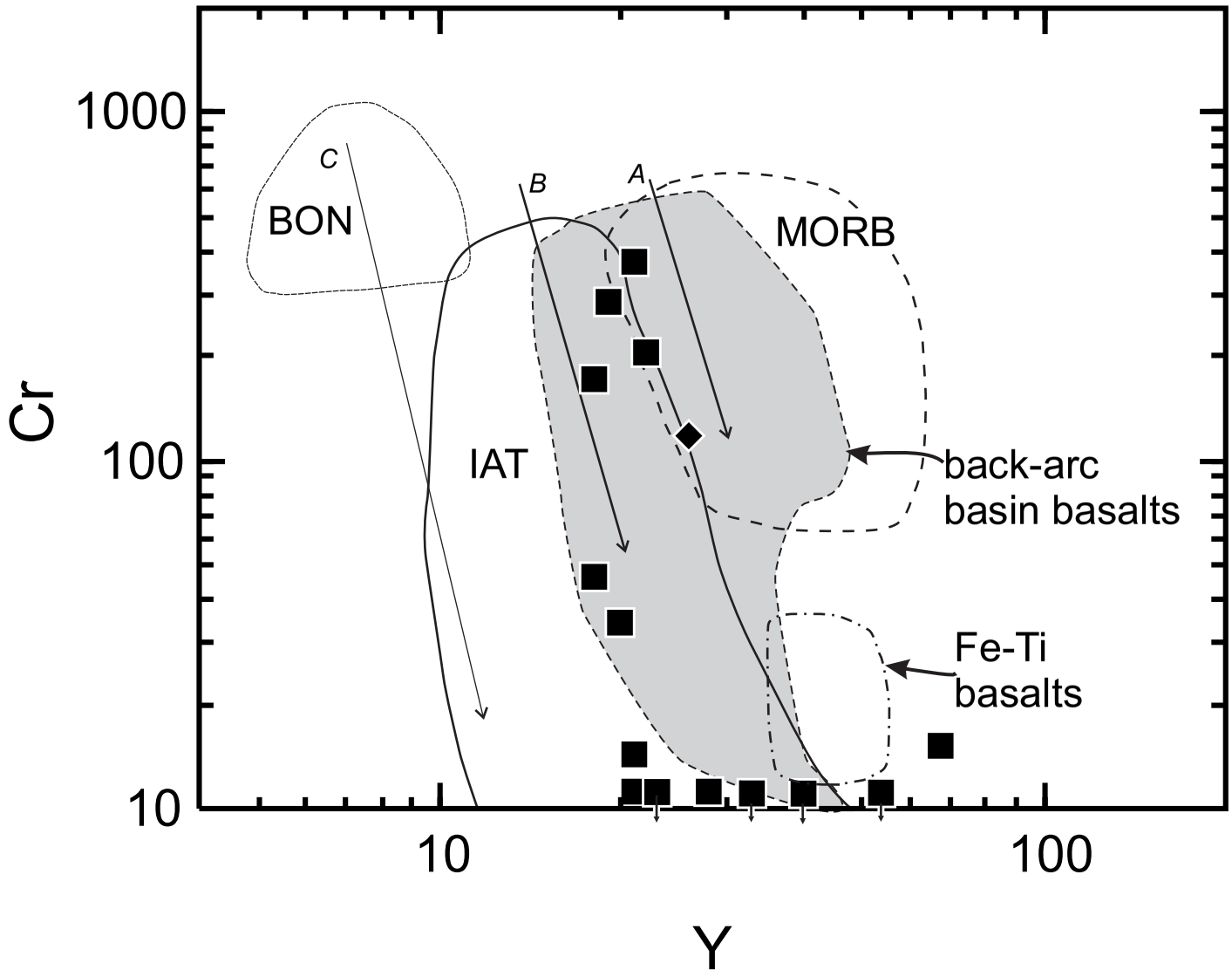
1000
100
10
Cr
10
100
Y
C
B
A
BON
IAT
MORB
back-arc
basin basalts
Fe-Ti
basalts

Figure 60. Zr vs. TiO_2 diagram. Zr increases with increasing fractionation. Symbols are the same as figure 56. The decrease in TiO_2 for each trend is the result if the onset of Fe-Ti fractionation (e.g., Perfit et al., 1983). Modified from Harper (2003b). Reference trends from three MORB affinity propagating spreading centers are: Galápagos Rift at 85°W (Perfit et al., 1983); Galápagos Rift at 95°W (Clague et al., 1981); and Central Lau spreading center (CLSC) (compiled by Harper, 2003b; figure 5, page 778).

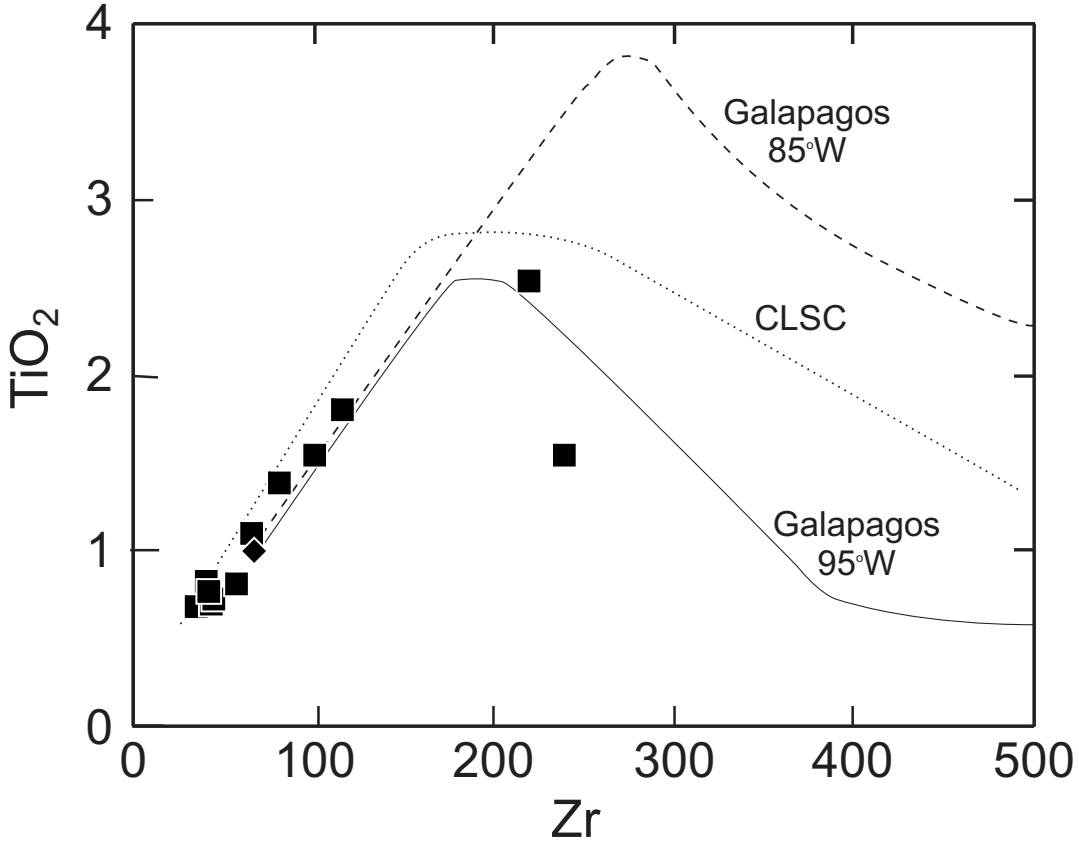
4
3
2
1
0
TiO2
0
100
200
300
400
500
Zr
Galapagos
85°W
CLSC
Galapagos
95°W

Figure 61. Concordia diagrams for Lookout Mountain Formation detrital zircons. Error ellipses are 2σ. A. $^{206}Pb/^{238}U$ *vs.* $^{207}Pb/^{235}U$ diagram. B. $^{207}Pb/^{206}Pb$ *vs.* $^{238}U/^{206}Pb$ diagram.

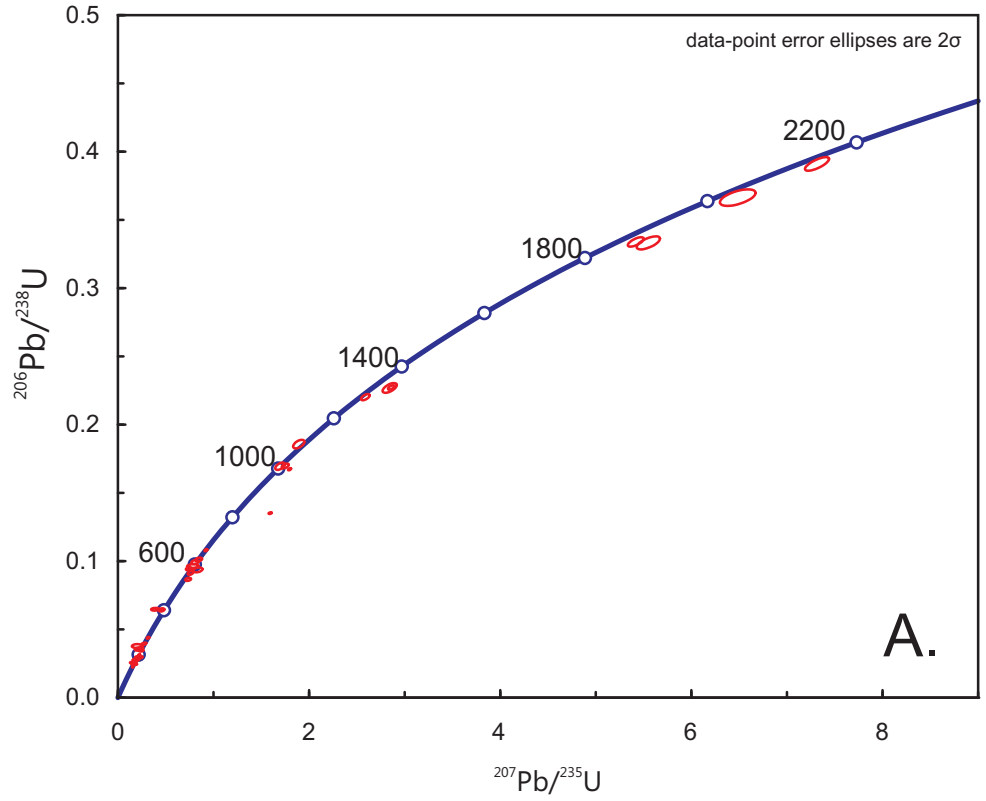
data-point error ellipses are 2σ
A.
0.5
0.4
0.3
0.2
0.1
0.0
0
2
4
6
8
2200
1800
1400
1000
600
$^{206}Pb/^{238}U$
$^{207}Pb/^{235}U$

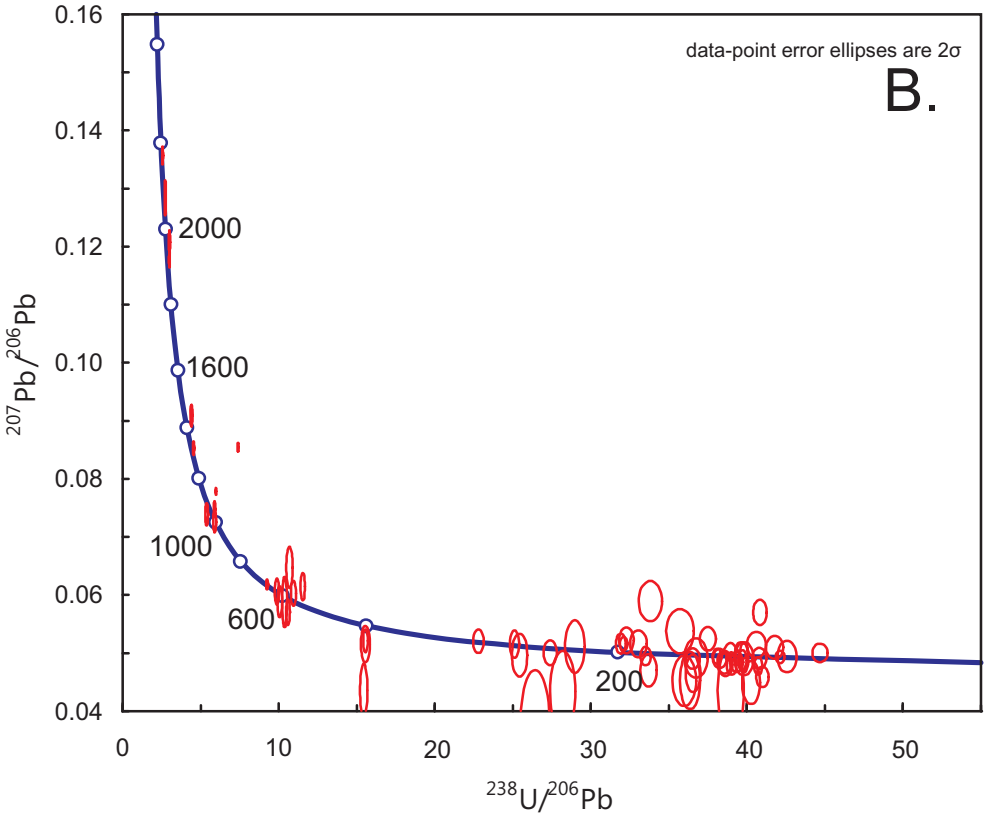
data-point error ellipses are 2σ
B.
0.16
0.14
0.12
0.10
0.08
0.06
0.04
0
10
20
30
40
50
2000
1600
1000
600
200
$^{207}Pb/^{206}Pb$
$^{238}U/^{206}Pb$

Figure 62. Age histograms and probability density distributions for detrital zircons from the Lookout Mountain Formation. Boundaries of geologic ages on graph are taken from Gradstein et al. (2004).

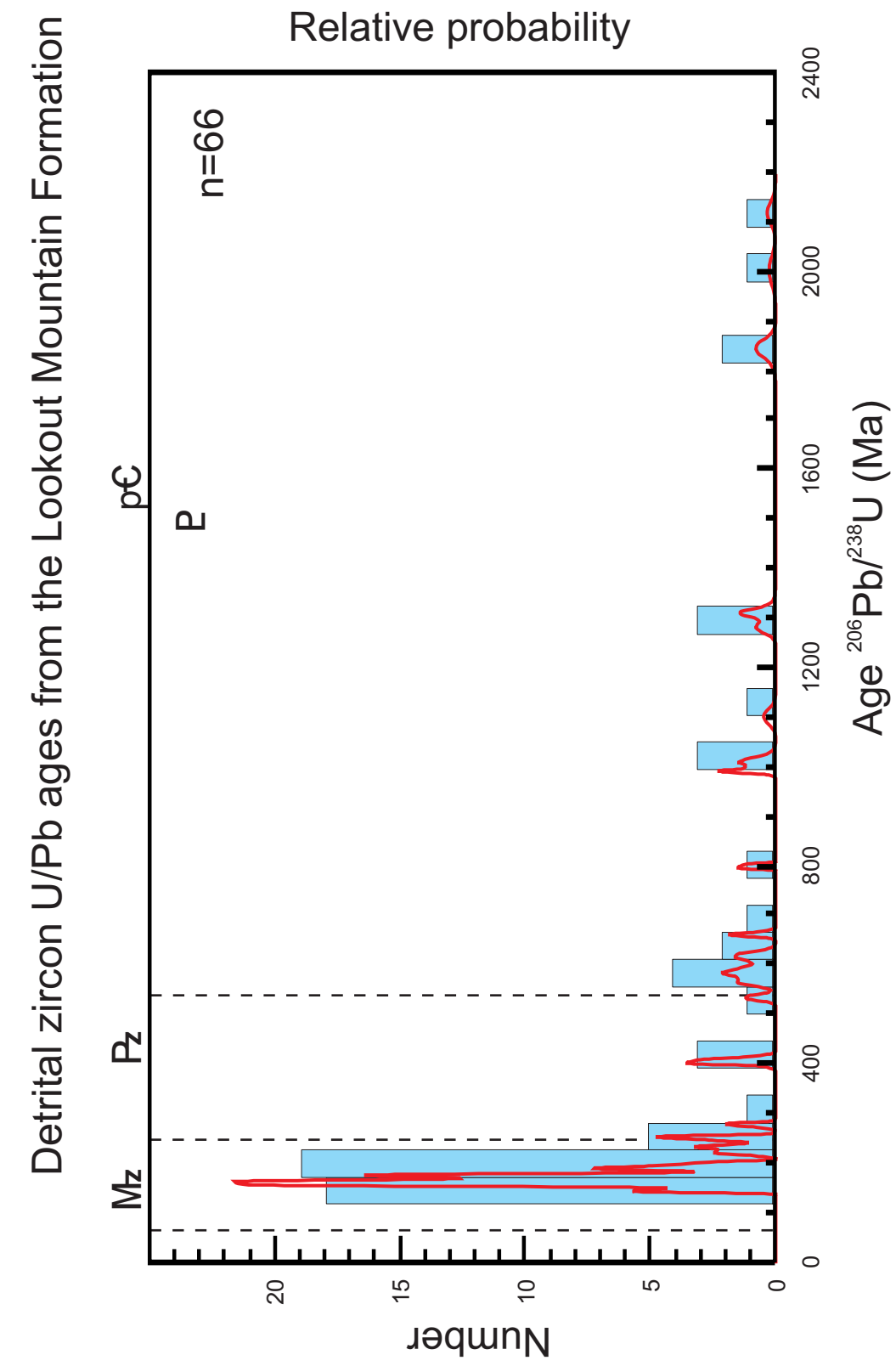
Detrital zircon U/Pb ages from the Lookout Mountain Formation
Relative probability
n=66
Mz
Pz
pЄ
P
Number
0
5
10
15
20
0
400
800
1200
1600
2000
2400
Age $^{206}Pb/^{238}U$ (Ma)

Figure 63. Age histograms and probability density distributions for the youngest (n = 43) detrital zircons from the Lookout Mountain Formation. Boundaries of geologic ages are taken from Gradstein et al. (2004).

Youngest detrital zircon U/Pb ages from the Lookout Mountain Formation

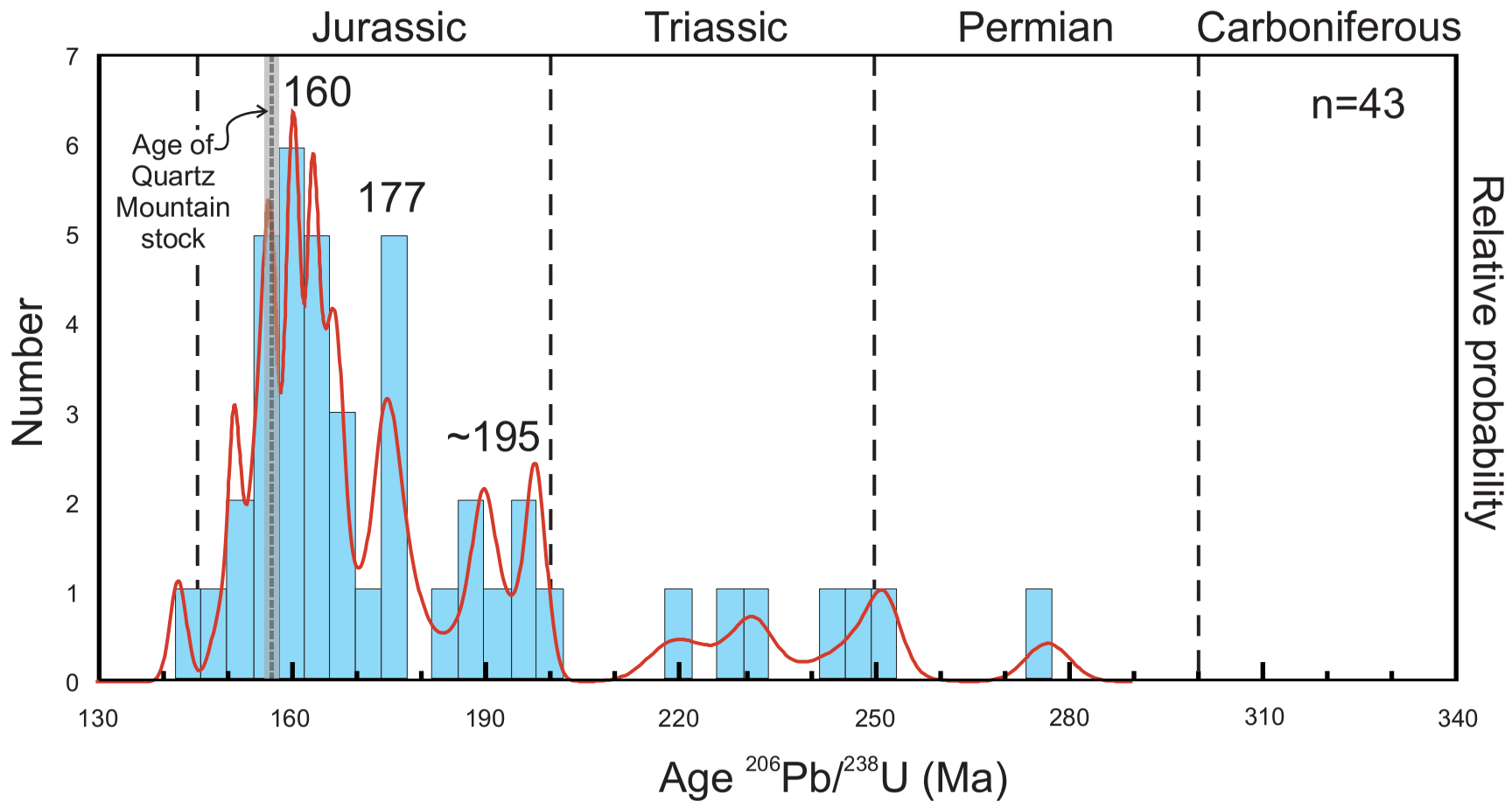

Figure 64. A. $^{206}Pb/^{238}U$ *vs.* $^{207}Pb/^{235}U$ concordia diagram for zircons from the Quartz Mountain stock. Error ellipses are 2σ. B. Average mean $^{207}Pb/^{206}Pb$ age of all 10 analyses from the Quartz Mountain stock. Error bars are 2σ.

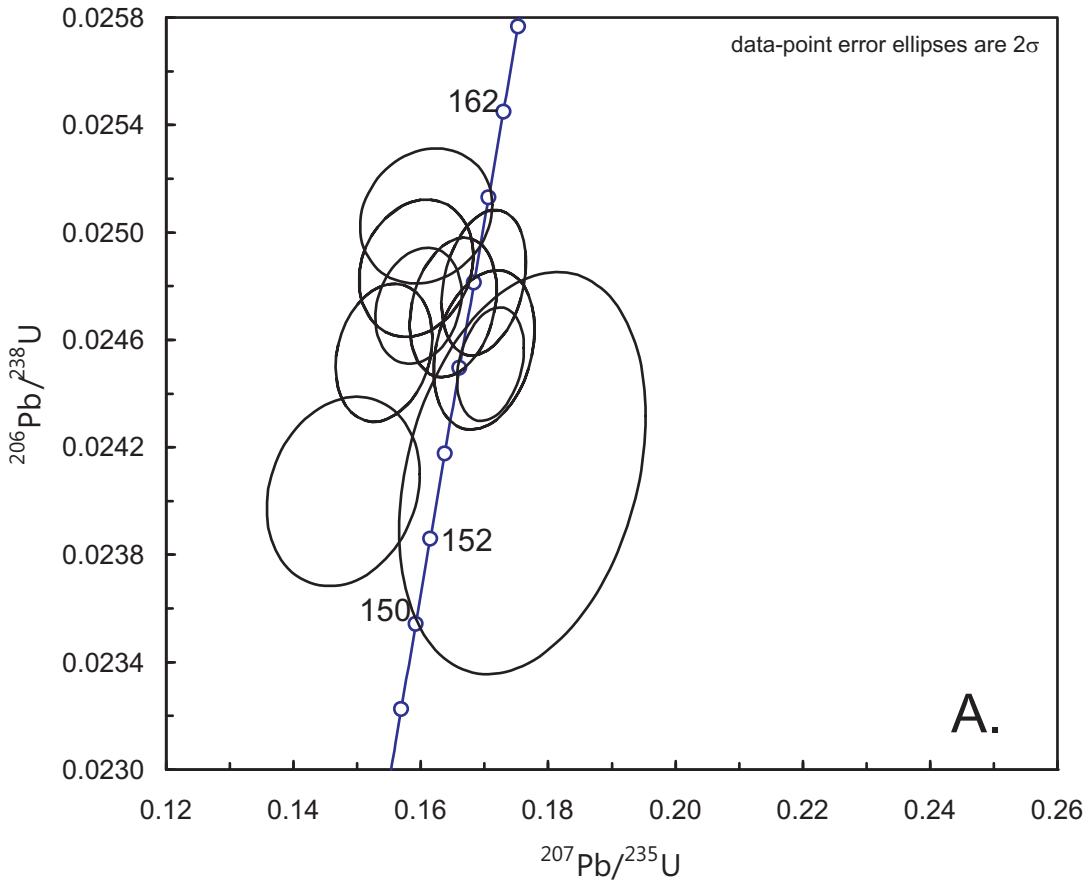
data-point error ellipses are 2σ
162
152
150
A.
0.0258
0.0254
0.0250
0.0246
0.0242
0.0238
0.0234
0.0230
206Pb/238U
0.12
0.14
0.16
0.18
0.20
0.22
0.24
0.26
207Pb/235U

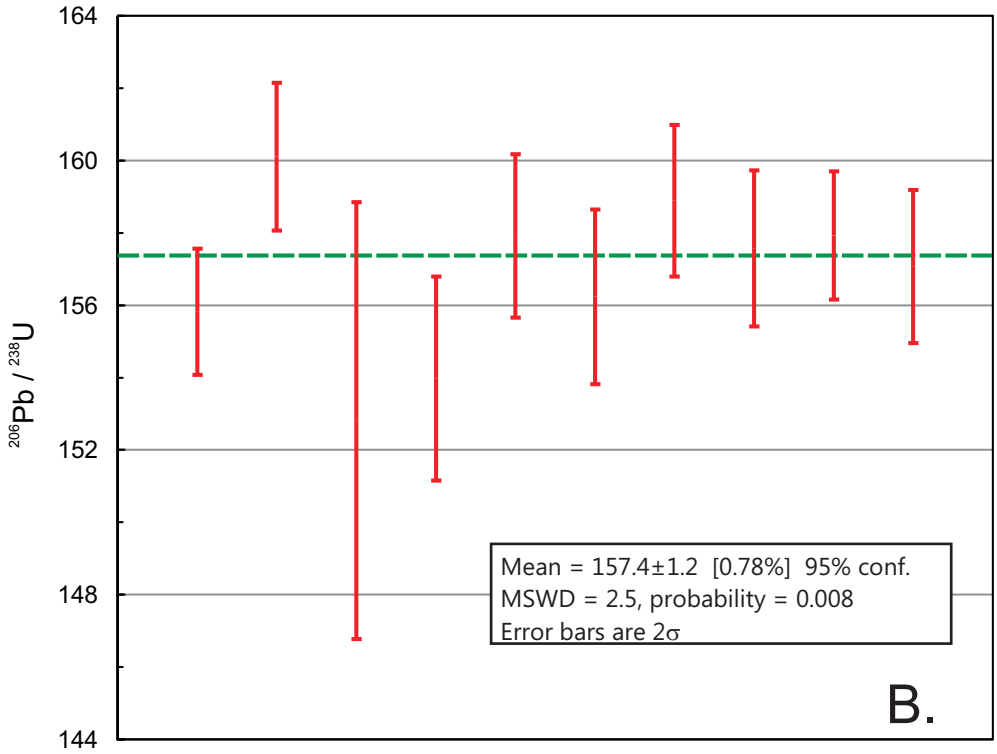
164
160
156
152
148
144
206Pb / 238U
Mean = 157.4±1.2 [0.78%] 95% conf.
MSWD = 2.5, probability = 0.008
Error bars are 2σ
B.

Figure 65. A. Aluminum saturation index (ASI) *vs.* SiO_2 diagram for Quartz Mountain stock samples. See text for calculation of ASI. B. Modified alkali-lime index (Na_2O+K_2O-CaO) *vs.* SiO_2 diagram for Quartz Mountain stock samples. Fields from Frost et al. (2001). C. $FeO^T/(FeO^T + MgO)$ *vs.* SiO_2 diagram for Quartz Mountain stock samples. Also plotted on all diagrams are the average values for A-type, I-type, M-type, and S-type granites (Collins et al., 1982; Whalen et al., 1987; Chappell and White, 1992; compiled by Winter, 2001).

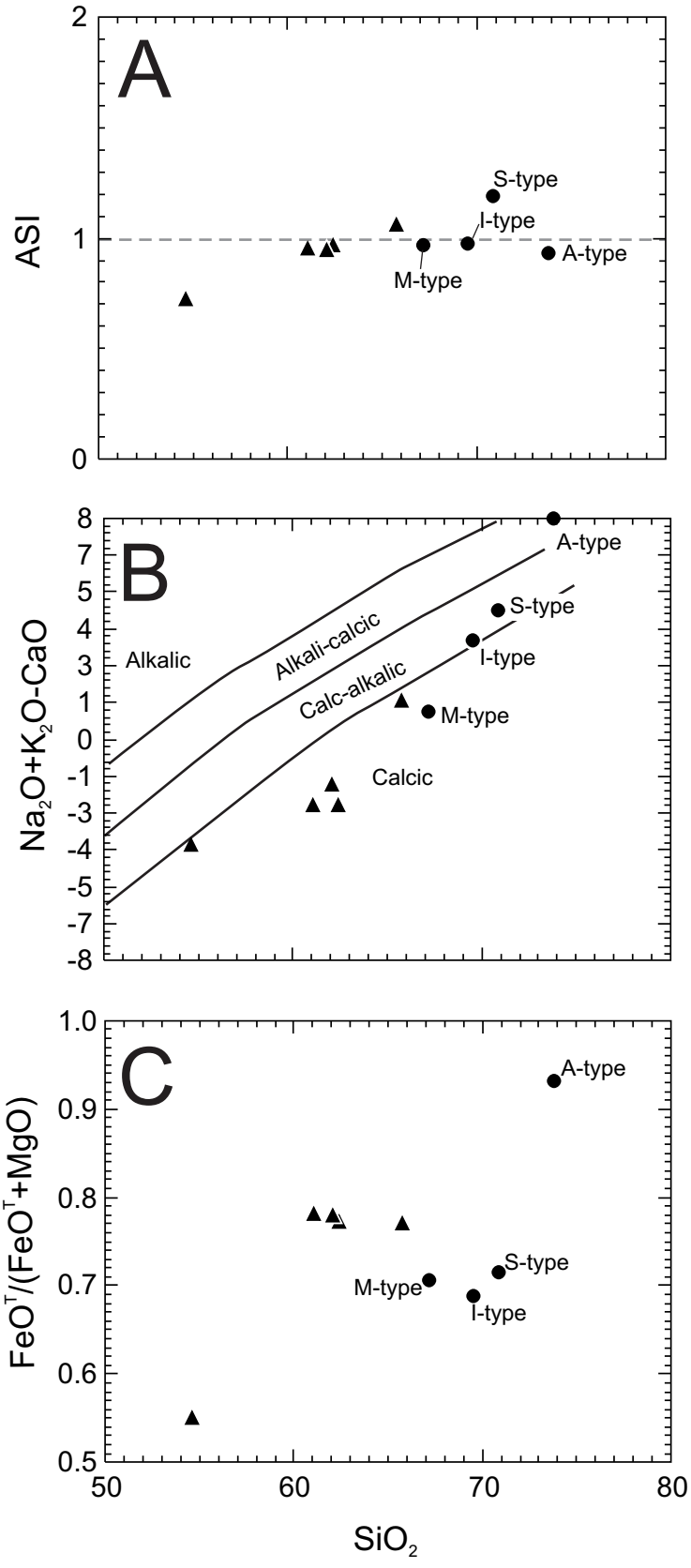
A
ASI
S-type
I-type
A-type
M-type
B
Na_2O+K_2O-CaO
Alkalic
Alkali-calcic
Calc-alkalic
Calcic
C
$FeO^T/(FeO^T+MgO)$
SiO_2

Figure 66. A. Ta-Y discrimination diagram for granitic rocks from Pearce et al. (1984b) for samples from the Quartz Mountain stock. B. Rb-Y+Nb discrimination diagram for granitic rocks from Pearce et al. (1984b) for samples from the Quartz Mountain stock. Also plotted on all diagrams are the average values for A-type, I-type, M-type, and S-type granites (Collins et al., 1982; Whalen et al., 1987; Chappell and White, 1992; compiled by Winter, 2001). ORG = ocean ridge granites; syn-COLG - syn-collision granites; VAG = volcanic arc granites; WPG = within-plate granites.

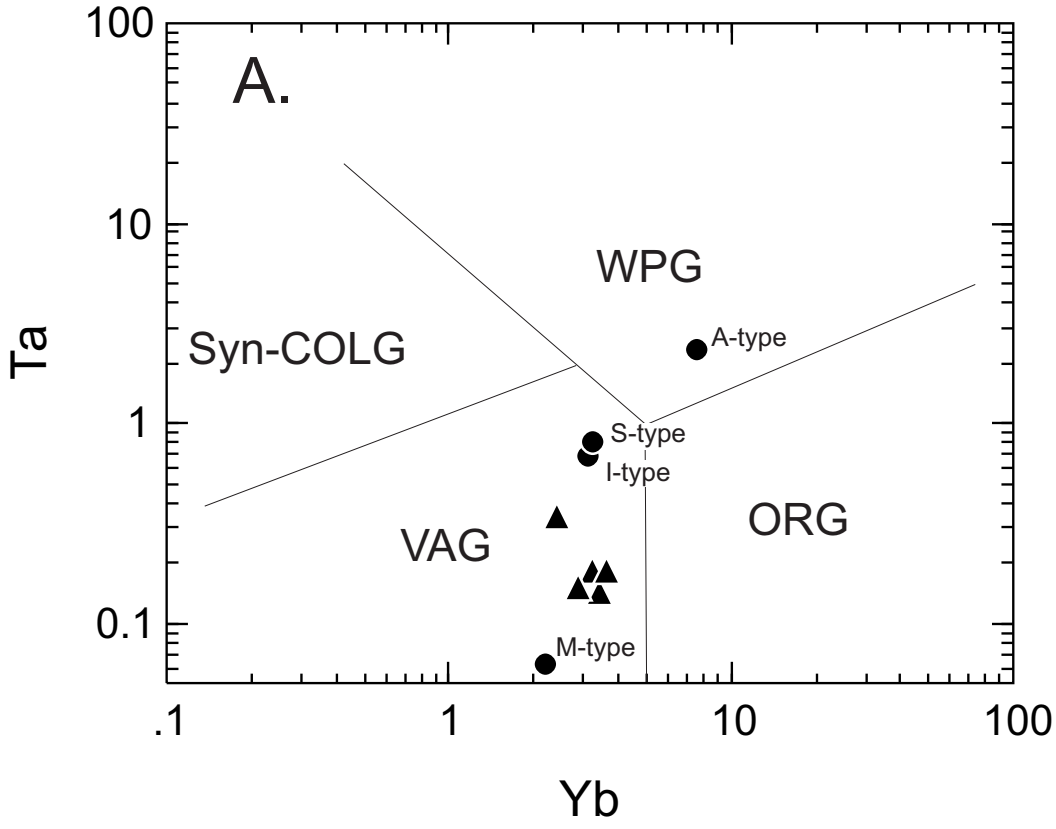
A.
100
10
1
0.1
Ta
.1
1
10
100
Yb
WPG
Syn-COLG
VAG
ORG
A-type
S-type
I-type
M-type

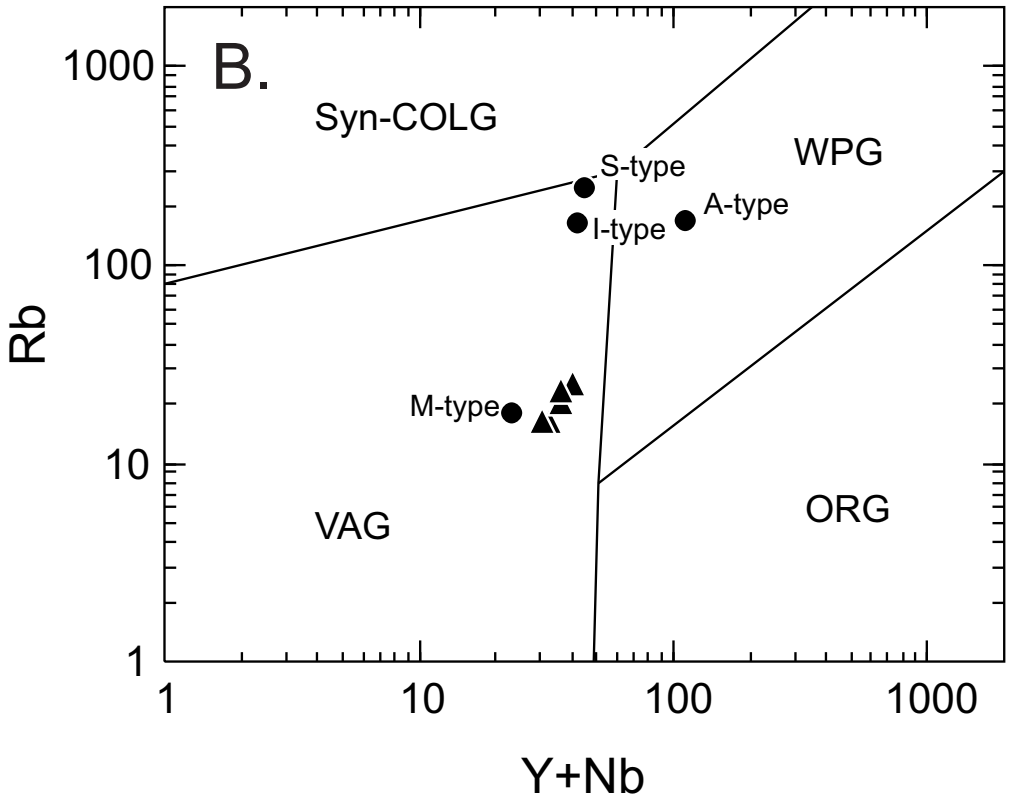
B.
1000
100
10
1
Rb
1
10
100
1000
Y+Nb
Syn-COLG
WPG
VAG
ORG
S-type
I-type
A-type
M-type

Figure 67. Th/Yb-Ta/Yb discrimination diagram for Quartz Mountain stock samples (Pearce, 1982). N-MORB, E-MORB and OIB normalizing values are from Sun and McDonough (1989). N-MORB = normal-mid-ocean ridge basalt; E-MORB = enriched-mid-ocean ridge basalt; OIB = ocean island basalt (= within-plate basalt). Field for volcanic arcs was compiled by Pearce (1982, 1983). Also plotted on all diagrams are the average values for A-type, I-type, M-type, and S-type granites (Collins et al., 1982; Whalen et al., 1987; Chappell and White, 1992; compiled by Winter, 2001).

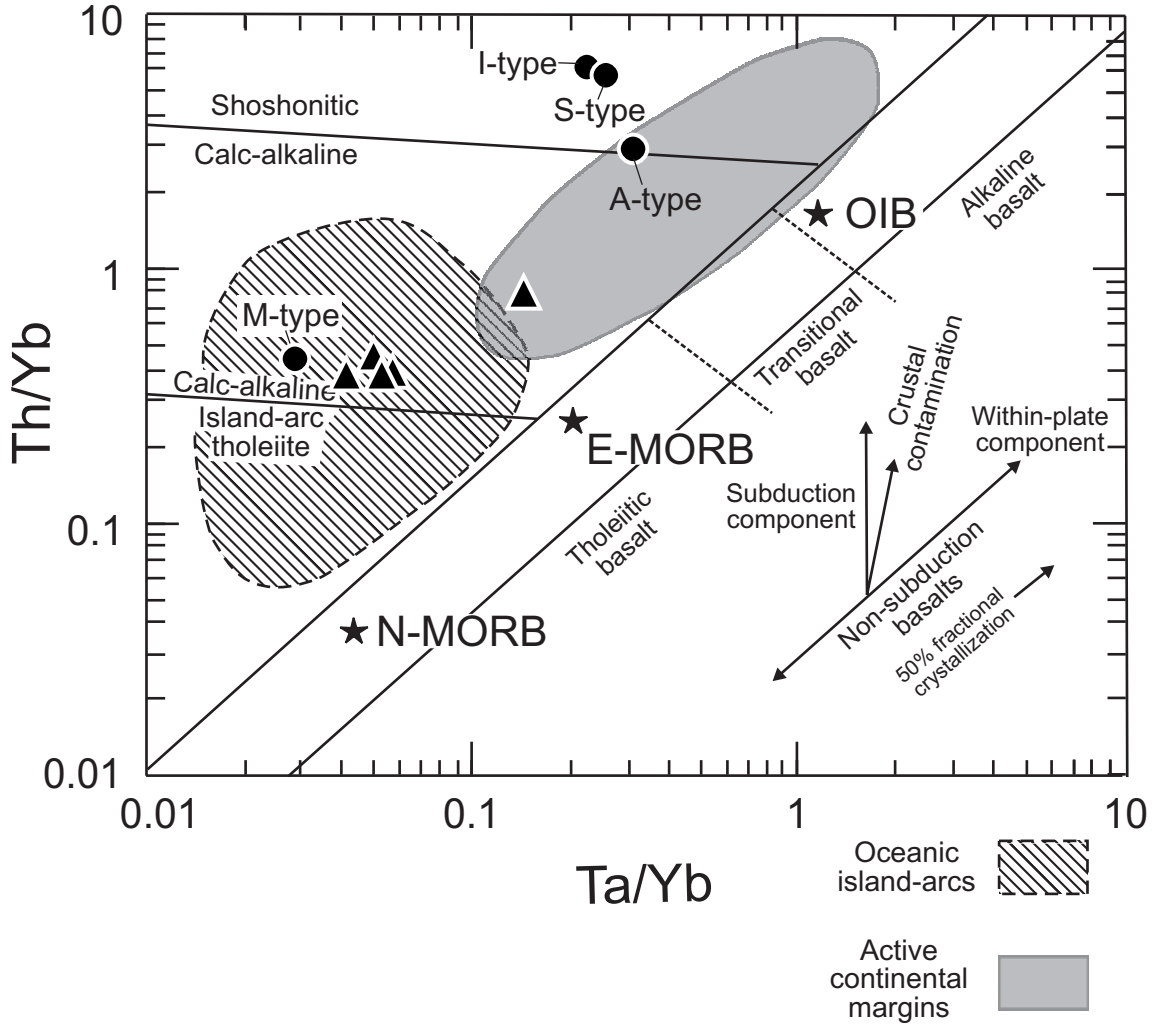
10
1
0.1
0.01
0.01
0.1
1
10
Th/Yb
Ta/Yb
I-type
S-type
A-type
Shoshonitic
Calc-alkaline
OIB
Alkaline basalt
Transitional basalt
M-type
Calc-alkaline
Island-arc tholeiite
E-MORB
Crustal contamination
Within-plate component
Subduction component
Tholeiitic basalt
Non-subduction basalts
50% fractional crystallization
N-MORB
Oceanic island-arcs
Active continental margins

Figure 68. Ti-Zr-Y basalt discriminant diagram (Pearce and Cann, 1973) for Helena-Haystack mélange of the Manstash inlier samples. Only basaltic compositions are plotted. Symbols are the same as Fig. 70. Also shown on this diagram is a shaded field for the De Roux unit and a dashed-line field for the Helena-Haystack mélange west of the Straight Creek fault. Older data taken from Ort and Tabor (1985), Tabor (1994) and Dragovich et al. (1998).

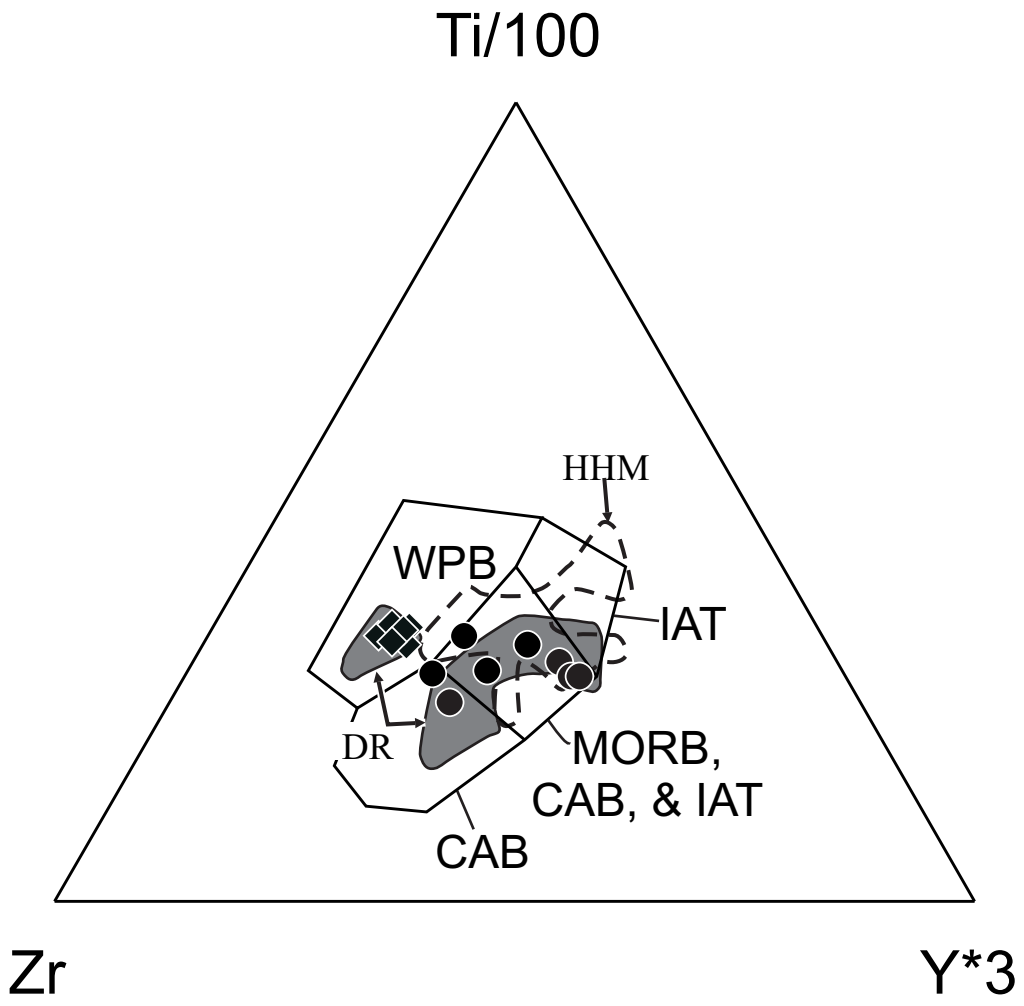
Ti/100
HHM
WPB
IAT
DR
MORB,
CAB, & IAT
CAB
Zr
Y*3

Figure 69. Ti-V discriminant diagram (Shervais, 1982) for Helena-Haystack mélange samples of the Manstash inlier. Only basaltic compositions are plotted. Symbols are the same as Fig. 70. Also shown on this diagram is a shaded field for the De Roux unit and a dashed-line field for the Helena-Haystack mélange west of the Straight Creek fault. Older data taken from Ort and Tabor (1985), Tabor (1994) and Dragovich et al. (1998).

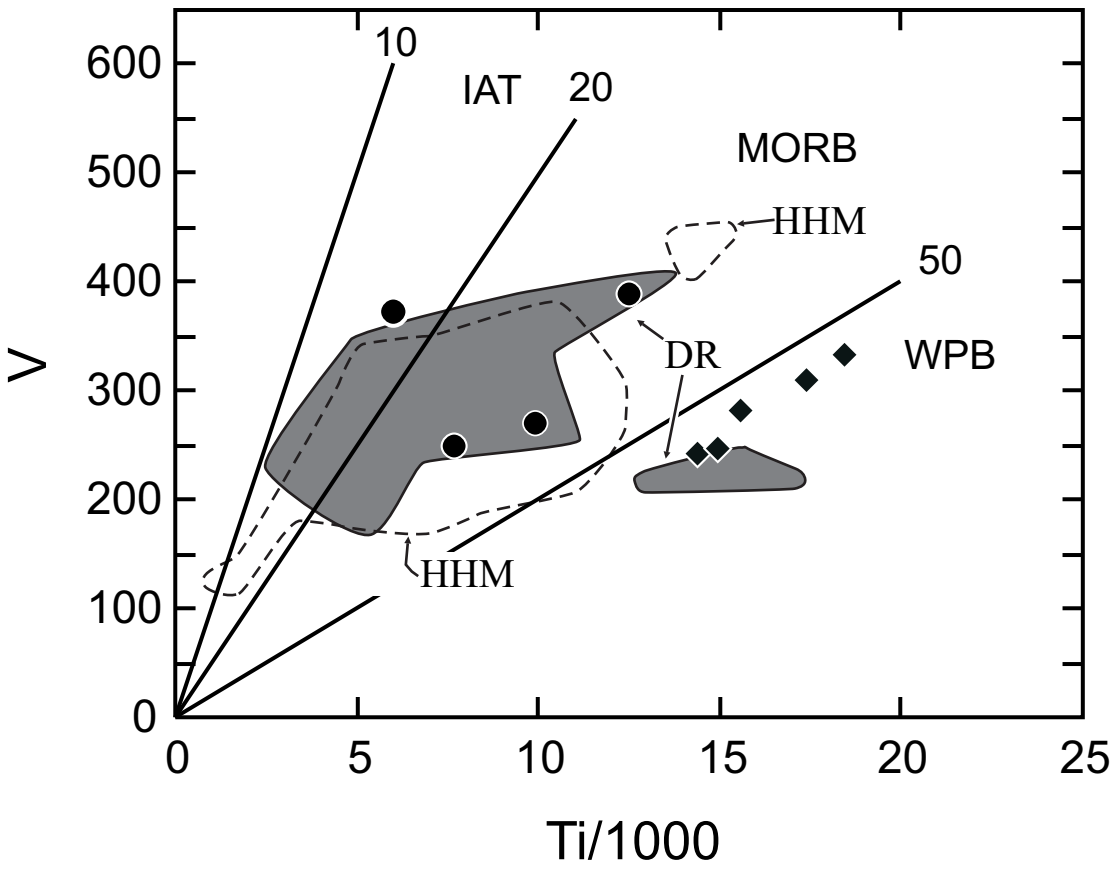
10
IAT
20
MORB
HHM
50
DR
WPB
HHM
600
500
400
300
200
100
0
V
0
5
10
15
20
25
Ti/1000

Figure 70. Th/Yb-Ta/Yb discrimination diagram for Helena-Haystack mélange and De Roux unit samples (Pearce, 1982). N-MORB, E-MORB and OIB normalizing values are from Sun and McDonough (1989). N-MORB = normal-mid-ocean ridge basalt; E-MORB = enriched-mid-ocean ridge basalt; OIB = ocean island basalt (= within-plate basalt). Also shown on this diagram is a shaded field for the De Roux unit and a dashed-line field for the Helena-Haystack mélange west of the Straight Creek fault (Ort and Tabor, 1985; Tabor, 1994; Dragovich et al., 1998).

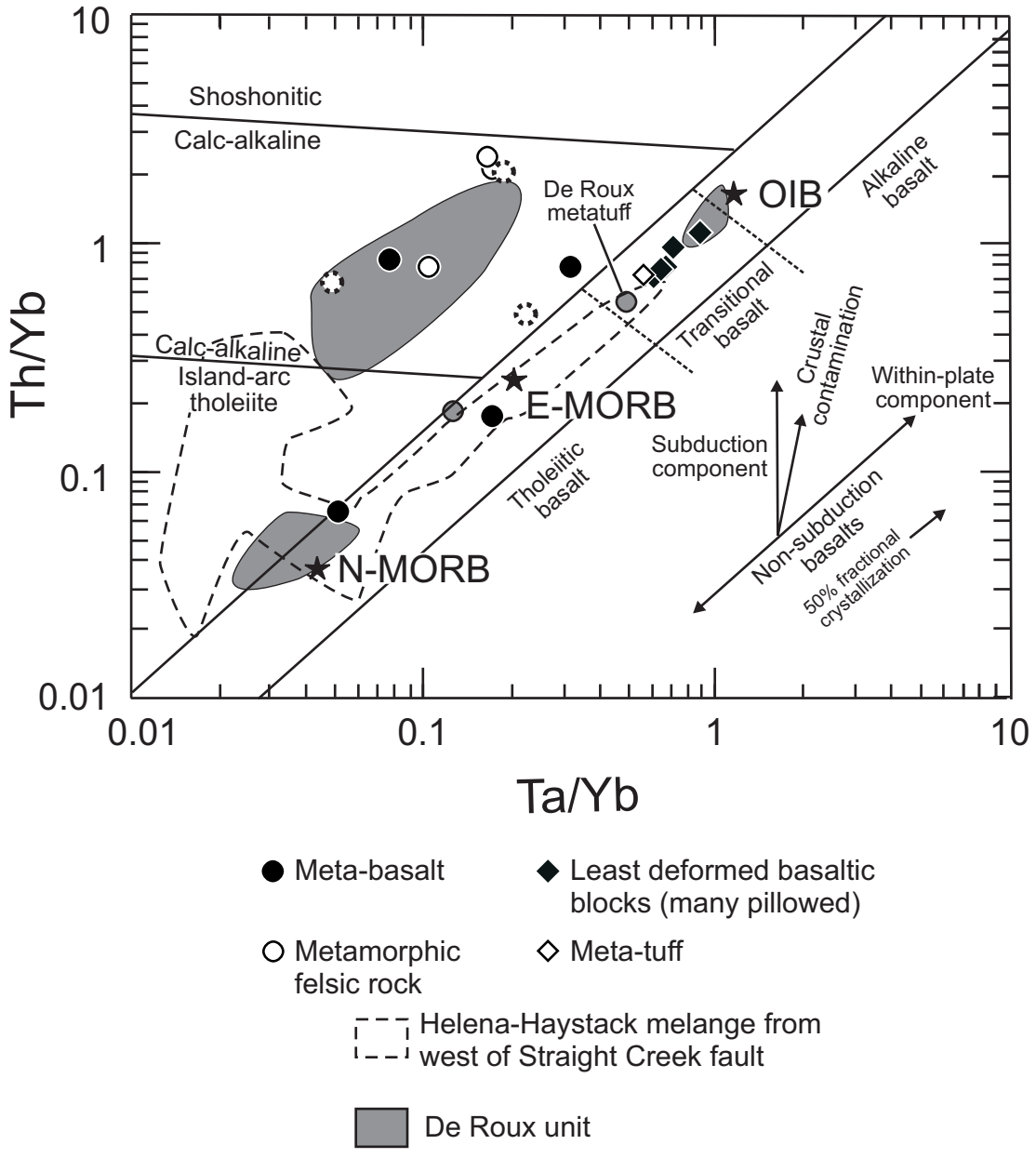
10
1
0.1
0.01
0.01
0.1
1
10
Th/Yb
Ta/Yb
Shoshonitic
Calc-alkaline
Calc-alkaline
Island-arc
tholeiite
De Roux
metatuff
OIB
Alkaline
basalt
Transitional
basalt
Crustal
contamination
Within-plate
component
E-MORB
Subduction
component
Tholeiitic
basalt
N-MORB
Non-subduction
basalts
50% fractional
crystallization
Meta-basalt
Least deformed basaltic
blocks (many pillowed)
Metamorphic
felsic rock
Meta-tuff
Helena-Haystack melange from
west of Straight Creek fault
De Roux unit

Figure 71. Chondrite- and N-MORB-normalized diagrams (see Fig. 70 for key to symbols). Chondrite and N-MORB normalized values are from Sun and McDonough (1989). A and B. Modern reference suite. N-MORB, E-MORB, and OIB from Sun and McDonough (1989); IAT and CAB from Pearce et al. (1995). C. Chondrite-normalized diagram for WPB and E-MORB affinity samples from the Helena-Haystack mélange of the Manastash inlier. D. N-MORB-normalized diagram for WPB and E-MORB affinity samples from the Helena-Haystack mélange of the Manastash inlier. E. Chondrite-normalized diagram for arc-affinity samples from the Helena-Haystack mélange of the Manastash inlier. F. N-MORB-normalized diagram for arc-affinity samples from the Helena-Haystack mélange of the Manastash inlier.

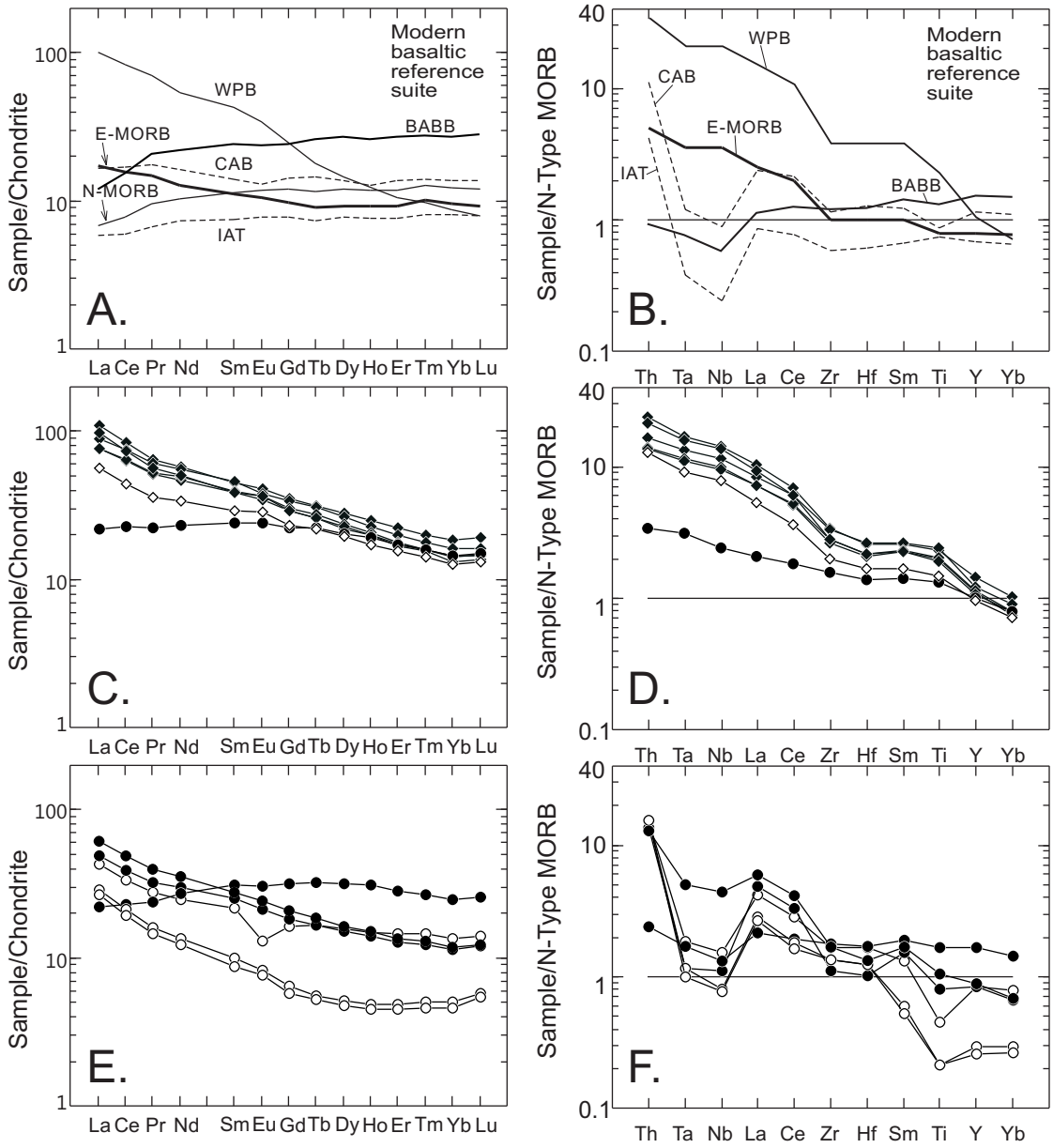
Modern basaltic reference suite
WPB
E-MORB
BABB
CAB
N-MORB
IAT
Sample/Chondrite
Sample/N-Type MORB
A.
B.
C.
D.
E.
F.
La Ce Pr Nd Sm Eu Gd Tb Dy Ho Er Tm Yb Lu
Th Ta Nb La Ce Zr Hf Sm Ti Y Yb

Figure 72. Geologic map of the type area of the De Roux unit. Modified from Miller (1980, 1985) and Tabor et al. (1982). New mapping done by J. MacDonald.

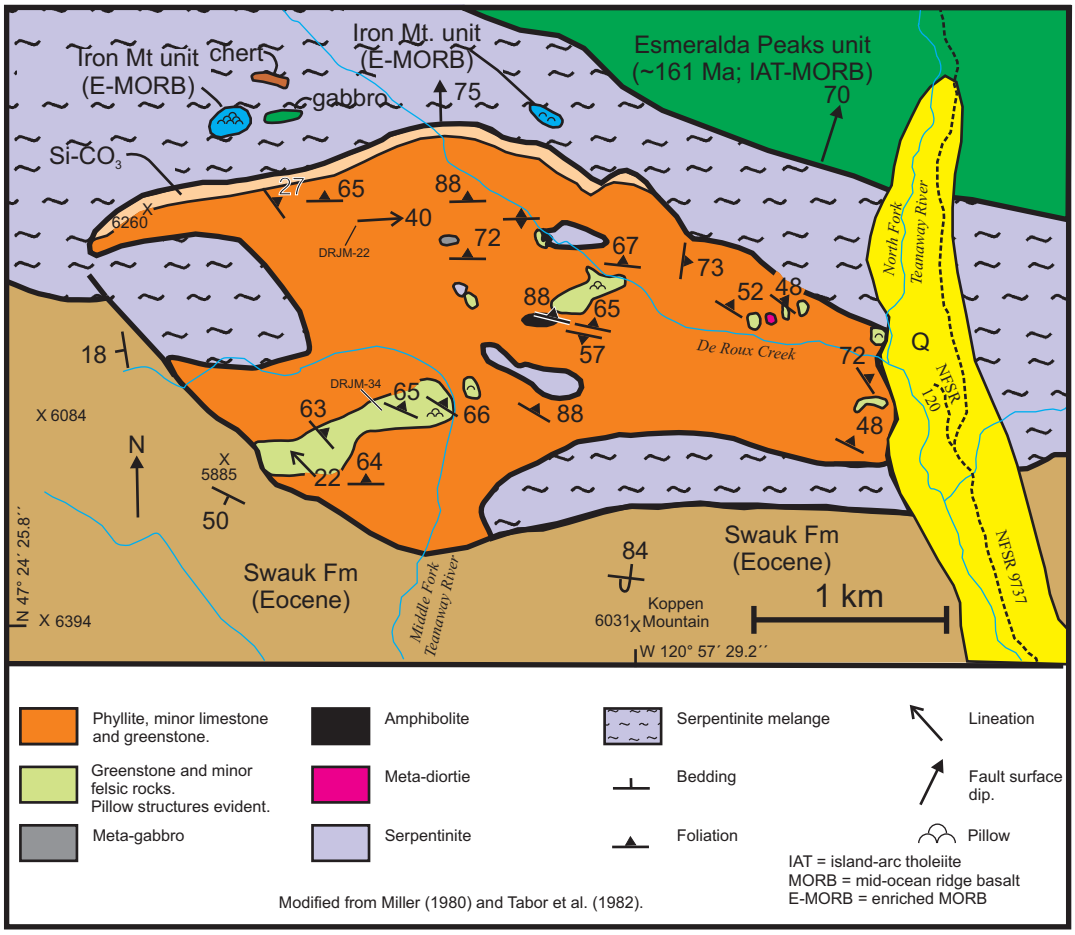

Modified from Miller (1980) and Tabor et al. (1982).

Figure 73. Schematic geologic map showing the study area in relation to first-order Precambrian basement provinces of western North America. Modified from Gehrels (2000, and references within).

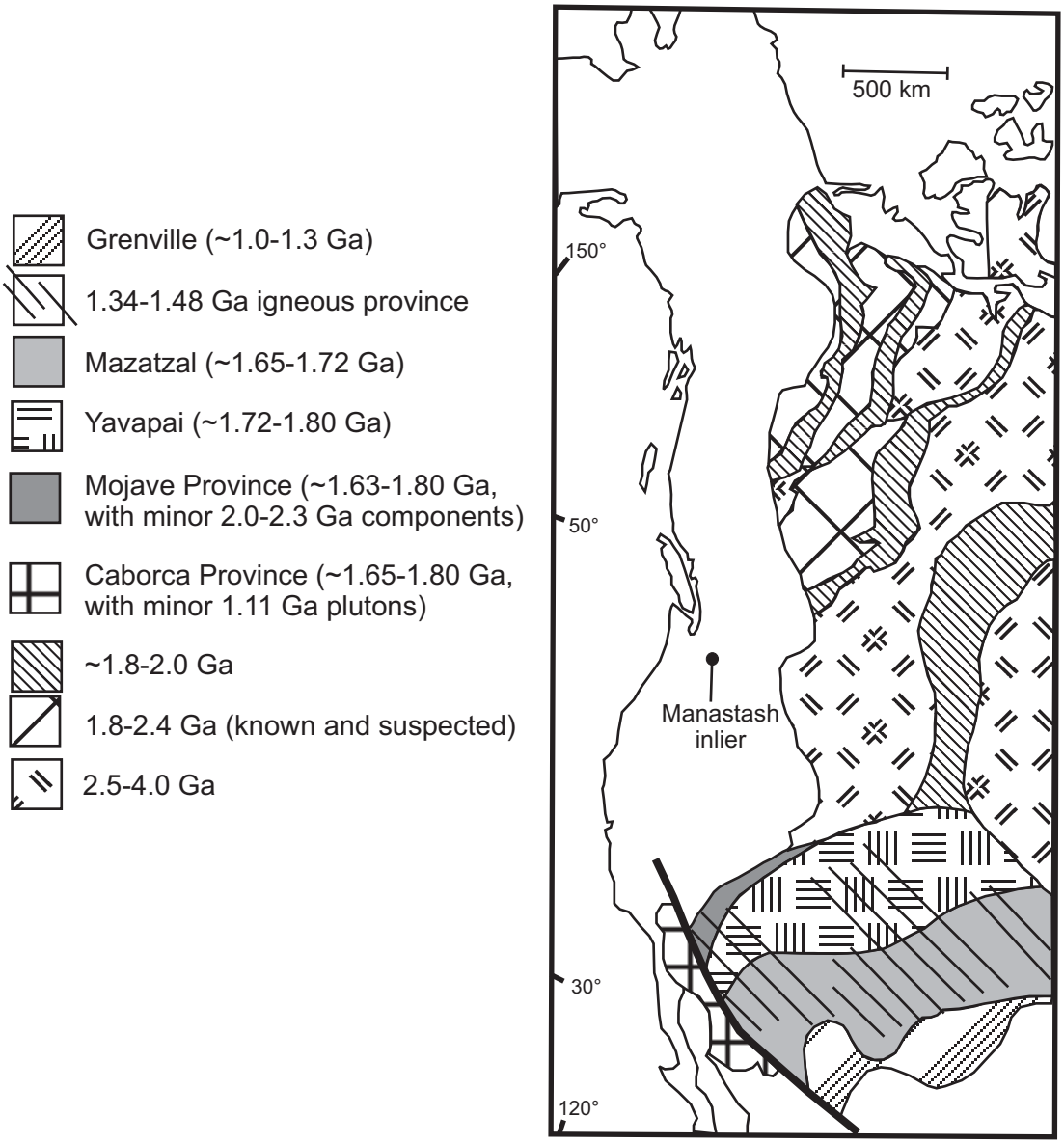
Grenville (~1.0-1.3 Ga)
1.34-1.48 Ga igneous province
Mazatzal (~1.65-1.72 Ga)
Yavapai (~1.72-1.80 Ga)
Mojave Province (~1.63-1.80 Ga, with minor 2.0-2.3 Ga components)
Caborca Province (~1.65-1.80 Ga, with minor 1.11 Ga plutons)
~1.8-2.0 Ga
1.8-2.4 Ga (known and suspected)
2.5-4.0 Ga
500 km
150°
50°
30°
120°
Manastash inlier

Figure 74. Reconstruction of the pre-Tertiary rocks in western Washington after ~98 km of displacement on the Straight Creek fault. HHM = Helena-Haystack mélange; NWCS = Northwest Cascade System; WEMB = western and eastern mélange belts. Modified from Tabor et al. (1989), Miller et al. (1993), and Tabor (1994).

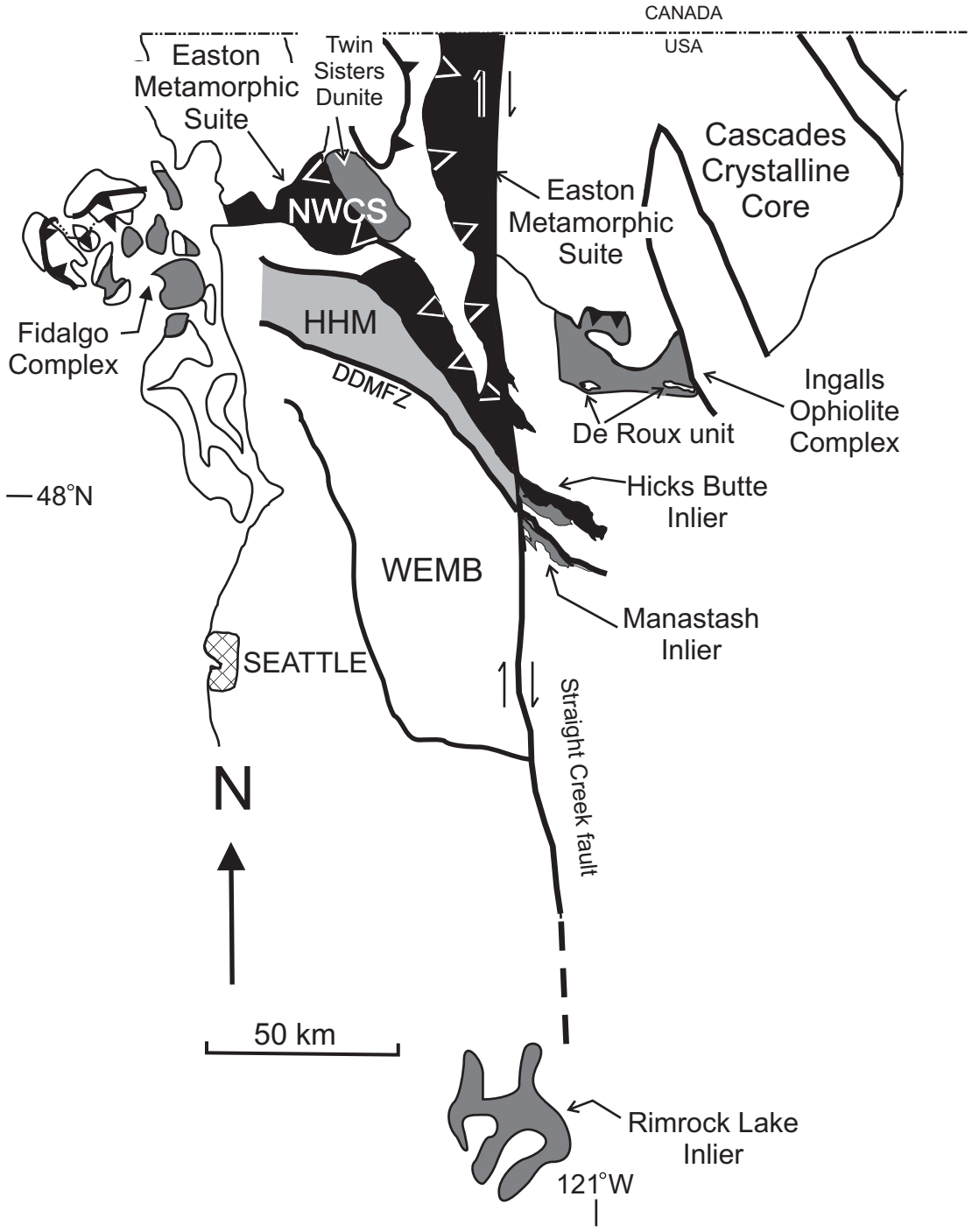
CANADA
USA
Easton
Metamorphic
Suite
Twin
Sisters
Dunite
NWCS
Easton
Metamorphic
Suite
Cascades
Crystalline
Core
HHM
Fidalgo
Complex
DDMFZ
Ingalls
Ophiolite
Complex
De Roux unit
48°N
Hicks Butte
Inlier
WEMB
Manastash
Inlier
SEATTLE
Straight Creek fault
N
50 km
Rimrock Lake
Inlier
121°W

Figure 75. Tectonic model for the formation of the Lookout Mountain Formation and Quartz Mountain stock. A. Oblique subduction during the Middle Jurassic. B. Forearc rifting and sedimentation during the Upper Callovian to Lower Oxfordian. This rifting may have been the result of a ridge subduction event. C. Rogue-Chetco arc formation, including the Quartz Mountain stock, and Ingalls-Josephine basin formation during the Upper Oxfordian.

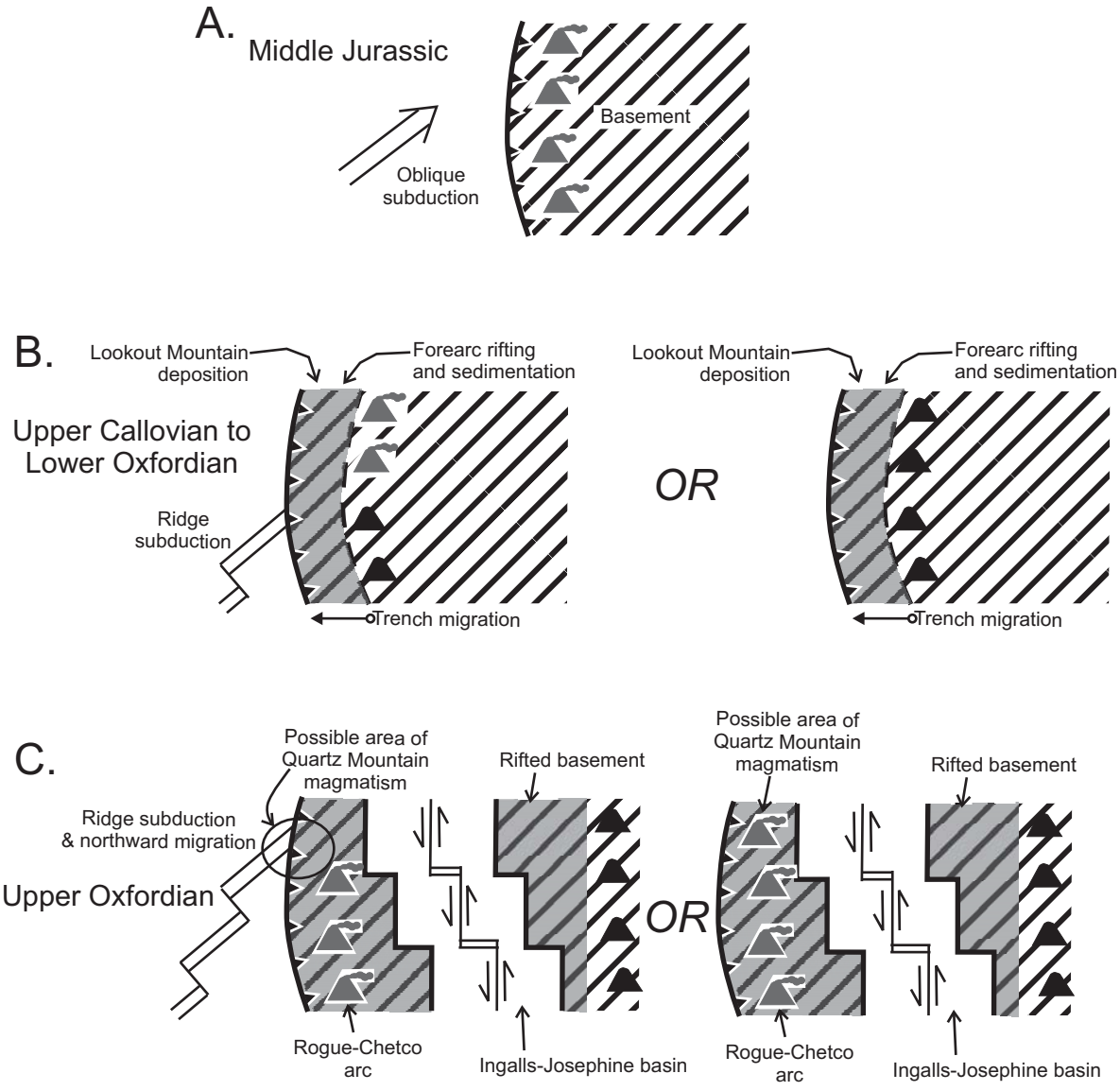
A.
Middle Jurassic
Basement
Oblique
subduction
B.
Lookout Mountain
deposition
Forearc rifting
and sedimentation
Upper Callovian to
Lower Oxfordian
Ridge
subduction
Trench migration
OR
Lookout Mountain
deposition
Forearc rifting
and sedimentation
Trench migration
C.
Possible area of
Quartz Mountain
magmatism
Rifted basement
Ridge subduction
& northward migration
Upper Oxfordian
Rogue-Chetco
arc
Ingalls-Josephine basin
OR
Possible area of
Quartz Mountain
magmatism
Rifted basement
Rogue-Chetco
arc
Ingalls-Josephine basin

APPENDIX B

OUTCROP MAP OF IRON MOUNTAIN AREA

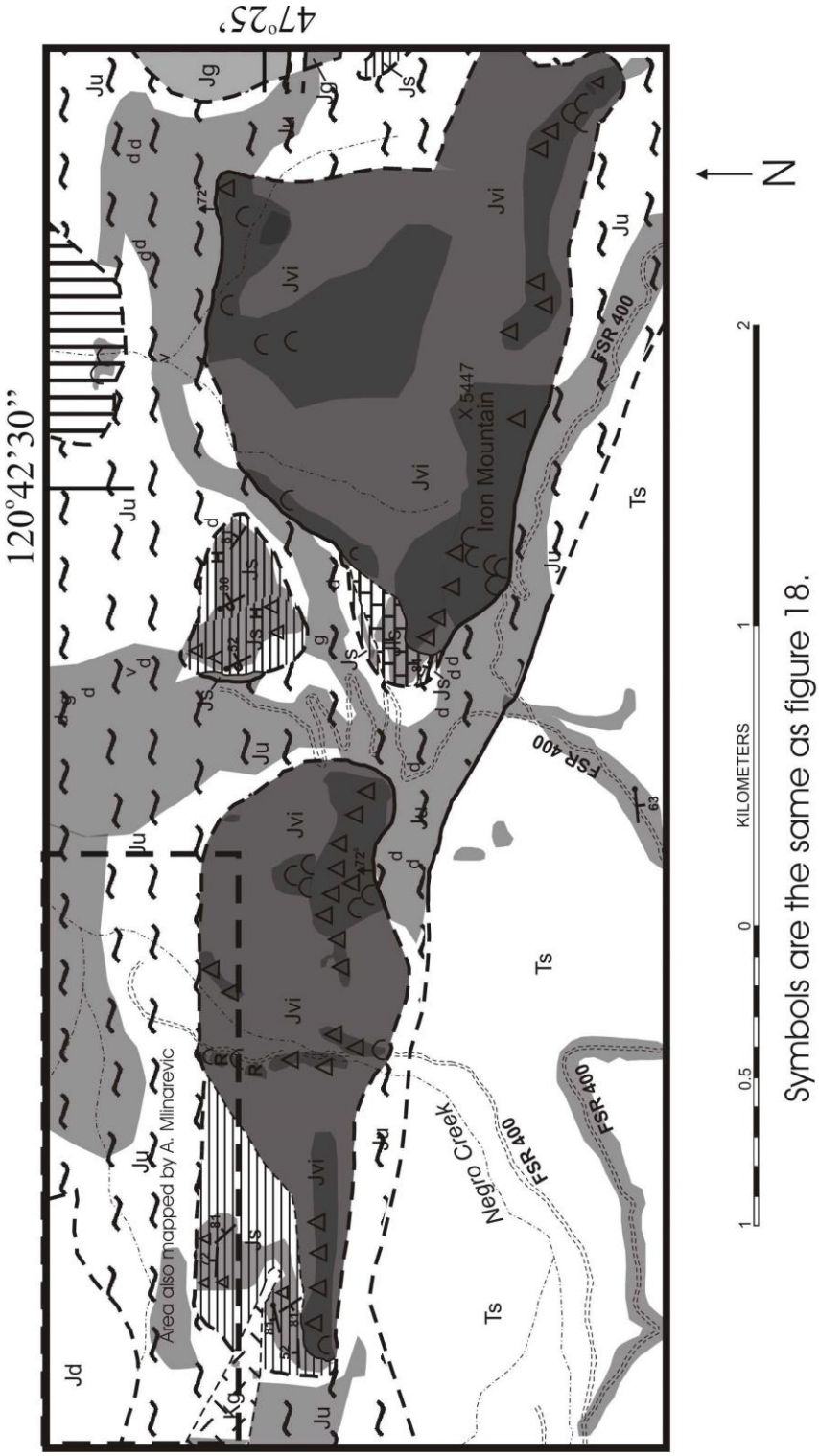

APPENDIX C

OUTCROP MAP OF ESMERALDA PEAKS AREA

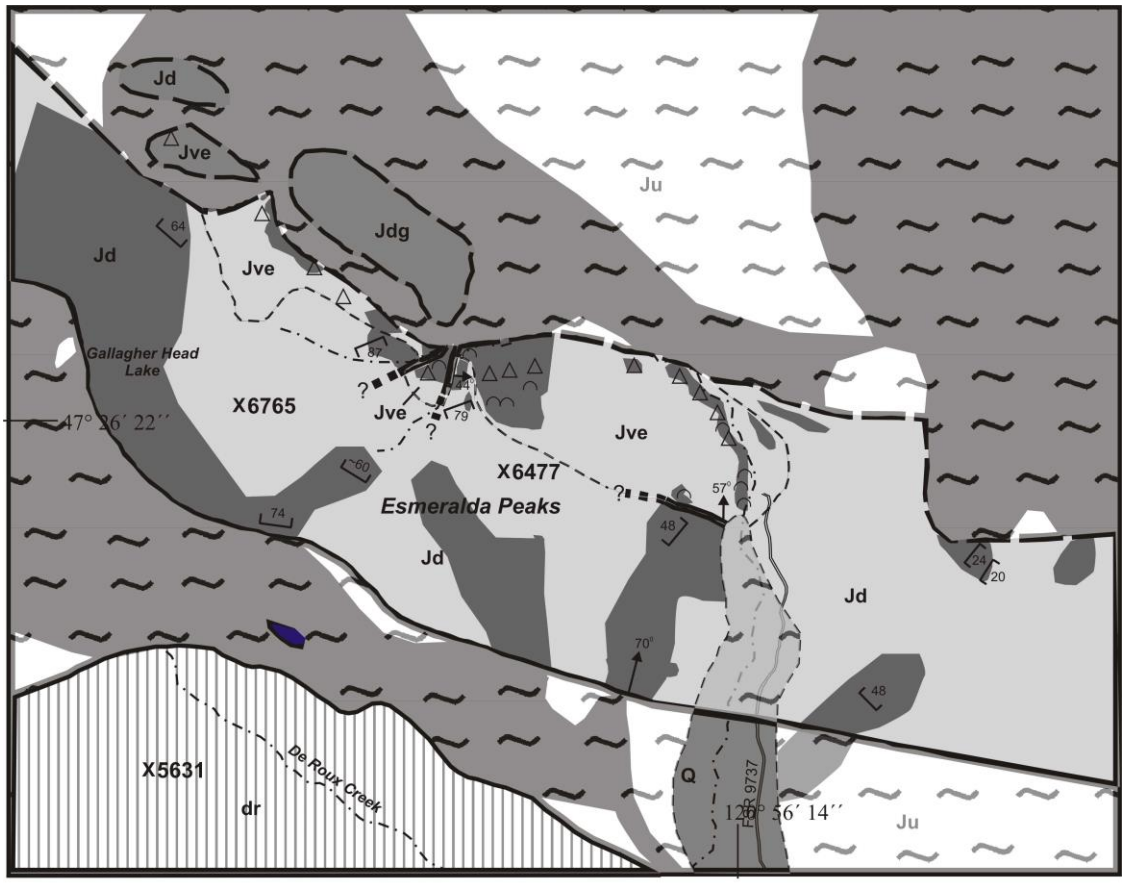

Symbols are the same as Figures 29 and 30.
Dark gray areas are outcrop

APPENDIX D

OUTCROP MAP OF QUARTZ MOUNTAIN AREA

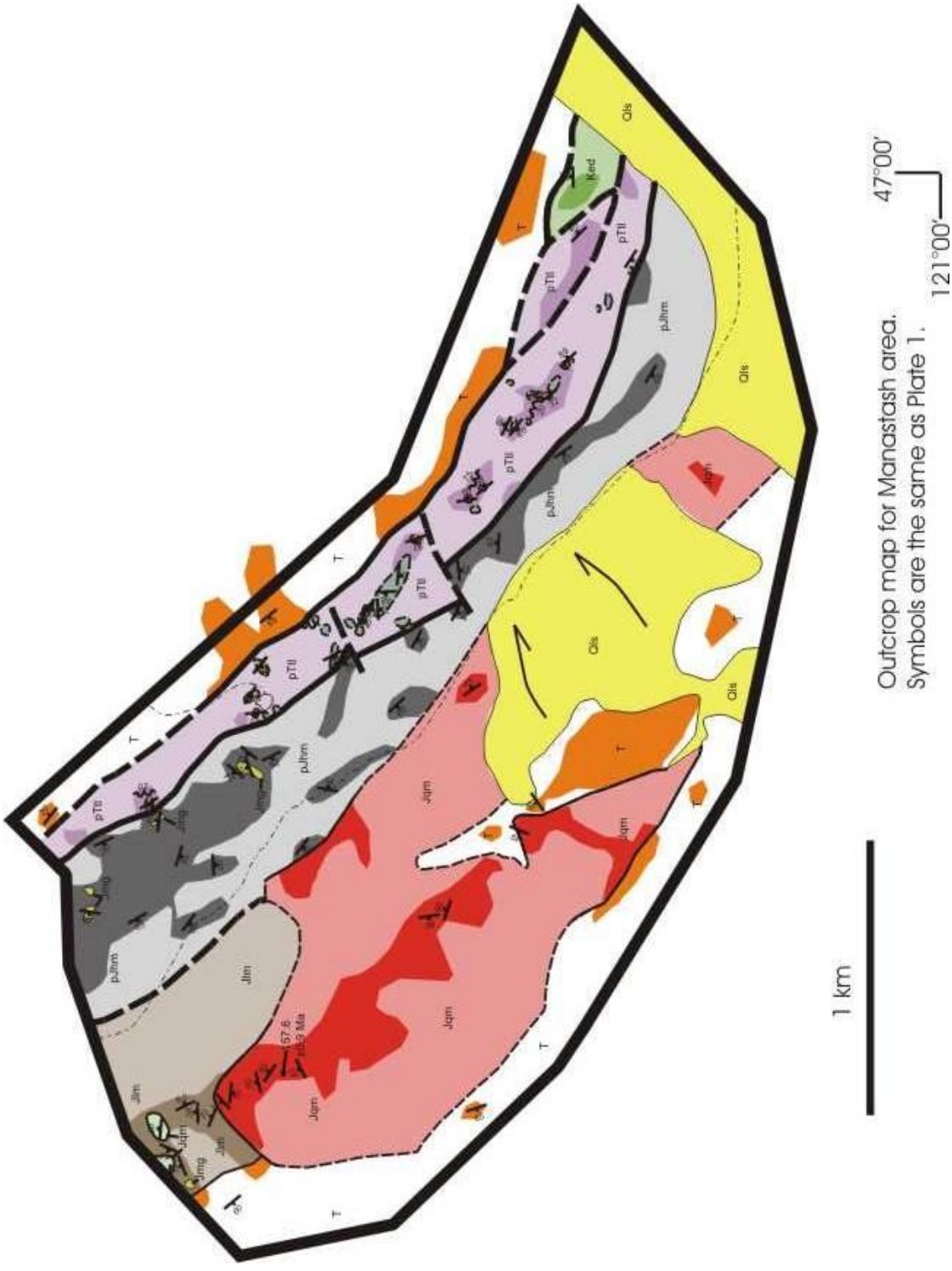

APPENDIX E

OUTCROP MAP OF DE ROUX CREEK AREA